Modifying layered double hydroxide nanoparticles with peptide to penetrate blood brain barrier for gene delivery

Huali Zuo

Bachelor of Science, Master of Science

A thesis submitted for the degree of Doctor of Philosophy at

The University of Queensland in 2016

Australian Institute for Bioengineering and Nanotechnology

Abstract

Blood–brain barrier (BBB) is a formidable barrier interface that exists between blood and brain, therefore, preventing therapeutic drugs or particles to enter the brain tissue. Nano-medicine is emerging as a prospective way for enhancing pharmaceutical product delivery to the brain with the development of various nano-biotechnologies. In particular, non-viral inorganic layered double hydroxide (LDH) nanoparticles have unique advantages over others in terms of various instinctive properties, such as low cytotoxicity, good biocompatibility and high drug loading capacity. Importantly, previous studies have demonstrated that LDHs can efficiently deliver siRNAs into the neuronal cells, resulting in the knockdown of the target protein. Despite the previous results, two major hurdles still exist before LDHs can be employed as an efficacious central nervous system (CNS) drug delivery system: (i) LDH aggregation upon exposure to the serum environment and (ii) non-specificity in the BBB penetration.

This thesis focuses on developing novel engineered LDH delivery system with enhanced suspension stability, redispersion capability and brain targeting ability based on the bovine serum albumin (BSA) coating strategies. Angiopep2 (Ang2) and rabies virus glycoprotein peptide (RVG) are selected as targeting ligands as they can target to the low-density lipoprotein receptor-related protein (LRP) over-expressed on U87 glioma cells and nicotinic acetylcholine receptor (nAchR) on Neura 2a (N2a) cells, respectively. These two ligands can also target the endothelial cells which form the BBB. Moreover, the manganese ions are incorporated into the LDHs system to form magnetic nanoparticles that can act as the potential theranostic agent for simultaneous brain imaging and delivery.

First of all, BSA coated LDHs are further crosslinked by glutaraldyhyde (GTA) to improve the suspension stability and residpersion capability based on previous BSA coating strategies. Enhanced colloidal stability and excellent redispersity have been achieved compared with uncrosslinked BSA-LDHs and pristine LDH nanoparticles, with negligible effect on cell cytotoxicity and cell uptake. Thus, the newly developed GTA crosslinking strategy provides a solid LDH-based platform for the following in vitro and in vivo studies.

Subsequently, LDHs-based targeting delivery system has been developed by conjugating ligand Ang2 or RVG with LDHs through BSA (Ang2-NPs and RVG-NPs) for brain tumour targeting. In vitro cell uptake shows that the Ang2-NPs and RVG-NPs have enhanced delivery efficiency and demonstrated specificity to relative cells. MTT assay and hemolysis study shows that the newly fabricated various LDH formulations have good blood compatibility and less

cytotoxicity. Moreover, incorporating anticancer drug 5-FU with the LDH targeting system results in increased cell growth inhibition in comparison with the unmodified LDHs. Thus, this research provides a facile approach for ligand modification and synchronous maintenance of colloidal stability with narrow batch-to-batch variation.

Then, in vivo and in vitro brain targeting ability of ligand modified LDHs has been evaluated. Endothelial cells (bEnd.3 cells) are the major cells that constitute BBB with both Ang2 and RVG receptors overexpressed. In the in vitro cellular uptake study and in the in vitro BBB model, the Ang2/RVG-NPs demonstrate increased cellular uptake and BBB penetration compared with NPs. In vivo confocal neuroimaging (ICON) results clearly show that the ligand modified LDH nanoparticles have longer retention time in the retina vessel. The in vivo optical imaging study confirms that the Ang2 ligand better target the mouse brain than RVG, which is consistent with the ICON observation that RVG-NPs disappear much more quickly than Ang2-NPs.

Moreover, we have synthesised a new manganese-based bifunctional LDHs (Mn-LDHs) for brain cancer theranostics. The newly designed Mn-LDHs exhibits similar biocompatibility and excellent gene delivery efficacy to normal LDHs. Incorporating the contrast agent Mn into the LDHs system endows themselve as contrast agents for MRI imaging. Compared with commercial Gd (DTPA)-based contrast agent ($r1 \approx 3.4$ mM^{-1} s^{-1}), the Mn-LDHs demonstrate relatively high r1 value (4.47 mM^{-1} s^{-1}). In consistence, the Mn-LDHs loaded with the cell death siRNA (CD-siRNA) show higher cytotoxicity to cancer cells than the free CD-siRNA, and cause significant brain tumour cell growth inhibition. Supportively, the amount of Mn-LDHs used for CD-siRNA delivery has been examined to be enough for MRI imaging of the cancer cells. Collectively, the obtained bifunctional Mn-LDHs show great potential applications as highly effective bimodal imaging and delivery for cancer diagnosis and chemotherapy simultaneously.

Declaration by Author

This thesis is composed of my original work, and contains no material previously published or written by another person except where due reference has been made in the text. I have clearly stated the contribution by others to jointly-authored works that I have included in my thesis.

I have clearly stated the contribution of others to my thesis as a whole, including statistical assistance, survey design, data analysis, significant technical procedures, professional editorial advice, and any other original research work used or reported in my thesis. The content of my thesis is the result of work I have carried out since the commencement of my research higher degree candidature and does not include a substantial part of work that has been submitted to qualify for the award of any other degree or diploma in any university or other tertiary institution. I have clearly stated which parts of my thesis, if any, have been submitted to qualify for another award.

I acknowledge that an electronic copy of my thesis must be lodged with the University Library and, subject to the policy and procedures of The University of Queensland, the thesis be made available for research and study in accordance with the Copyright Act 1968 unless a period of embargo has been approved by the Dean of the Graduate School.

I acknowledge that copyright of all material contained in my thesis resides with the copyright holder(s) of that material. Where appropriate I have obtained copyright permission from the copyright holder to reproduce material in this thesis.

Publications during candidature

1. **<u>H Zuo</u>**, Z Gu, H Cooper, ZP Xu. *Crosslinking to enhance colloidal stability and redispersity of layered double hydroxide nanoparticles*. Journal of colloid and interface science, **2015**, 459, 10-16.

2. Z. Gu, **<u>H. Zuo</u>**, L. Li, A. Wu, Z.P. Xu, *Pre-coating layered double hydroxide nanoparticles with albumin to improve colloidal stability and cellular uptake*, Journal of Materials Chemistry B, **2015**, 3, 3331-3339.

3. **<u>H Zuo</u>**, W Chen, H Cooper, ZP Xu. *A facile way of modifying layered double hydroxide nanoparticles with targeting ligand-conjugated albumin for enhanced delivery to brain tumour cells*. ACS Applied Materials & Interfaces (In revision).

Conference proceedings

1. 6th International NanoMedicine Conference. Sydney's Coogee Beach at the Crowne Plaza Hotel from July 6 to 8, 2015. Title: *Modifying layered double hydroxide nanoparticles with peptide to penetrate blood brain barrier for gene delivery* (Oral presentation).

2. Nano bio 2014 (7-10 July 2014), The University of Queensland. Title: *Modifying layered double hydroxide nanoparticles with peptide to penetrate through blood brain barrier for gene delivery* (post presentation).

3. Third Symposium on Innovative Polymers for Controlled Delivery (SIPCD 2014) held in Suzhou, China.16-19 Sep, 2014. *Stabilization of layered double hydroxide nanoparticles by bovine serum albumin pre-coating for drug/gene delivery* (post presentation).

4. Nanoparticles for Brain Applications: Diagnostic and Therapy. Otto-von-Guericke University Magdeburg, Germany. 15-16 Feb, 2016.

Publications included in this thesis

1. **<u>H Zuo</u>**, Z Gu, H Cooper, ZP Xu. *Crosslinking to enhance colloidal stability and redispersity of layered double hydroxide nanoparticles*. Journal of colloid and interface science, **2015**, 459, 10-16. Incorporated as Chapter 4

Contributor	Statement of contribution
Author Huali Zuo (Candidate)	Designed experiments (70%) Wrote the paper (70%)
Author Zi Gu	Designed experiments (10%) Wrote and edited paper (10%)
Author Helen Cooper	Statistical analysis of data in Figure 4.6
Author Zhiping Xu	Designed experiments (20%) Wrote and edited paper (20%)

<u>Contributions by others to the thesis</u>

XPS was performed by Dr. Barry wood (Chapter 7)

<u>Statement of parts of the thesis submitted to qualify for the award of another degree</u>

None.

<u>Acknowledgements</u>

Keywords

Layered double hydroxide, brain cancer, intracellular delivery, surface functionalization, drug/gene therapy, ligands, stability, theranostic, magnetic resonance imaging, active targeting.

Australian and New Zealand Standard Research Classifications (ANZSRC)

ANZSRC code: 100708, Nanomaterials, 30%

ANZSRC code: 090302, Biomedical Engineering, 40%

ANZSRC code: 111204 Cancer Therapy, 30%

Fields of Research (FoR) Classification

FoR code: 1007, Nanotechnology, 30%

FoR code: 1112, Oncology and Carcinogenesis, 30%

FoR code: 0903, Biomedical Engineering, 40%

Table of Contents

List of Figures and Tables

Figure 2.1 Barriers to CNS access. The neurovascular unit is composed of the endothelial lining, the basal lamina, ensheathed pericytes and astrocytic endfeet.

Figure 2.2 Therapeutic brain delivery strategies that target the physiological make-up of the BBB. (A) Transport mechanisms at the BBB. (B) A wide range of receptors mediate transport through transcytosis.

Figure 2.3 Strategies for enhanced drug delivery against brain tumour.

Figure 2.4 Schematic structure of different nanocarriers (liposomes, polymeric nanoparticles including nanospheres and nanocapsules, dendrimers, and micelles) for drug delivery to the brain tumour.

Figure 2.5 Schematic representation of LDH structure.

Figure 2.6 TEM images of (A) LDHFITC-HEX (same as LDHHEX-Cl) and (B) LDHFITC-ROD. (C) Delamination scheme of LDHs into LDH nanosheets.

Figure 2.7 Schematic illustration of LDH particle endocytosis and endosomal escape.

Figure 2.8 Adsorption of Intimin β (IB) to clay nanomaterials. Schematic diagrams showing possible interactions of LDH nanoparticles with IB through electrostatic interactions between -COO$^-$ groups along the IB chain and the positive charges on the LDH surface.

Figure 2.9 Schematic representation of (A) Fluorescent images of dissected organs from a mouse sacrificed after i.v. injection of Cy5.5-labeled LDH–NH$_2$, LDH–NH–PEG5000 and LDH–NH–COOH for 3 h. (B) in vivo T1-images from a SD rat scanned at different time intervals of post-injection (dose: 3.1 mg or 197.1 mmol Gd/kg). (C) In vivo PET imaging in 4T1 tumour-bearing mice shows stronger signal with ^{64}Cu-LDH-BSA. (D) CT (a) and T1-weighted MR images (b) of tumour after intravenous injection LDH-Gd/Au-heparin (dosage: 72.4 mg Au/kg for CT imaging ; 3.0 mg or 190.8 mmol Gd/kg for MR imaging) in 4T1 murine breast tumour-bearing mice for 0 h, 1 h and 4 h.

Figure 3.1 Schematic illustration of LDHs synthetic process.

Figure 3.2 Schematic illustration of LDH nanoparticle coating with BSA coating (Step A) and subsequent GTA crosslinking (Step B).

100 µl of the theoretic amount for quantitative cross-linking of the 59 amino groups in the BSA molecule were employed.

Figure 6.4 The blood-retinal barrier as a model for BBB was used to evaluate the ligands modified LDHs and unmodified LDHs retention time.

Figure 6.5 The biodistribution and fluorescence intensity of NPs, Ang2-NPs and RVG-NPs in the major organs.

Figure 6.S1 Flow cytometry analysis of Cy3 labelled nanoparticles uptake by bEnd.3 cells following incubation with Ang2-NPs/NPs (A) and RVG-NPs/NPs (B) with different ligands density for 2 h.

Figure 6.S2 ICON results of BSA-FITC (A), Ang2-NPs (B) and RVG-NPs (C) after i.v. injection of the nanoparticle formulations with molar ratio of BSA: BSA-ligands at 49:1, (D) Plot of fluorescence intensity in each timepoint based on FITC signal.

Figure 7.1 (A) Particle size distribution; and (B) FTIR spectrum of Mn-LDH nanoparticles; XPS of Mn-LDH nanoparticles for survey (C) and Mn 2p (D);

Figure 7.2 TEM (A) and SEM (B) images of Mn-LDH nanoparticles (scale bar = 200 nm); Elemental mapping of Mn (C), Al (D) and O (E) in Mn-LDHs, and the merged image (F) (scale bar = 50 nm).

Figure 7.3 Cell viability of N2a cells after treated with Mn-LDHs at concentrations from 0 to 500 μg/ml.

Figure 7.4 Histogram showing the percentage of N2a cells internalizing dsDNA-Cy3 in three cases (40 nM dsDNA-Cy3) for 4 h, measured by flow cytometry.

Figure 7.5 Fluorescence microscopic images showing N2a cells treated with DNA-Cy3 or DNA-Cy3/LDH for 4 h.

Figure 7.6 MTT assay on the viability of N2a cells treated with free CD-siRNA at 40 nM and CD-siRNA/LDHs at the CD-siRNA concentration range from 5 to 40 nM for 72 h at 37 ℃.

Figure 7.7 T_1 (A) and T_2 (B) weighted MR images; and T_1 (C) and T_2 (D) relaxivity of LDHs depending on pH 6.0 (1-7) and pH 7.4 (1'-7') and Mn concentration (1, 1': 0.015 mM; 2, 2': 0.031 mM; 3, 3': 0.063 mM; 4, 4': 0.125 mM; 5, 5': 0.25 mM; 6': 0.50 Mm; 7':1.00 mM).

Figure 7.8 T_1 weighted MR images (A) and T_1 relaxivity (B) of N2a cells treated with corresponding amount of Mn-LDHs from 0 to 21.6 μg/ml. (1: 0. μg/ml; 2: 2.7 μg/ml; 3: 5.4 μg/ml; 4: 10.8 μg/ml; 5: 21.6 μg/ml ;).

List of Abbreviations used in the Thesis

LDHs: layered double hydroxide nanoparticles   RES: reticuloendothelial system

BBB: blood-brain barrier   PEG: polyethylene glycol

DOX: doxorubicin   BSA: bovine serum albumin

DNA: deoxyribonucleic acid   GTA: glutaraldehyde

CME: clathrin-mediated endocytosis   Ang2: angiopep2

siRNA: small interfering RNA   FDA: food and drug administration

DMEM: dulbecco's Modified Eagle's Medium   PBS: phosphate buffered saline

DAPI: 4'-6-diamidino-2-phenylindole   FITC: fluorescein-5-isothiocyanate

PFA: paraformaldehyde   TEM: transmission electron microscopy

SEM: scanning electron microscopy   PAMAM: polyamidoamine

Cy3: cyanine 3   FACS: fluorescein-activated cell sorting

XPS: X-ray photoelectron spectroscopy   DLS: dynamic light scattering

MFI: mean fluorescence intensity   ZP: zeta potential

3D: three-dimensional   FCS: fetal calf serum

CLSM: confocal laser scanning microscopy   nAchR: nicotinic acetylcholine receptor

RVG: rabies virus glycoprotein peptide   GBM: gliboblastromaMultiforme

MEN: meningiomas   CD-siRNA: cell Death siRNA

PNAs: peptide nucleic acids   ODNs: antisense ligonucleotides

5-FU: 5-Fluorouracil   HS-tk: herpes simplex thymidine kinase

AS: astrocytoma

NB: neuroblastoma

MET: metastatis

Dox: doxorubicin

CSF: cerebrospinal fluid

MRI: magnetic resonance imaging

AMT: adsorptive-mediated transcytosis

CPPs: cell-penetrating peptides

CED: convection-enhanced delivery

PLA: poly (lactic acid)

EPR: enhanced permeability retention effect

PGA: poly (glycolic acid)

PLGA: poly (lactic-co-glycolic acid)

PEO: poly (ethylene oxide)

NIR: near-infrared fluorescence dye

CT: computed tomography

PET: positron emission tomography

T1: longitudinal relaxation time

IONP: iron oxide nanoparticles

T2: traverse relaxation time

EGFR: epidermal growth factor receptor

PAA: polyacrylamide

RH: raloxifene hydrochloride

NAA: α-naphthaleneacetate

EDS: energy-dispersive X-ray spectroscopy

DFUR: doxifluridine

CPT: camptothecin

TLR: toll-like receptor

APTES: (3-aminopropyl)triethoxysilane

OVA: ovalbumin

SiO$_2$@LDH: SiO$_2$ nanodot coated LDHs

IB: Intimin β

SPECT: single-photon emission

XRD: powder X-ray diffraction

MW: molecular weight

FA: flip angle

TOF: time of flight mass spectrometer

XPS: X-ray photoelectron spectroscopy

MTX: methotrexate

BRB: blood-retina barrier

Pgp: P-glycoprotein

SSC: Side scatter

EMSA: electrophoretic mobility shift assay

FSC: forward scatter channel

ICON: In vivo confocal neuroimaging

Pdi: polydispersity index

CNS: central nervous system

CCD: charge coupled device

RISC: RNA-induced silencing complex

mRNA: messenger RNA

ROS: reactive oxygen species

GSH: glutathione

FR-FSE: Fast-recovery spin-echo

FOV: field of view

NSF: nephrogenic systemic fibrosis

LRP: low-density lipoprotein receptor-related protein

SPIONPs: superparamagnetic iron oxide nanoparticles

MALDI: Matrix-assisted laser desorption/ionisation

MTT: 3-[4,5-dimethylthiazol-2-yl]-2,5-diphenyl tetrazolium bromide

PID1: phosphotyrosine Interaction Domain containing 1; NYGGF4

Mn-LDHs: manganese-based layered double hydroxide nanoparticles

ATR-FTIR: attenuated total reflectance -Fourier transform infrared spectroscopy

Chapter 1

Introduction

1.1 Significance of the project

At the moment there are no effective non-toxic particle carriers for diagnostic agent and new drug delivery to the brain cancer.[1,2] Layered double hydroxide (LDH) nanoparticles (NPs) have great potential as a drug delivery and imaging system.[3-6] However, two major hurdles remain before they can be used for this purpose. LDHs aggregate once upon exposure to the bloodstream and the blood-brain barrier (BBB) prevents the passage of most molecules and particles from the blood into the brain.[7, 8] The goal of this project is to overcome these obstacles using novel nano-engineering strategies to prevent LDHs aggregation and enhance their passage across the BBB. In this project we will develop next-generation LDH nanoparticles that are able to act as Trojan horses to carry drugs into the brain and simultaneously provide imaging capacity for therapeutic efficiency prediction.

Ideally, one would like to administer LDH-based drugs via the intravenous route. Unfortunately, LDH aggregation and rapid clearance from the bloodstream have limited this approach, thus improvement in the suspension stability is necessary.[9, 10] This project aims to use a facile way to engineer LDH nanoparticles with improved colloidal stability and BBB penetration ability as well as imaging capability. Therefore, the significance of this project is the development of efficacious LDH formulations that are suitable for intravenous injection and are able to efficiently penetrate the BBB. Moreover, understanding the surface engineering of LDH NPs will provide essential insights into the design and development of many other NP-based drug delivery systems. Any advancement in the specific aspect would produce huge scientific, social and economic impacts. Of further significance is the development of an effective delivery system for siRNA, thereby allowing RNA interference to realise its therapeutic potential.

1.2 Research objectives and scope

The leading goal of this research is to establish a stabilised LDH nano-composite platform by gaining insights into LDH surface functionalisation and doping element Mn into LDHs for brain tumour targeting and imaging performance. This thesis does not only develop a facile approach to surface modifying nanoparticles with the novel hierarchy, but also provides some guidelines in designing multifunctional nanoparticle-based platform for various biomedical applications.

The objectives of this project are specified as follows:

1) To enhance LDH suspension stability and redispersion capability through cross-linking albumin coated on LDHs;

2) To improve cellular uptake of LDH NPs by U87 glioma cells and neuroblastoma N2a cells through conjugating targeting ligand (Ang2 or RVG) via surface-coated albumin;

3) To confirm the increased BBB penetration of ligand modified-LDHs in the in vitro and in vivo models;

4) To develop dual-functional Mn-containing LDHs for simultaneous brain magnetic resonance imaging and siRNA delivery.

1.3 Thesis outline

This thesis is written according to the guidelines of the University of Queensland. The outcomes of this PhD thesis are presented in the form of journal publications. The chapters in this thesis are presented in the following sequence.

Literature on recent advances in brain cancer diagnostic/treatments is comprehensively reviewed in Chapter 2. Nanoparticle-based systems for brain accumulation and targeting, especially the current strategies to engineer LDH nanoparticles as effective delivery/imaging system are reviewed in details. In Chapter 3, the strategies and approaches utilised in the whole PhD project are summarized, including material synthetic methods for layered double

hydroxide nanoparticles and surface modification, and the techniques for material characterisations and biology experiments.

One of the key challenges for nanoparticles to be used as the delivery and imaging system for in vivo application is their colloidal stability. Therefore, Chapter 4 presents our surface modification of LDH NPs, i.e. BSA coating and further GTA crosslinking, the enhanced colloidal stability regardless of dilution times and solutions (e.g., PBS) and the improved redispersion capability. This modification does not affect the delivery efficiency and in vitro cytotoxicity to either normal cells or cancer cells. The new strategy therefore provides a much more effective method to prevent LDH nanoparticle aggregation and improve LDH nanoparticle dispersion for usage in a wide variety of bio-applications in vitro and in vivo.

Active targeting is supposed to increase the therapeutic index. Therefore, Chapter 5 describes the details of conjugating two brain tumour targeting ligands (Ang2 and RVG) onto LDHs and subsequent targeting tests. It is known that Ang2 and RVG ligands are able to target to low density lipoprotein (LRP) receptors and nicotinic acetylcholine receptors (nAchR) that are expressed on U87 and N2a cells, respectively. Ligands are conjugated to the LDHs through inter-matrix bovine serum albumin (BSA), rendering the LDHs simultaneously excellent colloidal stability and targeting ability. Such modification is reproducible with narrowly batch to batch variation. In vitro studies have demonstrated higher cellular uptake efficiency for ligand conjugated LDHs compared to unmodified LDHs. This new approach may contribute to rationally design of targeted nanoparticles, showing great potential as a promising platform for selective and effective therapeutic treatment of neural diseases.

Chapter 6 further presents our examination of the brain targeting ability of ligand-modified LDHs through in vitro and in vivo models. LDHs labelled with fluorescent markers and targeting ligands (Ang2 and RVG) are significantly taken up by endothelial cells and much more quickly penetrate through the simulated BBB constructed with the endothelial cells in comparison with non-targeted LDHs. The in vivo model also reveals that Ang2 modified LDHs demonstrated better brain accumulation ability compared to RVG modified LDHs and non-targeted LDHs. This work implies that ligands have different affinity towards receptor-expressed cells, and thus smart selection of ligands is able to achieve greater efficacy.

Currently, the nanoparticle-based systems have come to a multifunctional era. Thus Chapter 7 reports a new dual functional manganese-based layered double hydroxide nanoparticles (Mn-LDHs) as an effective anticancer drug (Cell Death siRNA (CD-siRNA)) delivery system and

biological T1-weighted magnetic resonance imaging (MRI) modality for cancer theranostics. The newly designed system shows simultaneously highly effective bimodal imaging and gene delivery for brain cancer diagnosis and therapy.

Chapter 8 finally presents our general discussion of the work in this thesis and the outlook for the future work, as a conclusion of this thesis.

1.4 References

1. Koo, Y.-E. L.; Reddy, G. R.; Bhojani, M.; Schneider, R.; Philbert, M. A.; Rehemtulla, A.; Ross, B. D.; Kopelman, R., Advanced drug delivery reviews 2006, 58 (14), 1556-1577.

2. Pardridge, W. M., NeuroRx 2005, 2 (1), 3-14.

3. Liu, Z.; Ma, R.; Osada, M.; Iyi, N.; Ebina, Y.; Takada, K.; Sasaki, T., Journal of the American Chemical Society 2006, 128 (14), 4872-4880.

4. Xu, Z. P.; Kurniawan, N. D.; Bartlett, P. F.; Lu, G. Q., Chemistry–A European Journal 2007, 13 (10), 2824-2830.

5. Desigaux, L.; Belkacem, M. B.; Richard, P.; Cellier, J.; Léone, P.; Cario, L.; Leroux, F.; Taviot-Guého, C.; Pitard, B., Nano letters 2006, 6 (2), 199-204.

6. Xu, Z. P.; Niebert, M.; Porazik, K.; Walker, T. L.; Cooper, H. M.; Middelberg, A. P.; Gray, P. P.; Bartlett, P. F.; Lu, G. Q. M., Journal of Controlled Release 2008, 130 (1), 86-94.

7. Zuo, H.; Gu, Z.; Cooper, H.; Xu, Z. P., Journal of colloid and interface science 2015, 459, 10-16.

8. Gu, Z.; Zuo, H.; Li, L.; Wu, A.; Xu, Z. P., Journal of Materials Chemistry B 2015, 3 (16), 3331-3339.

9. Sarparanta, M.; Bimbo, L. M.; Rytkönen, J.; Mäkilä, E.; Laaksonen, T. J.; Laaksonen, P. i.; Nyman, M.; Salonen, J.; Linder, M. B.; Hirvonen, J., Molecular pharmaceutics 2012, 9 (3), 654-663.

10. Wu, L.; Zhang, J.; Watanabe, W., Advanced drug delivery reviews 2011, 63 (6), 456-469.

Chapter 2

Literature Review

This chapter reviews the advances in the nanoparticles-based medications for brain cancer therapy and imaging, beginning with an introduction of inhibitory biomolecules for the brain cancer treatment. Therapeutic chemotherapeutic drugs and genetic molecules as promising medications for brain cancer therapy will be introduced in details in this section. The existence of BBB as a major challenge of brain tumour treatment is subsequently interpreted. The current therapeutic strategies including invasive local delivery methods and systemic treatments, and advances in nanoparticle-based theranostic strategies for brain tumour will be then summarized. In specific, the engineering of layered double hydroxide (LDH)-based nanoparticles will be systematically described. Finally, a summary of current state-of-the-art technologies and challenges to fabricate bio-applicable LDHs for BBB passage are provided, and the basic research strategies for this thesis are outlined.

2.1 Brain tumour and inhibitory biomolecules

2.1.1 Brain tumour

Brain serves as a control centre of the nervous system, which is responsible for speech, memory, intelligence and movement, and precise functions for coordination and regulation of many organs.[1] Problems, such as loss of brain cells, lead to stroke that can affect the ability to think clearly while inflammation in the brain can cause vision loss, weakness and paralysis. There are many brain diseases happening to people with age-related neurodegenerative conditions, such as Alzheimer's disease, Parkinson's disease and stroke.[2] Some brain diseases like brain tumours may press on the adjacent nerves and interfere with normal brain functions. Some brain diseases are neurogenic diseases such as Huntington's disease and muscular dystrophy, some other diseases like spinal cord and head injury belong to trauma. Depending on the specific problems, the symptoms of brain diseases vary widely. Some damages are permanent while sometimes, treatments such as medicines, surgery, or physical therapy can cure or at least weaken symptoms.[3, 4] This thesis will involve in the brain tumour study.

Tumour can be defined as tissues that grow in an undisciplined manner other than normalised growth. Brain tumours can be classified as two categories, namely benign and malignant cancer, depending on the tumour phase. The periphery margin of benign cancer is easy to be identified, therefore, it is easy to be removed and there is rare recurrence. However, the malignant brain cancer is composed of cancerous cells which invade and infect the surrounding healthy part of brain. Such a spread of malignant cancer to the border of the other tissues is called metastasis. Classified by different original area, neuroblastoma, glioblastoma, meningioma and astrocytoma can be categorised into the primary brain tumour. Metastasis tumours originated from cancers such as breast cancer or melanoma are classified into secondary brain tumour.[5] Of all the primary brain cancer, the glioblastomas account for 40% while neuroblastoma is a common solid tumour derived from primitive cells of the sympathetic nervous system.[6] This thesis will involve in the study of glioblastomas and neuroblastoma. As an essential complex and interconnected network, brain is able to balance regional segregation and functional specialisation with strong integration. However, the devastating results can happen when the brain tumour occur. Due to the intrinsically persistent severity and infiltrative nature, treatment of both primary and metastatic brain tumours remain as a formidable challenge.[7]

2.1.2 Inhibitory biomolecules as potential brain tumour therapeutics

Inhibitory biomolecules including gene-based and chemotherapeutics have been widely applied in the tumour treatment at the moment. Brain tumours induced by hereditary genetic factors with aberrant proteins expression imply a potential gene therapy by targeting and suppressing the mutant proteins at the gene expression level.[8] Abundant research work has been conducted on the use of antisense oligonucleotides (ODNs), peptide nucleic acids (PNAs) and more recently, small interfering RNA (siRNAs) as potential therapeutics.[9,10] Complementarily, chemical substances such as 5-Fluorouracil (5-FU), Doxorubicin (Dox) and paclitaxel based chemotherapy are also employed for brain cancer treatment, aiming to kill the cancer cells, thereby prolonging patient's life and reducing the disease symptoms.[11]

2.1.2.1 Gene-based drugs

Gene therapy now is applied as a new treatment for neurodegenerative diseases or brain cancers to target the specific disease area where the encoded protein will be produced or the mutant protein will be knocked down. The transferred gene could also correct a mutation or encode a protein with therapeutic function.[12] Several reports have successfully used the gene to treat brain cancer. Asgharzadeh et al. reported that the PID1 (Phosphotyrosine Interaction Domain

containing 1; NYGGF4) has tumour inhibition function in glioblastomas.[13] Retroviral vector with herpes simplex thymidine kinase (HS-tk) gene insertion is produced by murine fibroblasts. The vectors were intratumoral stereotaxic injected into rats planted with cerebral glioma, with the aid of anti-herpes drug ganciclovir at 5 days, gliomas were found to regress completely.[14] Despite the encouraging results, the degradation of the naked gene by serum nucleases has intensively limited its clinical application once upon exposure to the blood after administration injection. Responding to the insufficiency in therapeutic delivery, many research efforts have recently made on the exploration of new strategies to offer more effectively gene delivery to the central nervous system (CNS).[15] In this thesis, a cell death siRNA (CD siRNA) which is believed to have the ability to kill cancer cells in some way was employed.

2.1.2.2 Chemotherapeutic drugs

Several chemotherapeutic drugs are used to treat brain cancers. Dox is one of the most widely used anticancer agents. Studies of free Dox find efficient inhibition of the malignant brain tumour growth when injected directly into the brain tumour site.[16] Delivery system like liposomes encapsulating Dox shows enhanced accumulation in the brain tumour with increased life span.[17, 18] Paclitaxel is another kind of hydrophobic chemotherapeutic drugs used for brain tumour treatment.[19] The systemic treatment by paclitaxel is always not sufficient enough for cancer cure, therefore, a lot research is focused to encapsulate paclitaxel into microspheres for localised delivery to brain tumour.[20] Cell cycle and cytotoxicity studies of paclitaxel to C6 glioma cells show that the cells are inhibited in G2/M phase and increased cytotoxicity compared with control group is observed.[21, 22] In addition, the other chemotherapeutic drugs used for brain tumour treatment including the camptothecin and temozolomide are not so popular, but also investigated.[23, 24] Hydrophilic 5-FU belongs to anti-metabolic drugs, working through irreversible inhibition of thymidylate synthase.[25, 26] An investigation by using the combination of 5-FU with hyperbaric oxygen for treating malignant tumours has found that the concomitant hyperbaric oxygen enhanced the antitumor effects of 5-FU by reducing the tumour volume more than one time.[27] Clinical phase I trial of 5-FU formulations for glioma treatment by Menei with 10 patients was performed, and the overall median survival was 40 weeks, with 2 long-term survivors (71 and 89 weeks).[28] These results clearly indicate that the chemotherapeutic drugs are useful for brain tumour treatment in some situations.

2.2 Blood brain barrier: a challenge in the brain tumour treatment

2.2.1 History

The first hint of BBB existence was shown when a bacteriologist Paul Ehrlich using chemical dyes to stain biological structures by microscope. All the organs can be stained except the brain area after intravenous administration. At that time, it was attributed to the brain that has a low affinity for the dye. Then later in 1913, Edwin Goldmann performed an experiment, in which he injected the dye directly to the cerebrospinal fluid (CSF) rather than the vein. He found that the brain was stained but the rest of the tissues were not. In this case, he claimed that there was something acting as a barrier to separate the CSF and blood. However, due to the lack of an advanced technique for observing the existence of the barrier, this concept has only widely accepted after the employment of the scanning electron microscope to medical research.[29]

2.2.2 Structure
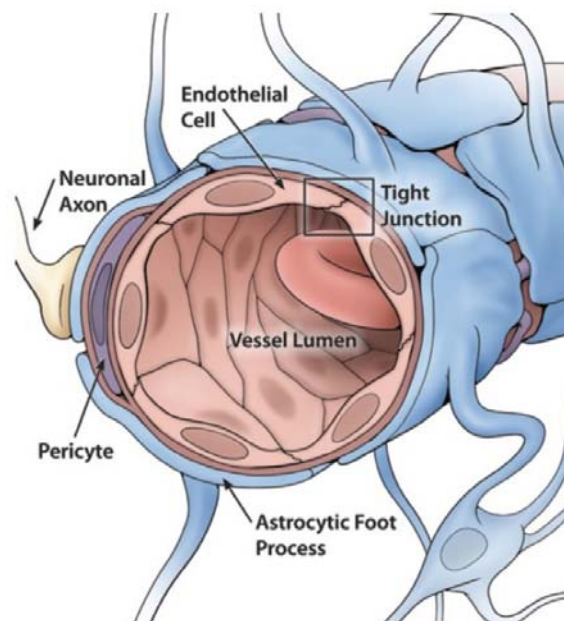
Figure 2.1 Barriers to CNS access. The neurovascular unit is composed of the endothelial lining, the basal lamina, ensheathed pericytes and astrocytic endfeet.[30]

The necessary of maintaining central nervous system homeostasis prompts the BBB to develop into a strictly complicated interface between the blood and the CNS. The BBB is mainly formed by the cerebral endothelial cells along the brain and spinal cord capillaries, connected by tight continuous junctions and surrounded by a series of perivascular cells including smooth muscle

cells, pericytes, microglial cells and astrocytes (Figure 2.1).[31, 32] In this way, the central nervous system is separated from the peripheral environment and can be protected from the fluctuations action of compounds transporting into or out of the periphery, thereby decreasing the interference to neuronal exchange to a larger extent. Protecting the neurons within the brain and spinal cord is the main element that facilitates BBB evolution. Not all the creatures own such a complicated BBB structure, apart from the advanced nervous system creatures. Cuttlefish has an intermediate level of BBB participating with pericytes in the development of barrier in big veins. Insects, molluscs and fish have the lower BBB evolution, and their barriers are only formed by glial cells.[33-35] Ionic homeostasis maintenance is treated as the most significant consequence of the BBB development. Creatures with a higher level of homeostasis maintenance in the interstitial medium of the cerebrospinal fluid possess a much advanced evolutionary level.[36]

2.2.3 Possible transportation ways across the BBB
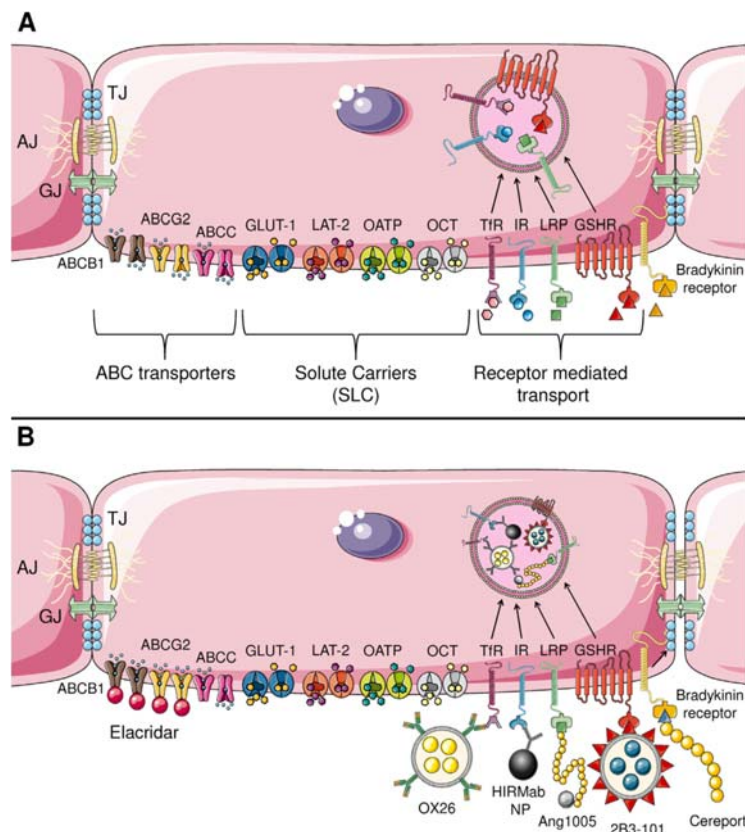
Figure 2.2 Therapeutic brain delivery strategies that target the physiological make-up of the BBB. (A) Transport mechanisms though the BBB. (B) A wide range of receptors that mediate transport through transcytosis.[37]

The existence of BBB selectively allows free passage of molecules such as water, O_2, CO_2 and small hydrophobic substances that are crucial to neural functions. However, vast majority of substances that are useful for brain tumour therapy or diagnostic are characterised to possess low BBB permeability.[38, 39] In an attempt to functionally access the BBB, it is necessary to comprehensively understand the intrinsic BBB features and meanwhile combine with the possible transport routes in a full-scale. The transcellular route plays a much important role in the delivery of different substances such as peptides, antibodies and siRNA through the BBB. These routes consist of paracellular aqueous pathway, carrier-mediated transport, receptor-mediated transcytosis and adsorptive-mediated transcytosis (Figure 2.2A).[40]

2.2.3.1 Passive diffusion into brain

BBB permeability through passive diffusion of compounds is associated with their lipophilic properties. Many lipid-soluble molecules and gaseous molecules such as O_2 and CO_2 can diffuse though the BBB and enter the brain passively, hence compounds of greater lipophilicity generally show higher permeability. However, these molecular and physicochemical factors are not always absolute elements for CNS penetration. In contrast, there are many examples of effective therapeutic CNS drugs that are lipophilic but not BBB-permeable. Sometimes, the solutes with positive charge is considered probably to be able to interact with the negatively charged cell membrane, which facilitates their entry through the BBB.[41]

2.2.3.2 Adsorptive-mediated trans-BBB delivery

Adsorptive-mediated transcytosis (AMT) provides a means for brain drug delivery through electrostatic interactions between cationic molecules and anionic cell membrane of the brain capillary endothelial cells. AMT-based drug delivery to the brain can be achieved using cationic proteins or basic peptides such as cell-penetrating peptides (CPPs) as the ligand. Large therapeutic molecules such as peptides and proteins can be transported across BBB to brain parenchyma through AMT.[42]

2.2.3.3 Transporter-mediated trans-BBB drug delivery

A wide range of solutes and drugs such as glucose, amino acids, purine bases, nucleosides and choline have a much lower CNS entry rate. It is because these substances and many of their metabolites are able to be actively effluxed from the brain by ABC transporter (ATP-binding cassette) family.[31] Among energy-dependent transporters, P-glycoprotein (Pgp) is one of typical member and displays recognition specificity towards hydrophobic substrates. The

major role of the ABC transporters in the BBB is to function as active efflux pumps consuming ATP and transport a diverse range of lipid-soluble compounds out of CNS. In other words, they remove potential neurotoxic endogenous or xenobiotic molecules from the brain and carry out a vital neuroprotective and detoxifying function.[43] In this way, the brain penetration of drugs that are substrates for these ABC efflux transporters is significantly reduced by this transport activity.

2.2.3.4 Receptor-mediated transcytosis

A series of receptors expressing on the BBB provide possible active targeting through ligand-receptor, antigen–antibody and other forms of molecular recognition to a specific location (Fig. 2B).[44] Receptor-mediated transcytosis could increase penetration rate and reduce potential side effects.[45]

One example of large molecule drugs that have shown promising clinical results are the angiopeps, the receptor of which is low-density lipoprotein receptor (LRP) that ubiquitously expressed on BBB cells. Among the ligands for LRP, Angiopep-2 (Ang2) shows a higher brain penetration capability than other proteins of LRP-related family and most other proteins that target to the BBB, such as aprotinin and transferrin.[46, 47] Moreover, Angiopep-2 is proven to be a dual-functional ligand for brain tumour-targeting, which is also overexpressed on glioma cells.[48] Nicotinic acetylcholine receptors (nAChRs) are widely expressed in the BBB and neurons that located in various parts of the central nervous system. A 29 amino-acid short peptide derived from the rabies virus glycoprotein (RVG) is applied as another dual targeting ligand for brain as RVG can bind to acetylcholine receptors.[49] In addition, lactoferrin, transferrin and insulin are also reported to have great potential in targeted drug delivery across the blood brain barrier.[50]

2.2.4 Summary

Treatment of brain cancers remains as a challenge due to the BBB and potential inefficient drug concentraiton. As a brief conclusion, the receptor-mediated transcytosis strategy for overcoming BBB holds great potential for highly improved drug delivery towards brain. Due to the dual targeting ability of Ang2 and RVG peptide towards brain cells, they were selected for the brain targeting work in this thesis.

2.3 Therapeutic strategies for brain

Due to the infiltrative nature of primary brain tumours and the rigorous BBB features, it is extremely hard to diagnose and treat the brain tumour, and advanced techniques are required to improve the therapeutic outcomes towards this devastating disease. During the last decades, numerous strategies have been investigated for improved drug delivery to the dreadful brain tumours and overcome the BBB (Figure 2.3). There are invasive and non-invasive techniques that are not maturely developed for brain tumour treatment.[51] In this section, the pitfall and potential of current methodologies will be briefly discussed. Nanoparticle-based strategy that are used to deliver a spectrum of chemotherapeutic, diagnostic and imaging agents for various applications will be intensively interpreted.[52]
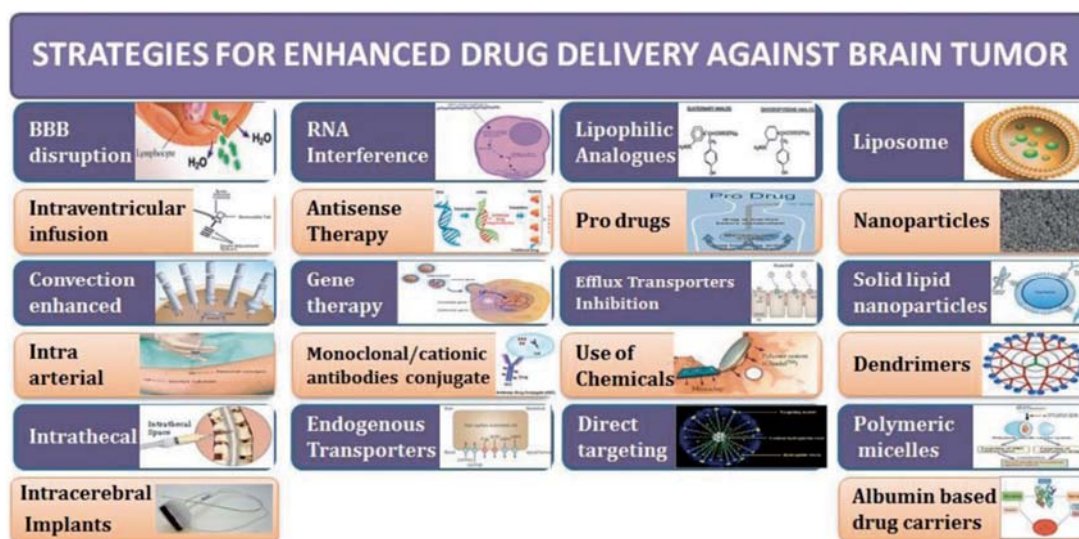
Figure 2.3 Strategies for enhanced drug delivery against brain tumour.[53]

2.3.1 Invasive local delivery methods

To mediate the direct drug administration to brain parenchyma, local delivery methods include the convection-enhanced delivery, gliadel wafers, osmotic BBB disruption and ultrasound-induced BBB opening have been investigated. These methods have the potential benefit of decreasing systemic toxicities and overcoming the lack of BBB permeability.[53, 54]

Convection-enhanced delivery (CED) uses the implanted infusion catheters that allows continuous drug delivery during surgery. A hydrostatic pressure gradient via convective flow through the parenchyma enables the drugs to reach all the tumour cells.[55] Gliadel wafers are implantable polymer wafers placed at the tumour resection site. Due to the high cost, gliadel

wafers are rarely used. Both of these two techniques are confronted by the problems that drugs are washed away in the systemic circulation which is known as sink effect.[56] The hyperosmolar agent mannitol is another option for brain malignancies treatment. By injecting mannitol solution in advance to the carotid artery, the inner and outer brain pressure environment maybe changed due to the administration of hypertonic solution which leads to alteration of BBB structure. After a period of 30 seconds, administering antitumor compounds to the same artery through the same method, the BBB passage ability of compounds are greatly increased.[57] It is reported that the antitumor agents in brain were increased by 3 to 20 times while the penetration ability was increased by 2 to 6 times in the existence of mannitol. However, side effects are accompanied with this method, and injection with mannitol causes apoptotic in the brain relevant cells as a result of the tiny transformation in the central nervous system. A high concentration of this foreign substances may even make the patients convulsive and decrease their cognitive ability.[57, 58] Transient physical modulation of the BBB also attracts much attention. One popular technique is ultrasound which could increase paracellular distance and increase passive diffusion of hydrophobic agents by reducing the efflux transporters capacity.[59, 60] Some common issues arise from BBB transient disruption still severely limits its widely usage, including artificial complexity, immature technology, potential of pernicious tumours or products invasion from BBB to peripheral tissues. Apart from these challenging problems, evaluation of the BBB transit efficiency is another issue that needs consideration.[61]

All above mentioned methods offer some improvements of the treatment outcomes. Obviously, in the other side, all these invasive treatments are associated with complications that we cannot ignore. Although combining different strategies may use their strength, these techniques need to be intensively improved and promoted to reach an acceptable drug accumulation concentration for the remedy of brain diseases. Besides, due to lack of protective shield, these techniques also tend to easily lose drug activity. In addition, the healthcare costs of treatments are likely to be enormous in the long recovery period.[51]

2.3.2 Systemic treatment strategies

In systemic therapy, drugs are delivered either orally or intravenously as well as via the olfactory route, while adequate delivery to the brain relies on BBB penetration. This type of therapy is less invasive, however, the drug concentration at the brain disease site often falls to sub-therapeutic levels due to the restriction of BBB, plaguing by the fact of offsite toxicity. In general, for enhanced brain accumulation, the drugs should either be able to overcome the

efflux transporters or take advantages of innate influx transporter systems expressed at the BBB. For inhibiting the efflux transporters, it is achievable through chemical modification to reduce their efflux liability. A typical studies of efflux transporters inhibition were performed through engineering the efflux substrate GNE-317 with less substrate activity, and finally GNE-317 was found to be uniformly distributed throughout tumour and normal brain regions.[62] Receptor-mediated transcytosis and transporter-mediated trans-BBB drug delivery are two methods that mediate active transport.These two methods are able to take advantages of innate influx transporter systems expressed at the BBB for systemic brain cancer treatments.[63]

2.3.3 Nanotechnology-based strategy

The research about nanoparticle is currently a field of great interest for applications in biomedical, optical materials and electronic devices. Nano-carriers are delivery systems that range from 1 to 100 nm (not strictly to 500 nm) and can be fabricated from all sorts of substances, including lipids, inorganic salts, polymers and carbon nanotubes (Figure 2.4).[64,65,66] Among these nano-carriers, layered double hydroxide nanoparticles are the focus of this thesis and used throughout the research.

Traditionally, enhanced permeability and retention (EPR) effect with vascular leakage is always expected to benefit for drug penetration into tumour area, however, EPR effect is not applicable for brain metastases as vascular defect is not exist in such an area.[67] Achieving an adequate "targeted bioavailability" to the brain is essential in the treatment of brain tumours. A promising way to deliver drugs to the targets within the CNS is through active targeting nanoparticles-based system.[68, 69] The goal of the present review is to highlight the recent findings concerning this strategy. The use of nanoparticles for imaging is also within the scope of the review. Moreover, nanoparticle-based brain tumour treatment could be combined with other BBB circumvention strategies to achieve the best therapeutic outcome.
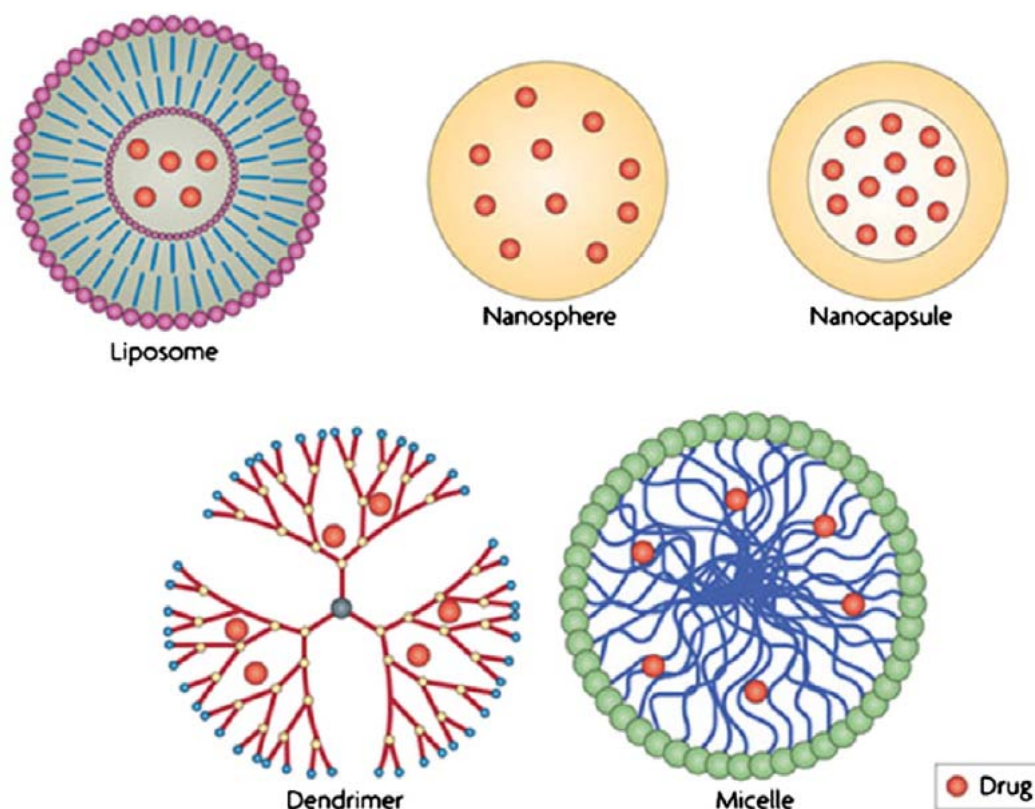
Figure 2.4 Schematic structure of different nanocarriers (liposomes, polymeric nanoparticles including nanospheres and nanocapsules, dendrimers, and micelles) for drug delivery to the brain tumour.[70]

2.3.3.1 Polymeric materials and micelles

A polymer is large molecular mass material constituted by multiple repeated monomers and is made via polymerization of these monomers. Large molecule or macromolecule containing a wide variety of properties can be plastics such as polystyrene or derives from natural biopolymers such as nucleic acid or proteins that possess biological structure and function.[64]

The far-ranging original materials used for polymer synthesis render these polymers many specific physical properties such as tenacity, viscoelasticity, semicrystallinity and biological functions.[71] Many researches have been done to examine the potential of polymers as candidates in biological area, especially polyesters, including poly (lactic acid) (PLA), poly (glycolic acid) (PGA) and their copolymer poly (lactic-co-glycolic acid) (PLGA).[72]

A micelle is composed of amphiphilic surfactant molecules or large amphiphilic block copolymers that are self-assembled in water into a structure of spherical vesicle with a

hydrophobic core and a hydrophilic exterior. Hydrophobic core in the centre of micelle allows the micelle to carry and protect hydrophobic drugs until they are released by some drug delivery mechanism while the hydrophilic surface shields the micelles from the instant recognition by the immune system and subsequent clearance. Traditional micelles are formed by the hydrocarbon portion of long fatty acids, with a polar or hydrophilic or charged head group and a hydrophobic tail. The size of micelles is often less than 100 nm and determined by the component size and geometrical features. Polymers have variable hydrophilic and hydrophobic features and can form micelles in water.

The most famous copolymer is PEO (poly (ethylene oxide))–PPO (poly (propylene oxide))–PEO with the trade names of Pluronic® and Poloxamer™. Drug delivery by micelles is ubiquitous and has been undergoing a long history. Block copolymer micelles conjugated with cell-penetrating peptide promote brain targeting delivery and thus have attracted a lot attention.[73, 74] Angiopep-2 conjugated PEG-PLA micelles were prepared by film hydration method. Near-infrared (NIR) fluorescence dye, DiR was loaded into micelles to evaluate the brain-targeting ability of micelles by fluorescence imaging in vivo and ex vivo. Compared with the micelles without ligand modification, significant NIR fluorescent signal was detected in the brain after angiopep-anchored micelle administration. Further the whole brain and brain slice imaging confirmed the observations. The angiopep-PEG-PLA micelles show high brain accumulation for up to 24 h after intravenous administration in mice. These results indicate that angiopep-modified PEG-PLA micelle is a promising brain-targeting nanocarrier for lipophilic drugs.[75]

2.3.3.2 Liposomes

Liposomes are applied in drug or gene delivery for a long period, which is comprised by amphiphilic molecules with polar and nonpolar components. In the 1960s, liposome platforms were first well-established for managing the therapeutic and imaging agents. Only until 1973, the potential of liposomes as nano-scale delivery vehicle has been investigated by Gregorialdis.[76] Since then, an explosion research on the nano-scale liposomes has been conducted due to their comparable simple preparation, non-immunogenic, high biocompatible and relatively low cost. All these features have confirmed the indisputable status of liposomes as a drug delivery vehicle. Generally, liposome is formed by phospholipids that generate unilamellar or multilamellar lipid bilayer structures under various technological conditions, surrounding by an internal aqueous core. Practically, liposomes components are varied with

amphoteric ionic, anionic and cationic lipid, therefore, the surface charge can be adjusted through balancing a different amount of the lipid. In the drug delivery field, the self-assembly liposomes are attractive because their amphiphilic feature give them superiority to encapsulate hydrophilic agents in the aqueous core or the hydrophobic molecules in the lipid bilayer. Therefore, the therapeutic drugs can be protected to keep their bioavailability. Given the assemblable structure and the phospholipids composition, liposomes have become an incontrovertible choice at one time.[77]

However, there are many controversies as liposomes are unstable and easily to be captured by the reticuloendothelial system (RES) when the surface is coated by opsonisation proteins after intravenous administration into the bloodstream. Moreover, liposomes may be dissolved due to electrostatic, hydrophobic and other forces, and thus the system stability needs to be improved and many methods have been applied to address these problems. Some work has demonstrated that conjugated lipids with PEG tethers can increase liposome stability, allowing the liposomes to circulate for many days by reducing opsonin adsorption and avoiding rapid clearance by RES. Besides an increase in the duration of liposome circulation by modifying their surface with PEG, many ligands can be conjugated modified to the surface of liposomes in order to direct their binding to a specific receptor and alter the system random distribution in the organism. Evidence suggest that liposomes conjugated with ligands (transferrin, lactoferrin, low-density lipoprotein) show promise for drug delivery across BBB.[78]

2.3.3.3 Dendrimers

Dendrimers are a class of well-defined branched molecules with high degree of dispensability that surround an inner core. Typically, dendrimers can be synthesised by polyamidoamine (PAMAM) in an algorithmic step-by-step pattern, the more repeating units of branch layers, and the higher generation of the dendrimer. With functional groups on the surface, the dendrimers can be engineered with various targeting ligands for diverse applications. Negatively charged cargos (plasmid DNA, antisense oligonucleotide, and siRNA) can be absorbed to the high-density positively charged surface or encapsulated into the interior of the dendrimer. To form stable nano-composites, the dendrimer formulation should be cautiously modulated to achieve sufficient electrostatic repulsion.

Moreover, the immunogenicity and toxicity are determined by the surface charge. For example, compared with anionic PAMAM dendrimers, cationic PAMAM dendrimers are generally more cytotoxic.[79, 80] Targeting PAMAMs are prepared by conjugating angiopep through bifunctional

PEG, and then complexed with DNA to from PAMAM–PEG–Angiopep/DNA nanoparticles. The angiopep-modified NPs were observed to be internalized by BCECs through a clathrin- and caveolae-mediated energy-depending endocytosis.The cellular uptake of the angiopep-modified NPs was also inhibited by angiopep-2, indicating that LRP-mediated endocytosis may be the main mechanism of cellular internalisation of angiopep-modified NPs. The in vitro BBB model and in vivo investigation have both demonstrated that angiopep-modified NPs show higher efficiency in crossing BBB and accumulated more in brain than unmodified counterparts.[81]

2.3.3.4 Nanoparticles as MRI contrast agents

Magnetic nanoparticles can be stimulated by magnetic field and used as contrast agents for magnetic resonance imaging (MRI). The current state of brain tumour imaging contributes greatly to improving diagnosis, tumour grading and prognosis prediction, surgery planning and navigation, and treatment response assessment.[82, 83] MRI imaging technique together with computed tomography (CT) imaging and positron emission tomography (PET) imaging play a pivotal role for brain tumours management. CT imaging is especially useful for acute calcifications, haemorrhage and osseous features, providing important complementary information. The usage of PET imaging is limited when there are contraindications such as heart pacemaker existence.[84]

Due to inherent depth of imaging, relatively high resolution and good contrast between healthy and abnormal tissues, the imaging of brain tumour has been mostly relying on the MRI. MRI images result from the interaction of contrast agents with surrounding tissue water protons in the presence of an external magnetic field.[85] There are two different contrast agents for enhanced imaging modalities, the positive contrast agents by shortening the longitudinal relaxation time (T1) or the negative contrast agents by shortening the traverse relaxation time (T2) of the surrounding water protons. Paramagnetic gadolinium chelates and manganese complexes belongs to the T1-weighted contrast agents and create bright T1-weighted signal intensity. On the other hand, superparamagnetic iron oxide nanoparticles (SPIONPs) belongs to the T2-weighted contrast agents and generate the dark T2-weighted MR signal. Nanoparticles are comprised by different matrices, by incorporating different contrast agents into the nanoparticle system, and can be endowed with MRI imaging capability.[86, 87]

Nanotechnology-based systems for versatile payload delivery with favourable pharmacokinetics and synchronously imaging represent a new era of "theranostic" for

enhanced therapeutic index. Multi-functionality can be engineered into magnetic nanoparticle systems for tumour specific detection, treatment, and follow-up monitoring.[88, 89] Xu et al. reported an $Gd(DTPA)^{2-}$ intercalated layered double hydroxide (LDH) nanomaterials. The new LDH complexes exhibited 4 times enhancement of longitudinal proton relaxvity compared with free $Gd(DTPA)^{2-}$ in solution.[90] Hadjipanayis et al. synthesised an iron oxide nanoparticles (IONP) that are conjugated with an antibody for targeting to epidermal growth factor receptor (EGFR) expressed on the human glioblastoma multiform cells. The IONP systems are used for target brain tumour therapeutic and MRI contrast enhancement imaging. These functionalised nanoparticles are preferentially uptake by the glioma cells, activating cell apoptosis and inducing strong T2-weighted contrast MRI imaging. In vivo studies demonstrate increased survival rate of tumour implanted animals with injection of antibody conjugated IONPs, and these particles show selective MRI contrast enhanced images of tumour cells and target therapy of tumour cells.[91] In another study, the polyacrylamide (PAA) nanoparticles with a core for encapsulating superparamagnetic iron oxide crystals and photosensitisers (Photofrin®) were prepared with a vascular-targeting peptides conjugation. In vivo MRI of brain tumour in a rat 9L glioma model showed significantly higher and longer MRI enhancement of tumour in comparison with normal brain tissues. The therapy by PDT is also significantly improved with high animal survival rate and cellular water diffusion rate by the targeted PAA nanoparticles.[85,88]

The multifunctional clinical nature of nanotechnology provides great potential for targeting, therapy and imaging of malignant brain tumours.[89, 92] Magnetic nanoparticles have great potential to be used in combination with conventional therapeutic strategies for better brain tumour treatment.[93]

2.3.3.5 Summary

Apart from the magnetic nanoparticles which can response to external magnetic stimuli and organic compounds mentioned above, inorganic nanoparticles including gold-, carbon- and clay-based nanoparticles are widely used for therapeutic and diagnostic purpose.[94, 95] Among them, layered double hydroxide nanoparticles (LDHs), as one kind of clay nanoparticles which benefit from high drug loading capacity, good biosafety and immune system evasion have attracted much attention.[96-98] In addition, incorporating LDHs with above mentioned ligands has great potential for further enhanced brain targeting.

2.4 Layered double hydroxide nanoparticles (LDHs)

Since discovered in 1842 by Swedish scientists, great research interests have been attracted on the syntheses and applications of LDHs.[99] As one type of nano-clays, LDHs show great promise in the theranostic, energy storage and environmental treatment area.[100-102] Particularly, the physiochemical features and bioapplications of LDHs have been extensively investigated in the past few decades.[103, 104] This section summarises the recent advances in the LDH-based nanomedicine, mainly focusing on the structure, therapeutic agent delivery, imaging and LDHs-based hybrids.

2.4.1 LDH structure

LDHs, also known as anionic clays or hydrotalcite-like materials, are a class of two dimensional synthetic lamellar compounds that are made up of positively charged layers with an interlayer region containing balanced anions and water molecules (Figure 2.5).[105, 106] The structure is brucite-like ($Mg(OH)_2$), where the hydroxyl anions are hexagonally close packed with the divalent magnesium cation filling the octahedral centres. Consequently, each magnesium cation is surrounded by six hydroxyl groups to form an octahedron. These octahera share the edges to form a infinite 2-D layer. The layers are held together by weak hydrogen bonds and stacked on top of each other. Part of the cations can be isomorphically replaced by trivalent cations with the similar size, giving positively charged layers.[107, 108] The different stack ways of brucite-like layers result in different LDH structure, where rhombohedral and hexagonal are the most typical ones.[107]

The LDHs can be presented by the general formula $[M^{II}_{1-x}M^{III}_x(OH)_2]^{x+}(A_{n-})_{x/n} \cdot yH_2O$, where the M^{II} and M^{III} represent divalent and trivalent cations.[109] The preferred M^{2+}/M^{3+} molar ratio in the natural occurring LDHs and most of the synthetic ones usually ranges between 2 and 4.[110] Generally, the isomorphical substitution with anyl divalent or trivalent cations is possible, giving LDHs various functions for practical applications.[111, 112]
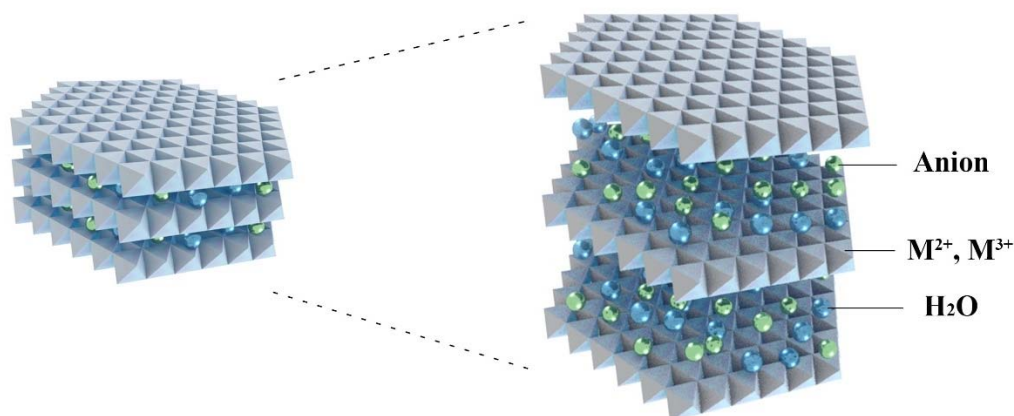
Figure 2.5 Schematic representation of LDH structure.

The most commonly used cations in the layers are Mg^{2+}, Zn^{2+}, Ca^{2+}, Co^{2+}, Ni^{2+}, Cu^{2+} or Mn^{2+}, and Al^{3+}, Cr^{3+}, Co^{3+}, Fe^{3+} or Mn^{3+}. Other LDHs containing monovalent such as Li^+ and tetravalent metal cations such as Zr^{4+} have been also synthetised.[113-115] The basic principle for substitution of divalent or trivalent cations without distortion of the LDHs structure is that the elements have similar radii. The radius of cations that can form LDHs can be found in Table 1.[116] The LDH stability relative to the metal cations is in the order of $Zn < Ni \approx Co < Mn < Mg$ for M^{II} and $Fe < Al$ for M^{III}.[117]

Compared to cations, there are no strict selection criterion to the interlayer anions. Many different anionic species have been successfully intercalated. The already known interlayer anions include: inorganic anions (carbonate, nitrate, chloride, halides, etc.),[118] organic anions (acrylate, lactate, terephthalate, etc.),[119, 120] polymeric anions (polyoxometalates, poly(vinyl sulfonates, etc.)[121] and biomolecules compounds (ATP, DNA, GMP, amino acid, etc.).[122-124] Anions exchange occurs with the preference following order: $NO_3^- < Br^- < Cl^- < OH^- < SO_4^{2-} < CrO_4^{2-} < HAsO_4^{2-} < HPO_4^{2-} < CO_3^{2-}$. The only constraint of the anions to be intercalated is that the charge of anions should be properly balanced with positive charges in the sheets. Otherwise, the desired LDHs cannot be form by large anions with relatively low charge.[125] Notably, due to high affinity of CO_3^{2-}, CO_2 tends to contaminate LDHs when the other anions are used for the preparation. However, the nitrogen bubble can be of help to reduce CO_2 contamination.

Table 2.1 Ionic radii of some cations. LDHs consisting of Al^{3+} and Mg^{2+} or Mn^{2+} were primarily studied in this thesis.[116]

M^{2+}	Radius (nm)	M^{3+}	Radius (nm)
Fe	0.061	Al	0.054
Co	0.065	Co	0.055
Ni	0.069	Fe	0.055
Mg	0.072	Mn	0.058
Cu	0.073	Ga	0.062
Zn	0.074	Rh	0.067
Mn	0.083	Ru	0.068
Pd	0.086	Cr	0.069
Ti	0.086	V	0.074
Cd	0.095	In	0.080
Ca	0.100	Y	0.090
		La	0.103
V^{4+}	0.058	Li^+	0.076
Ti^{4+}	0.061	Na^+	0.102
Sn^{4+}	0.069		
Zr^{4+}	0.072		

2.4.2 LDH morphology

The most typical morphology of LDH is hexagonal sheets-like (Figure 2.6A) with 50-150 nm laterally width and 10-20 nm thickness. A particular rod-like LDH nanoparticles (Figure 2.6B) with 30-60 nm width and 100-200 nm length were reported by Xu's group. The new rod-like LDH nanoparticles were identical to the hexagonal-like LDHs regarding the chemical composition while distinct in the synthesis conditions.[126] Similarly, there is a kind of

delaminated LDH nanoparticles that are synthesised by directly exfoliating the well-crystallised LDHs in the nitrate form into single sheets. The newly delaminated nanosheets have a lateral size of several micrometres and thickness of 0.8 nm. The delamination scheme is shown in the Figure 2.6C.[127, 128] There is not too much morphology variation of LDH nanomaterials. The other already known morphology change of LDHs is relevant to the hybrid LDHs with the other materials. A hollow LDH nanoshell was fabricated using the exfoliated LDH nanosheets as a shell building block and polystyrene beads as a sacrificial template (Figure 2.6D).[129] By in situ growth, the flowerlike morphology $Fe_3O_4@SiO_2@NiAl$-LDH microspheres with three components were synthesised, in which the LDH nanoplatelets form the shell on the SiO_2-coated Fe_3O_4 magnetite core.[130]
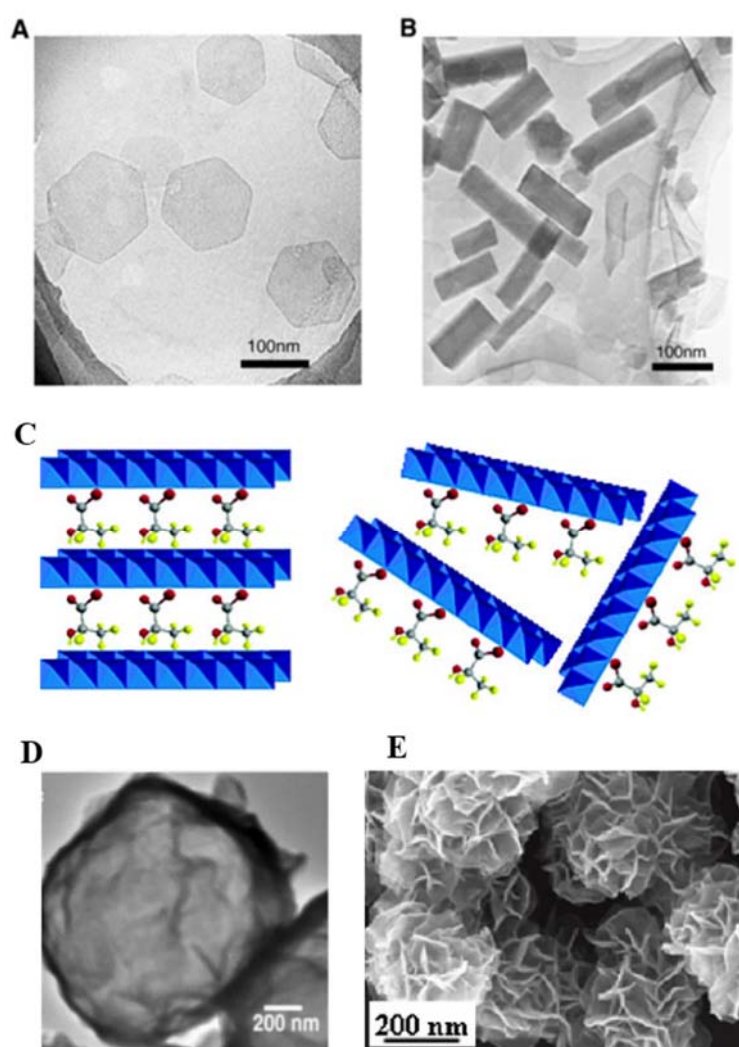
Figure 2.6 TEM images of (A) LDHFITC-HEX (same as LDHHEX-Cl) and (B) LDHFITC-ROD. Reproduced from Ref [126]; (C) Delamination scheme of LDHs into LDH nanosheets.[127] (D) TEM images of LDH hollow shells after treatment in air of 95% humidity.[129] (E) SEM images $Fe_3O_4@SiO_2@NiAl$-LDH microspheres.[130]

2.4.3 Pharmaceutical applications of LDHs

Owing to the unique features such as anion exchange properties and high positive surface area, the pharmaceutical applications of LDHs have attracted wide interests. A lot of therapeutic agents and biochemical compounds such as protiens/peptides, chemotherapeutic drugs, vitamins and DNAs have been incorporated with LDHs through anion exchange or electrostatic interaction and evaluated for biomedical applications.[131] Normally, LDHs have a positive zeta potential of 30-40 mV, which makes the LDHs suitable for adhering onto the negatively charged cell membrane and facilitating the subsequent cell uptake.[132, 133] Moreover, LDHs own peculiar characteristics, such as good biocompatibility and pH-dependent dissolution, which aid to design smart drug delivery systems.[134] The following section will interpret these advantages of LDHs and summarize the progresses of LDHs as delivery systems.

2.4.3.1 Sustained/controlled release

Controlled release refers to the delivery compounds in response to time or stimuli including pH, enzyme, light, magnetic field, temperature, ultrasound, osmosis, etc.[135, 136] In the pharmaceuticals area, controlled drug release does not only intend to prolong the drug release, but also attempts to maintain drug level within the therapeutic window to mitigate side effects accompanying with potentially hazardous drug accumulation following administration.[137 138] As interpreted in the LDH structure part, the stacked layers are balanced by interlayer anions and the interlayer anions are exchangeable, therefore, under certain conditions of temperature, pH (4-7), or anion concentration, the precursor drug-LDHs could release the drug, undergoing the following reaction:[139]

$$[Mg_2Al(OH)_6] \, (drug) \cdot 2H_2O + 3H^+ \rightarrow 2Mg^{2+} + Al(OH)_3 + drug^- + 3H_2O$$
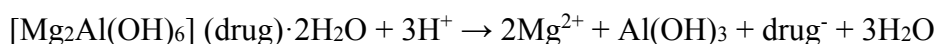
The dissolution of LDHs together with the anion exchange (also known as diffusion) results in the release of intercalated drug. The physiological conditions can be adjusted to control the drug release profile by altering the temperature, pH or anions.[140, 141]

Senapati et al. synthesised a series of MgAl-LDHs with various charge density anions for hydrophobic anticancer drug (raloxifene hydrochloride (RH)) delivery. As reported, 80% RH was released from LDH-phosphate-RH within 1 h and totally released at around 7 h. On the other hand, the LDH-nitrate-RH showed a relative slow release rate with 60% drug released at 6 h, then followed by a sustained release and reached total release at 42 h. The differential drug release rate is interpreted by interactions of drug molecules and anions with LDH constituents.

24

The charge density of nitrate and phosphate leads to different electrostatic interactions with LDH positive layers, therefore, leaving rest of layers interact with drug in different strength.[142]

Two kinds of anti-inflammatory compounds (ibuprofen and fenbufen) were intercalated into the LDH interlayers via ion-exchange and co-precipitation, respectively. The release profile shows that 60 % of ibuprofen was released from LDH-ibuprofen at the initial 20 mins and sustained released to 100 % after 100 mins by ion exchange in the PBS buffer (pH=7.5). Fenbufen drug release was studied in a simulated intestinal fluid (buffer pH 7.8), rapid fenbufen release was observed during the first 15 mins and then increased linearly to 59 % after 120 mins.[143, 144] Various pH influences on the drug release are also investigated. For example, rapid release pattern of α-naphthaleneacetate (NAA) from LDHs was observed at both pH 14 and pH 1 where the LDH structure was completely collapsed at pH 1.[145] O'Hare et al. investigated the release behaviour of a series drugs including diclofenac, gemfibrozil, 4-biphenylacetic acid, 2-propylpentanoic acid, naproxen, ibuprofen and tolfenamic acid at pH 4 or 7. Except for the gemfibrozil which has an identical release profile at pH 4 and 7, the other drugs all showed faster release at pH 4 than pH 7.[146] Plenty of anticancer drugs such as 5-fluorouracil and methotrexate (MTX) release from LDH carrier research are shown to be fast initially and followed with sustained release.[147, 148]

2.4.3.2 Drug delivery

Chemotherapeutic anticancer drugs intercalated into the LDH interlayers through anion exchange/coprecipatation have been investigated intensively in the past two decades. Choy et al. reported that anticancer drug, MTX was successfully hybridised with LDHs by ion-exchange reaction without changing significant structural and functional properties in the hybrids. Cellular uptake test by Saos-2 cells shows that LDHs facilitated delivery efficiency of MTX–LDH hybrids than MTX alone where the proliferation of Saos-2 cells was more strongly suppressed.[149] Another study by Choy et al. successfully intercalated MTX into LDHs through conventional co-precipitation method. Anticancer efficacy of MTX-LDH nanohybrids was tested with the bone cancer cell culture lines (Saos-2 and MG-63), which showed same effective cell suppression at the MTX concentration 5000 times lower, showing the excellent delivery efficiency of MTX via LDHs delivery vector.[150] A comparative cell proliferation suppression test between MTX and MTX-LDH nanohybrid on MTX sensitive and resistant cells found that the MTX-LDH nanohybrid could also bypass the MTX resistance and eventually effectively inhibited wild-type HOS cells and MTX-resistant HOS

cells proliferation compared to free MTX. They presented that the results were associated with uptake mechanism as the MTX-LDH nanohybrid is taken up by clathrin-mediated endocytosis. In this process, the nanohybrid is surrounded by clathrin-coated pit after internalisation, which is completely different from the cellular uptake mechanism for MTX only.[151]

An interesting comparative study has evaluated the anticancer potential of chemotherapy agents (MTX, 5-FU, Dox) and drug-LDH compounds (MTX-LDH, 5-FU-LDH). The anticancer effect is in the order of MTX-LDH > MTX > Dox > 5-FU-LDH > 5-FU in all cell lines (Hep1, A549 and HOS).[152] Other drugs such as Floxuridine, Doxifluridine (DFUR) and Camptothecin (CPT) are also studied and loaded into LDHs by anion exchange or precipitation by controlling the pH or temperature.[153]

2.4.3.3 Gene delivery

Remarkable researches have been done in the gene delivery using LDHs. Ladewig et al. reported that anti-MAPK1 (ERK2) siRNA was delivered to HEK293T cells by LDHs and resulted in a substantial knockdown of ERK2 expression by 80–90% 8 h after incubation, which was even quicker than the Lipofectamine.[154] Specially, Wong et al. reported that cortical neurons are more rapidly internalising nucleic acid-LDH complexes than NIH3T3 fibroblasts. Thus the siRNA delivered by LDHs resulted in effective 49% knockdown of axon guidance receptor, DCC through clathrin-mediated endocytosis pathway.[155] Moreover, the successful knockdown of DCC protein indicate that the siRNA is efficiently released from LDH nanoparticles prior to reaching the lysosome with a degradable environment.

The gene release mechanism has been interpreted in Xu's report. When foreign LDHs are internalised by the cells and transferred to the endosomal vesicles, the protons are pumped into the endosome, thereby facilitating the dissolution of LDHs, resulting in the release of Mg^{2+}, Al^{3+} and Cl^- ions. With the increasing concentration of ions, the water molecules enter the endosome and cause osmotic swelling and endosome bursting, thereby releasing the inside compounds into the cell cytoplasm (Figure 2.7). Most importantly, the siRNA is protected from the acidic environment within the endosome due to LDH's buffer capacity.[126]
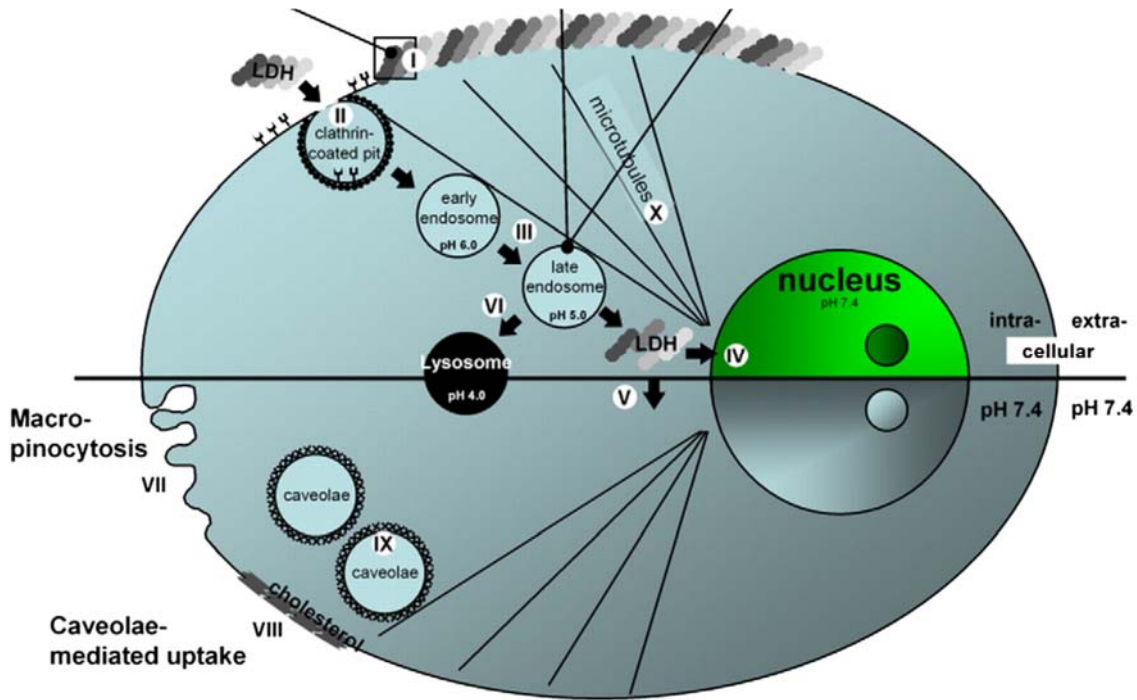
Figure 2.7 Schematic illustration of LDH particle endocytosis and endosomal escape. Reproduced from Ref [126].

Various factors determining gene function expression efficiency are studied. Wong et al. claimed that the nucleotide sequence affects their interaction with LDHs and governs the siRNA delivery efficiency.[156] Some studies suggest that the particle size determines the siRNA delivery efficiency. Chen et al. reported that LDHs with a smaller particle size (45 nm) are more efficient in delivering siRNA in HEK 293 T cells than the particles with large size (114 nm).[157] The pEGFP-N1 plasmid DNA are also successfully transfected NSC 34 cells with high transfection efficiency as reported by Li et al.[158] To enhance the cancer cell growth inhibition, a novelty system by simultaneously delivering anticancer drug 5-FU and Allstars Cell Death siRNA (CD-siRNA) via LDHs for effective cancer treatment are also established. The coordinate effect of CD-siRNA and 5-FU with the same LDH particles significantly enhances cytotoxicity to three cancer cell lines (MCF-7, U2OS and HCT-116) in comparison with either CD-siRNA-LDH or 5-FU-LDH.[159]

2.4.3.4 Protein delivery

The large positively charged surface enables LDH to carry zwitterionic biomolecules via electrostatic interactions. Xu et al. used LDHs to load an amount of as high as 1.1 mg Intimin β (IB) per mg LDHs (Figure 2.8) as adjuvant to induce strong immune responses against bacterial infections. IB is an outer-surface membrane protein of two dominant zoonotic enteric

pathogens: Escherichia coli and enteropathogenic E. coli, playing an essential role in the initial stage of infection. In this report, LDH-IB induces remarkable higher antibody and cell-mediated immune responses, compared with that induced by the potent adjuvant, QuilA. Particularly, the long term strong immune responses last for at least four months in the mouse model with no obvious histopathology of the major organs.[160]

Another report by Xu et al. presented that co-delivery of the toll-like receptor (TLR) ligand CpG and a model antigen, ovalbumin (OVA) by LDHs could modulate immune responses towards the preferred polarity for anticancer immunity. In this study, 0.125 mg OVA and 0.01 mg CpG were immobilized on the surface of one mg LDHs. The complex LDH-CpG-OVA does not only promot the secretion of IgG1 antibody but also stimulates much higher amount of IgG2a at day 21 and 35 after subcutaneous immunisation. In particular, the IgG2a/IgG1 ratio is six times higher than that induced by Alum-CpG-OVA. This observation indicates that the LDH is a more flexible vaccine adjuvant, capable of inducing both Th2 and Th1 immune responses. As Th1 response is suitable for anti-tumour treatment, the mice immunised with LDH-CpG-OVA first showed retarded tumour growth after challenge with OVA-expressing B16/F10 tumour cells.[161] Collectively, these data demonstrate the suitability of LDHs as useful adjuvants in new-generation vaccine formulations to control various infectious diseases and cancers.
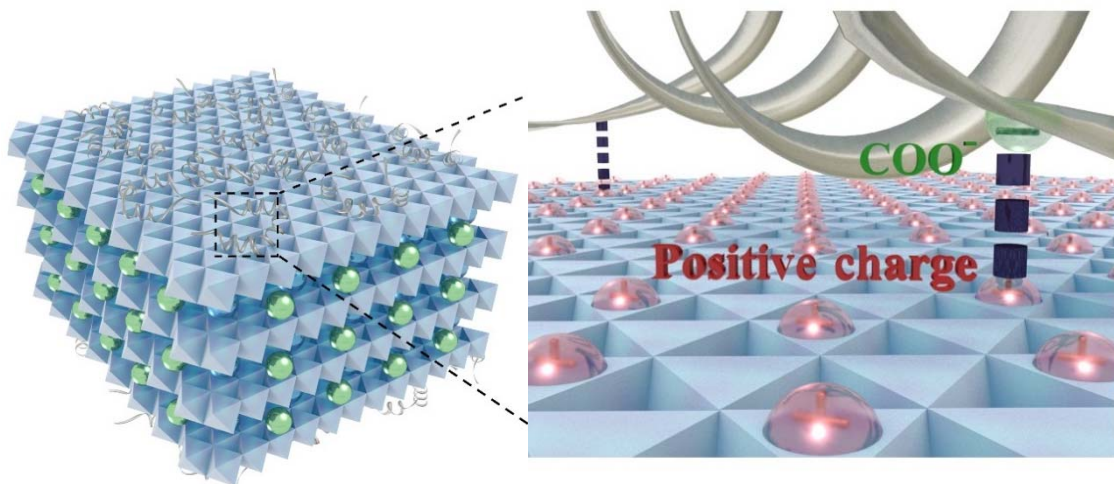
Figure 2.8 Adsorption of Intimin β (IB) to clay nanomaterials. Schematic diagrams showing possible interactions of LDH nanoparticles with IB through electrostatic interactions between -COO⁻ groups along the IB chain and the positive charges on the LDH surface.[160]

2.4.3.5 Good biocompatibility

Biocompatibility is an important evaluation parameter when applying a material for clinical usage. To be a safer material for bioapplication, the material should perform its intended function with desired efficiency in the host while without eliciting any unexpected local or systemic effect.[162] The in vitro biocompatibility test of LDHs regarding cell viability test, hemolysis assay, thrombosis assay, lactate dehydrogenase leakage assay, inflammatory mediators analysis, lipid peroxidation and reactive oxygen species generation have been intensively investigated.[163]

Choy et al. performed the toxicity test of LDHs in carcinoma A549 cells, normal L-132 cells, cervical adenocarcinoma cells (HeLa) and osteosarcoma cells (HOS). LDHs showed little cytotoxicity upon the cells proliferation and viability at the concentration below 250 μg/ml within 48 h. Compared with the toxicity caused by the other inorganic nanoparticles, silica triggered no considerable cell death but with an inflammation response, iron oxide caused cell death due to the cell membrane damage, and single walled carbon nanotube led to cell apoptosis by inducing oxidative stress. However, LDHs exhibited less cytotoxic effects on normal L-132 cells in terms of side effects accompanying with the nanoparticles at the concentration of less than 250 μg/ml.[164] Moreover, in comparison with polymer nanocarriers, Xu et al. reported that MgAl-LDH was approximately 10 times less cytotoxic than polyethyleneimine.[109]

Meanwhile, the in vivo toxicity tests of LDH materials have been also performed in various ways. The in vivo intramuscular implantation test is a much adequate scrutinisation as it allows the evaluation of full biological defence by the host immune system in comparison with the in vitro test performed under controlled conditions. Antigenicity and tissue integration capacity have been investigated histologically by implanting LDH formed tablets in rat abdominal wall after 7 and 28 days. No inflammatory response and fibrous capsule neighbouring the LDHs was triggered. Moreover, the LDHs show good tissue and appropriate extracellular matrix remodelling as well as the deposition of collagen.[163] To improve the bioavailability of LDHs in the colon, the oral delivery of LDHs has also been investigated by coating the pH-sensitive Eudragit copolymer on the surface of LDHs to protect it from extreme gastric pH. The histological analysis of major organs including liver and kidney has been conducted. The histopathology showed no obvious damage of liver and kidney tissue in comparison with the control group (no treatment mice). The tissues exhibited normal morphological appearance, no

inflammatory reactions and necrosis were observed. The author claimed that the LDH-polymer hybrids without hepatotoxicity or renal cytotoxicity show beneficial for oral administration.[165]

The biocompatibility of LDHs via jugular vein injection or intraperitoneal injections has been further studied to evaluate the LDH potential as an injectable drug delivery vehicle. Apart from the local irritation around tissues at the injection site which can be eliminated by meticulous intravenous technique, no systemic effects as indicated by clinical chemistry and histopathology were induced at administration doses of below 200 mg/kg. Therefore, the possibility of using LDH as an injectable drug delivery vehicle is suggested.[166]

Exemplified from naturally occurring minerals, another predominant property of LDH nanoparticles over the others is that the compositions are highly compatible with normal physiological conditions as the byproducts (Mg^{2+}, Al^{3+} or $Al(OH)_3$, Cl^-, H_2O) also normally exist within the cells. All these unique properties have prompted LDHs to be an effective non-viral agent as cellular drug and gene delivery vehicle.[109] Most importantly, in 2014 and 2015, the results of four Phase I pharmacokinetic (PK) and gastroduodenal irritation clinical trials with LDH/Ibuprofen and LDH/naproxen demonstrate that these two products significantly reduce irritation in the gastrointestinal tract compared with current standard ibuprofen and naproxen. It is, therefore, highly expected that the LDH nanoparticles can be used as an efficient vehicle for drug/gene/protein delivery.

2.4.4 Engineering of LDH nanoparticles

To efficiently deliver therapeutic agents to the target area, the nanoparticle based delivery system are normally surface-modified to overcome the physiochemical and biological barriers, especially when administered systematically.[167, 168] Numerous modification methods have been applied into nanoparticles engineering for improved colloidal stability, prolonged circulation time, target specificity and minimised side effects or immune response.[169, 170] In the past decades, the modifications of LDHs have been mainly focused on the intercalation of guests into the galleries such as small organic anions, metal complexes, biological macromolecules, providing fascinating details about the physical/chemical properties of the galleries. However, the development of surface modification and applications LDHs as imaging tool are relatively lack of investigation.[171, 172] The following part provides a review with respect to the engineering of LDHs for different biomedical applications.

2.4.4.1 Surface engineering for improved biomedical therapy

The modification of nanoparticles, also known as nanotechnologies, is an important research area for fabricating hybrid nanoconjugates by combining advantages of one or more materials to obtain multiple functions. Such techniques need to make balance among physiochemical properties and the cost for best outcomes. The development of nanohybrids is considered to be one of the most important achievements in the nanomedicine progress.[173] Many studies have successfully tailored LDHs based hybrid systems by integrating LDHs with the other materials such as organic or inorganic nanomaterials with improved properties for various biomedical applications as summarized below.

Our previous research has successfully applied the serum coating strategy to stabilise LDHs in various electrolyte solutions. By adding the LDHs into albumin solution dropwise with vigorous stirring, LDHs are well stabilised at the albumin/LDH mass ratio of 5: 2.[174] Thereby, our albumin pre-coating strategy has introduced a method for LDHs in vivo application. Also, such a pre-coating method provides for a way for LDH surface modification with ligands for targeting delivery, which will be interpreted applied in this thesis.

Eudragit® L-100 and Eudragit® S-100 are two kinds of enteric methylacrylic acid and methylmethacrylate anionic copolymers. These polymers can be used as materials for oral treatment of inflammatory bowel diseases or specific colonic delivery as they are insoluble at pH lower than 5 but soluble at intestinal pH > 6 for Eudragit® L-100 and pH > 7 for Eudragit® S-100. Due to the intrinsic nature of LDHs, the anionic L-100 and S-100 can associate with the surface of LDHs, therefore, preventing the dissolution of LDHs at gastric pH while accelerating release of delivered therapeutic agents at the colon area. Liu et al. used S100 coated and sulfasalazine prodrug intercalated LDHs for paw edema inflammation treatment by oral delivery. The drug release from LDH composites at pH 1.2 restricted to 5-8% for 2 h, followed by approximately 20% drug release at the pH 6.8 for 2 h, and finally reached around 70% drug release at pH 7.4 for 10 h. Moreover, this newly designed nanoformulation exhibited effectively scavenging activity of superoxide radical in a concentration dependent manner, anti-inflammatory activity in an in vivo animal model resulted in reduction in the inflammation especially at day 4.[165]

Xu et al. reported a well-dispersed SiO_2 nanodot-coated LDHs (SiO_2@LDH) via electrostatic interactions, which was developed into amine-functionalized LDH nanocomposite (NH_2-SiO_2@LDH) by condensating (3-aminopropyl)triethoxysilane (APTES). SiO_2@LDH and

NH$_2$-SiO$_2$@LDH showed excellent colloidal stability either in culture medium or in the phosphate buffer. Further in vitro study showed that the nanocomposite exhibited low cytotoxicity, whereas the NH$_2$-SiO$_2$@LDH nanocomposite was much more efficiently in delivering siRNA into the U$_2$OS cell line for cell proliferation inhibition as compared to the SiO$_2$@LDH.[175]

In vivo targeted delivery through LDHs is still lack of investigation especially in the development of RNA interference therapeutics. Choy et al. used the LDHs as Survivin siRNA delivery system to compare the passive and active tumour targeting ability in vivo by intraperitoneal injection. The targeted delivery system established by grafting LDHs external surface with amino silane and followed with folic acid conjugation. In vitro and in vivo results show that the LDH-FA/siSurvivin could avert biological barriers, enhance tumour-site accumulation and induce endosomal escape for targeting mRNA silencing in the cytoplasm. In vivo study with xenograft mice indicates that a 3.0-fold higher suppression of tumour volume than LDH/siSurvivin was achieved by LDH-FA/siSurvivin in vivo.[176]

2.4.4.2 Modifying LDHs as imaging tools

Medical imaging is an important technique for disease detection, prognosis and treatment intervention.[177, 178] There are several imaging modalities including optical imaging, magnetic resonance imaging (MRI), ultrasound imaging, X-ray CT, positron emission tomography (PET) and single-photon emission CT (SPECT).[179, 180] One or more imaging techniques can be used to give more precise prediction of disease development.[181] The intrinsic properties of inorganic nanoparticles endow them great potential for medical imaging. By incorporating various imaging molecules or magnetic elements, these nanoparticles can be applied in nearly all imaging modalities. There is a retarded development of LDHs as imaging tools, which has been just exploited in recent years (Figure 2.9). However, as non-invasive 2D materials, LDHs are recognised as ideal candidates for imaging purposes owing to their biocompatibility and other properties essential to nanomedicine.

In 2015, Lee et al. reported the charge effect on the distribution of LDHs by modifying LDHs surface with different organic groups and NIR fluorescent dye Cy5.5. By grafting the LDHs surface with amino acid and Cy5.5, the resulted positive amino-LDHs tends to accumulate in the lungs. The negatively charged LDHs modified with carboxylate groups cause susceptibility to rapid clearance from the blood circulation and mostly accumulated in the liver. It is

noteworthy that the neutral PEG5000 conjugated LDHs show enhanced blood circulation time, but no obvious fluorescence was observed in the major organs (Figure 2.9 A).[182]
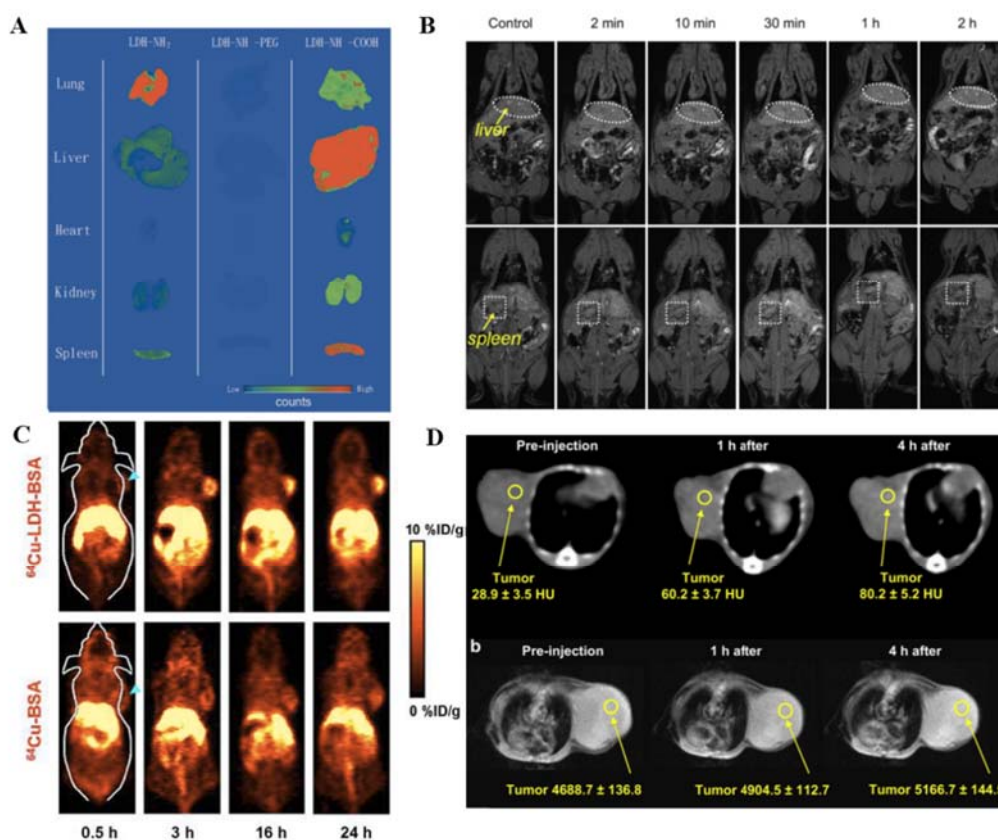
Figure 2.9 Schematic representation of (A) Fluorescent images of dissected organs from a mouse sacrificed after i.v. injection of Cy5.5-labeled LDH–NH$_2$, LDH–NH–PEG5000 and LDH–NH–COOH for 3 h.[182] (B) in vivo T1-images from a SD rat scanned at different time intervals of post-injection (dose: 3.1 mg or 197.1 mmol Gd/kg).[183] (C) In vivo PET imaging in 4T1 tumour-bearing mice shows stronger signal with ^{64}Cu-LDH-BSA.[185] (D) CT (a) and T1-weighted MR images (b) of tumour after intravenous injection LDH-Gd/Au-heparin (dosage: 72.4 mg Au/kg for CT imaging ; 3.0 mg or 190.8 mmol Gd/kg for MR imaging) in 4T1 murine breast tumour-bearing mice for 0 h, 1 h and 4 h.[183]

In the disease diagnostic field, two or more strategies integrated into one system have attracted great interest. Xu et al. reported a CT/MRI dual-modality imaging and anti-cancer drug delivery LDH-Gd/Au nanocomposite based platform. Compared with the commercial CT contrast agent iobitridol and MRI contrast agent Magnevist, the nanocomposite has been found to be better CT and T1-weighted MRI contrast agents either in vitro or in vivo. For breast

tumour imaging, the heparin, an anti-coagulant, was bind to the surface of LDH-Gd/Au surface for enhanced blood compatibility and blood circulation time. After 4-h intravenous injection, the CT and MR imaging signals increased to 80.2 and 5166.7 from original 28.9 and 4688.7, which are effective for tumour detection. Furthermore, the nanocomposite has been found to be able to cause cancer cells death after efficiently transport and release DOX into the cancer cell (Figure 2.9 B&D). This report provides the idea to construct multi-functional nanoplatforms for accurate cancer diagnostic and therapy in the early stage.[183]

A report presented the LDHs PET imaging by labelling LDH nanoparticles with radioisotopes: bivalent cations $^{64}Cu^{2+}$ and trivalent cations $^{44}Sc^{3+}$. With BSA coating on the surface of LDHs, the ^{64}Cu-LDH-BSA as found to prominently enrich in the tumour area with $7.7 \pm 0.1\%ID/g$ at 16 h post-injection (Figure 2.9 C).[184, 185]

2.4.5 Summary

The biodegradable LDH systems hold great promise for gene and drug delivery. Especially, in vivo targeted delivery of drugs through LDH still remains as a key challenge. Currently, investigation on the in vivo application have attracted great interest. Intraperitoneal injection of LDH/siRNA to compare the passive and active tumour targeting ability in vivo was investigated by Choy et al.[176] However, ideally, one would like to administer LDH-drug complexes via intravenous injection. Intravenous injection is the most rapid and effective injection route for therapeutic, especially for the central nervous system therapy.[186] In the past few decades, the biomedical application research of LDHs mostly focused on the in vitro part. As shown in our previous work, when exposure to the electrolyte solution (physiological environment), the LDHs tend to aggregate probably due to adsorption of ions on the LDH surface in salt solution to counteract the intrinsic surface charge of LDHs. Therefore, the major challenges inhibited the LDHs to be used as drug/gene delivery platform for in vivo delivery is their tendency to aggregate in the physiological environment, which is supposed to be induced by their large positively charged surface area adsorbing proteins in the blood.[187] The resulting large aggregates either block veins and capillaries or cause animals death, thus greatly restrict their in vivo application. Moreover, the adsorption of proteins to LDH surface is able to attract macrophages and dendritic cells, leading to immune system activation and nanoparticles clearance from the blood circulation.[188] Therefore, the propensity to aggregate and bind serum proteins once in the bloodstream are major impediments for LDHs application in CNS delivery.

2.5 Hypotheses of this thesis

Our studies provide strong evidence that LDHs possess the appropriate repertoire of chemical and physical properties essential for an effective, efficient and safe drug delivery vehicle for the CNS. We propose that precoating LDHs with albumin will greatly enhance their biocompatibility and biostability once in the bloodstream. The popular strategy used for efficient drug accumulation in the brain area is through ligand-receptor mediated endocytosis. Ideally, by simply conjugating the ligands to the albumin precoated LDHs, the LDHs stability and targeting ability for in vivo application could simultaneously obtained. We further propose that the conjugation of BBB-penetrating peptides will allow LDHs passage across the BBB. Since surface modification of LDHs progressed slowly, this project will focus on solving the remaining surface modification problem of LDHs for targeted CNS delivery. On the other hand, since magnetic nanoparticle provide imaging ability, therefore, in this study, we propose that the incorporating magnetic materials with LDHs enable brain tumour imaging and therapy simultaneously.

2.6 References

1. Grossberg, S., The adaptive brain II: Vision, speech, language, and motor control. Elsevier: 1987; Vol. 43.

2. Mattson, M.; Duan, W.; Pedersen, W.; Culmsee, C., Apoptosis 2001, 6 (1-2), 69-81.

3. Przedborski, S.; Vila, M.; Jackson-Lewis, V., The Journal of clinical investigation 2003, 111 (1), 3-10.

4. Donaghy, M., Brain's diseases of the nervous system. Oxford University Press Oxford: 2001.

5. Prajapati, S. J.; Jadhav, K. R., Brain 2015, 4 (3), 600-3.

6. Jain, R. K.; Di Tomaso, E.; Duda, D. G.; Loeffler, J. S.; Sorensen, A. G.; Batchelor, T. T., Nature Reviews Neuroscience 2007, 8 (8), 610-622.

7. Braun, U.; Muldoon, S. F.; Bassett, D. S., eLS 2015.

8. Vasen, H. F.; Watson, P.; Mecklin, J. P.; Lynch, H. T., Gastroenterology 1999, 116 (6), 1453-1456.

9. Sandilands, A.; O'Regan, G. M.; Liao, H.; Zhao, Y.; Terron-Kwiatkowski, A.; Watson, R. M.; Cassidy, A. J.; Goudie, D. R.; Smith, F. J.; McLean, W. I., Journal of Investigative Dermatology 2006, 126 (8), 1770-1775.

10. Aagaard, L.; Rossi, J. J., Advanced drug delivery reviews 2007, 59 (2), 75-86.

11. Floyd, J. A.; Galperin, A.; Ratner, B. D., Advanced drug delivery reviews 2015, 91, 23-7.

12. Sheridan, C., Nat Biotechnol 2011, 29 (2), 121-128. DOI Doi 10.1038/Nbt.1769.

13. Erdreich-Epstein, A.; Robison, N.; Ren, X.

14. Culver, K. W.; Ram, Z.; Wallbridge, S.; Ishii, H.; Oldfield, E. H.; Blaese, R. M., Science 1992, 256 (5063), 1550-1552.

15. Maguire, A. M.; Simonelli, F.; Pierce, E. A.; Pugh, E. N.; Mingozzi, F.; Bennicelli, J.; Banfi, S.; Marshall, K. A.; Testa, F.; Surace, E. M.; Rossi, S.; Lyubarsky, A.; Arruda, V. R.; Konkle, B.; Stone, E.; Sun, J. W.; Jacobs, J.; Dell'Osso, L.; Hertle, R.; Ma, J. X.; Redmond, T. M.; Zhu, X. S.; Hauck, B.; Zelenaia, O.; Shindler, K. S.; Maguire, M. G.; Wright, J. F.; Volpe, N. J.; McDonnell, J. W.; Auricchio, A.; High, K. A.; Bennett, J., New Engl J Med 2008, 358 (21), 2240-2248.

16. LESNIAK, M. S.; UPADHYAY, U.; GOODWIN, R.; TYLER, B.; BREM, H., Anticancer research 2005, 25 (6B), 3825-3831.

17. Arnold, R. D.; Mager, D. E.; Slack, J. E.; Straubinger, R. M., Clin Cancer Res 2005, 11 (24), 8856-8865.

18. Siegal, T.; Horowitz, A.; Gabizon, A., Journal of neurosurgery 1995, 83 (6), 1029-1037.

19. Song, T. T.; Yuan, X. B.; Sun, A. P.; Wang, H.; Kang, C. S.; Ren, Y.; He, B.; Sheng, J.; Pu, P. Y., Journal of applied polymer science 2010, 115 (3), 1534-1539.

20. Naraharisetti, P. K.; Ong, B. Y. S.; Xie, J. W.; Lee, T. K. Y.; Wang, C.-H.; Sahinidis, N. V., Biomaterials 2007, 28 (5), 886-894.

21. Xie, J.; Marijnissen, J. C.; Wang, C.-H., Biomaterials 2006, 27 (17), 3321-3332.

22. Ranganath, S. H.; Kee, I.; Krantz, W. B.; Chow, P. K.-H.; Wang, C.-H., Pharmaceutical research 2009, 26 (9), 2101-2114.

23. Zhang, Y.-H.; Yue, Z.-J.; Zhang, H.; Tang, G.-S.; Wang, Y.; Liu, J.-M., European Journal of Pharmaceutics and Biopharmaceutics 2010, 76 (3), 371-375.

24. Ozeki, T.; Kaneko, D.; Hashizawa, K.; Imai, Y.; Tagami, T.; Okada, H., International journal of pharmaceutics 2012, 427 (2), 299-304.

25. Menei, P.; Boisdron-Celle, M.; Croué, A.; Guy, G.; Benoit, J.-P., Neurosurgery 1996, 39 (1), 117-123.

26. Menei, P.; Capelle, L.; Guyotat, J.; Fuentes, S.; Assaker, R.; Bataille, B.; François, P.; Dorwling-Carter, D.; Paquis, P.; Bauchet, L., Neurosurgery 2005, 56 (2), 242-248.

27. Takiguchi, N.; Saito, N.; Nunomura, M.; Kouda, K.; Oda, K.; Furuyama, N.; Nakajima, N., Cancer Chemoth Pharm 2001, 47 (1), 11-14.

28. Menei, P.; Jadaud, E.; Faisant, N.; Boisdron-Celle, M.; Michalak, S.; Fournier, D.; Delhaye, M.; Benoit, J. P., Cancer 2004, 100 (2), 405-410.

29. Janzer, R. C., J Inherit Metab Dis 1993, 16 (4), 639-647.

30. Hendricks, B. K.; Cohen-Gadol, A. A.; Miller, J. C., Neurosurgical focus 2015, 38 (3), E10.

31. Begley, D. J., Curr Pharm Design 2004, 10 (12), 1295-1312.

32. Abbott, N. J., J Inherit Metab Dis 2013, 36 (3), 437-449.

33. R. Alyautdin, I. Khalin, M. I. Nafeeza, M. H. Haron and D. Kuznetsov, Int J Nanomedicine, 2014, 9, 795-811.

34. Simpson, I. A.; Appel, N. M.; Hokari, M.; Oki, J.; Holman, G. D.; Maher, F.; Koehler-Stec, E. M.; Vannucci, S. J.; Smith, Q. R., J Neurochem 1999, 72 (1), 238-247.

35. Abbott, N. J., Cell Mol Neurobiol 2005, 25 (1), 5-23.

36. Alyautdin, R.; Khalin, I.; Nafeeza, M. I.; Haron, M. H.; Kuznetsov, D., Int J Nanomedicine 2014, 9, 795-811.

37. Van Tellingen, O.; Yetkin-Arik, B.; De Gooijer, M.; Wesseling, P.; Wurdinger, T.; de Vries, H., Drug Resistance Updates 2015, 19, 1-12.

38. Wisniewski, H. M.; Lossinsky, A. S., Brain Pathol 1991, 1 (2), 89-96. 39. El-Bacha, R. S.; Minn, A., Cell Mol Biol 1999, 45 (1), 15-23.

40. Abbott, N. J., Journal of inherited metabolic disease 2013, 36 (3), 437-449.

41. Zhang, E. Y.; Knipp, G. T.; Ekins, S.; Swaan, P. W., Drug Metab Rev 2002, 34 (4), 709-750.

42. Hervé, F.; Ghinea, N.; Scherrmann, J.-M., The AAPS journal 2008, 10 (3), 455-472.

43. Dallas, S.; Miller, D. S.; Bendayan, R., Pharmacol Rev 2006, 58 (2), 140-161.

44. Haley, B. P.; Gronbech-Jensen, N., Phys Rev B 2010, 82 (11).

45. V. Mohanraj and Y. Chen, Trop J Pharm Res, 2006, 5, 561-573.   .

46. Demeule, M.; Regina, A.; Che, C.; Poirier, J.; Nguyen, T.; Gabathuler, R.; Castaigne, J. P.; Beliveau, R., J Pharmacol Exp Ther 2008, 324 (3), 1064-1072.

47. May, P.; Herz, J.; Bock, H. H., Cell Mol Life Sci 2005, 62 (19-20), 2325-2338

48. Demeule, M.; Currie, J. C.; Bertrand, Y.; Che, C.; Nguyen, T.; Regina, A.; Gabathuler, R.; Castaigne, J. P.; Beliveau, R., J Neurochem 2008, 106 (4), 1534-1544.

49. Liu, Y.; Huang, R.; Han, L.; Ke, W.; Shao, K.; Ye, L.; Lou, J.; Jiang, C., Biomaterials 2009, 30 (25), 4195-4202.

50. Bickel, U.; Yoshikawa, T.; Pardridge, W. M., Advanced drug delivery reviews 2001, 46 (1), 247-279.

51. Parrish, K.; Sarkaria, J. N.; Elmquist, W., Clinical Pharmacology & Therapeutics 2015, 97 (4), 336-346.

52. Chen, G.; Roy, I.; Yang, C.; Prasad, P. N., Chemical reviews 2016, 116 (5), 2826-2885.

53. Garg, T.; Bhandari, S.; Rath, G.; Goyal, A. K., Journal of drug targeting 2015, 23 (10), 865-887.

54. Bidros, D. S.; Liu, J. K.; Vogelbaum, M. A., Future oncology 2010, 6 (1), 117-125.

55. Lonser, R. R.; Sarntinoranont, M.; Morrison, P. F.; Oldfield, E. H., Journal of neurosurgery 2015, 122 (3), 697-706.

56. Xing, W.-k.; Shao, C.; Qi, Z.-y.; Yang, C.; Wang, Z., Drug design, development and therapy 2015, 9, 3341.

57. Patel, M. M.; Goyal, B. R.; Bhadada, S. V.; Bhatt, J. S.; Amin, A. F., Cns Drugs 2009, 23 (1), 35-58. DOI Doi 10.2165/0023210-200923010-00003.

58. Kroll, R. A.; Pagel, M. A.; Muldoon, L. L.; Roman-Goldstein, S.; Fiamengo, S. A.; Neuwelt, E. A., Neurosurgery 1998, 43 (4), 879-886.

59. Kinoshita, M.; McDannold, N.; Jolesz, F. A.; Hynynen, K., Biochem Bioph Res Co 2006, 340 (4), 1085-1090.

60. Sheikov, N.; McDannold, N.; Vykhodtseva, N.; Jolesz, F.; Hynynen, K., Ultrasound Med Biol 2004, 30 (7), 979-989.

61. Bryan, R. N., Radiology 2016, 281 (1), 1-3.

62. Salphati, L.; Shahidi-Latham, S.; Quiason, C.; Barck, K.; Nishimura, M.; Alicke, B.; Pang, J.; Carano, R. A.; Olivero, A. G.; Phillips, H. S., Drug Metabolism and Disposition 2014, 42 (7), 1110-1116.

63. Kumagai, A.; Eisenberg, J. B.; Pardridge, W., J Biol Chem 1987, 262 (31), 15214-15219.

64. Steichen, S. D.; Caldorera-Moore, M.; Peppas, N. A., Eur J Pharm Sci 2013, 48 (3), 416-427.

65. Iwamoto, T., Biological and Pharmaceutical Bulletin 2013, 36 (5), 715-718.

66. Cheng, Y.; Morshed, R. A.; Auffinger, B.; Tobias, A. L.; Lesniak, M. S., Advanced drug delivery reviews 2014, 66, 42-57.

67. Sneed, P. K.; Suh, J. H.; Goetsch, S. J.; Sanghavi, S. N.; Chappell, R.; Buatti, J. M.; Regine, W. F.; Weltman, E.; King, V. J.; Breneman, J. C., International Journal of Radiation Oncology* Biology* Physics 2002, 53 (3), 519-526.

68. Kreuter, J.; Gelperina, S., Tumori 2008, 94 (2), 271-277.

69. Kreuter, J., Adv Drug Deliver Rev 2001, 47 (1), 65-81.

70. Orive, G.; Anitua, E.; Pedraz, J. L.; Emerich, D. F., Nature Reviews Neuroscience 2009, 10 (9), 682-692.

71. Vicent, M. J.; Dieudonne, L.; Carbajo, R. J.; Pineda-Lucena, A., Expert Opin Drug Del 2008, 5 (5), 593-614.

72. Adhikari, A. R.; Rusakova, I.; Haleh, A.; Luisi, J.; Panova, N. I.; Laezza, F.; Chu, W. K., J Appl Phys 2014, 115 (5).

73. Miura, Y.; Takenaka, T.; Toh, K.; Wu, S. R.; Nishihara, H.; Kano, M. R.; Ino, Y.; Nomoto, T.; Matsumoto, Y.; Koyama, H.; Cabral, H.; Nishiyama, N.; Kataoka, K., Acs Nano 2013, 7 (10), 8583-8592.

74. Husseini, G. A.; Pitt, W. G., Adv Drug Deliver Rev 2008, 60 (10), 1137-1152

75. Shen, J.; Zhan, C. Y.; Xie, C.; Meng, Q. G.; Gu, B.; Li, C.; Zhang, Y. K.; Lu, W. Y., J Drug Target 2011, 19 (3), 197-203.

76. Gregoria.G, Febs Lett 1973, 36 (3), 292-296.

77. Preiss, M. R.; Bothun, G. D., Expert Opin Drug Del 2011, 8 (8), 1025-1040.

78. Barbara Haley, M. D., * Eugene Frenkel, M.D.

79. Astruc, D.; Boisselier, E.; Ornelas, C., Chem Rev 2010, 110 (4), 1857-1959.

80. Tekade, R. K.; Dutta, T.; Gajbhiye, V.; Jain, N. K., J Microencapsul 2009, 26 (4), 287-296.

81. Ke, W. L.; Shao, K.; Huang, R. Q.; Han, L.; Liu, Y.; Li, J. F.; Kuang, Y. Y.; Ye, L. Y.; Lou, J. N.; Jiang, C., Biomaterials 2009, 30 (36), 6976-6985.

82. Mabray, M. C.; Cha, S., Brain tumor research and treatment 2015, 3 (1), 8-23.

83. Wankhede, M.; Bouras, A.; Kaluzova, M.; Hadjipanayis, C. G., Expert review of clinical pharmacology 2012, 5 (2), 173-186.

84. Fay, M.; Bell, C.; Dowson, N.; Puttick, S.; Rose, S., 2015.

85. Koo, Y.-E. L.; Reddy, G. R.; Bhojani, M.; Schneider, R.; Philbert, M. A.; Rehemtulla, A.; Ross, B. D.; Kopelman, R., Advanced drug delivery reviews 2006, 58 (14), 1556-1577.

86. Strijkers, G. J.; Mulder, M.; Willem, J.; van Tilborg, F.; Geralda, A.; Nicolay, K., Anti-Cancer Agents in Medicinal Chemistry (Formerly Current Medicinal Chemistry-Anti-Cancer Agents) 2007, 7 (3), 291-305.

87. Yim, H.; Seo, S.; Na, K., Journal of Nanomaterials 2011, 2011, 19.

88. Kopelman, R.; Koo, Y.-E. L.; Philbert, M.; Moffat, B. A.; Reddy, G. R.; McConville, P.; Hall, D. E.; Chenevert, T. L.; Bhojani, M. S.; Buck, S. M., Journal of Magnetism and Magnetic Materials 2005, 293 (1), 404-410.

89. Gao, J.; Gu, H.; Xu, B., Accounts of chemical research 2009, 42 (8), 1097-1107.

90. Xu, Z. P.; Kurniawan, N. D.; Bartlett, P. F.; Lu, G. Q., Chemistry–A European Journal 2007, 13 (10), 2824-2830.

91. Hadjipanayis, C. G.; Machaidze, R.; Kaluzova, M.; Wang, L.; Schuette, A. J.; Chen, H.; Wu, X.; Mao, H., Cancer research 2010, 70 (15), 6303-6312.

92. McCarthy, J. R.; Weissleder, R., Advanced drug delivery reviews 2008, 60 (11), 1241-1251.

93. Zhou, J.; Atsina, K.-B.; Himes, B. T.; Strohbehn, G. W.; Saltzman, W. M., Cancer journal (Sudbury, Mass.) 2012, 18 (1).

94. Anselmo, A. C.; Mitragotri, S., The AAPS journal 2015, 17 (5), 1041-1054.

95. Eustis, S.; El-Sayed, M. A., Chemical society reviews 2006, 35 (3), 209-217.

96. Choi, S.-J.; Oh, J.-M.; Choy, J.-H., Journal of nanoscience and nanotechnology 2010, 10 (4), 2913-2916.

97. Kralj, M.; Pavelic, K., EMBO reports 2003, 4 (11), 1008-1012.

98. Gu, Z.; Wu, A.; Li, L.; Xu, Z. P., Pharmaceutics 2014, 6 (2), 235-248.

99. Zhang, K.; Xu, Z. P.; Lu, J.; Tang, Z. Y.; Zhao, H. J.; Good, D. A.; Wei, M. Q., International journal of molecular sciences 2014, 15 (5), 7409-7428.

100. Sun, X.; Dey, S. K., Journal of colloid and interface science 2015, 458, 160-168.

101. Park, D.-H.; Choi, G.; Choy, J.-H., Bio-layered double hydroxides nanohybrids for theranostics applications. In Photofunctional Layered Materials, Springer: 2015; pp 137-175.

102. Bitinis, N.; Hernández, M.; Verdejo, R.; Kenny, J. M.; Lopez-Manchado, M., Advanced Materials 2011, 23 (44), 5229-5236.

103. Chandra, S.; Barick, K.; Bahadur, D., Advanced Drug Delivery Reviews 2011, 63 (14), 1267-1281.

104. Tian, R.; Liang, R.; Wei, M.; Evans, D. G.; Duan, X., 2015.

105. Liu, Z.; Ma, R.; Osada, M.; Iyi, N.; Ebina, Y.; Takada, K.; Sasaki, T., Journal of the American Chemical Society 2006, 128 (14), 4872-4880.

106. He, J.; Wei, M.; Li, B.; Kang, Y.; Evans, D. G.; Duan, X., Preparation of layered double hydroxides. In Layered double hydroxides, Springer: 2006; pp 89-119.

107. Rives, V., Layered double hydroxides: present and future. Nova Publishers: 2001.

108. Ma, R.; Liang, J.; Liu, X.; Sasaki, T., Journal of the American Chemical Society 2012, 134 (48), 19915-19921.

109. Xu, Z. P.; Lu, G., Pure Appl. Chem. 2006, 78 (9), 1771-1779.

110. López-Salinas, E.; Garcia-Sanchez, M.; Montoya, J.; Acosta, D.; Abasolo, J.; Schifter, I., Langmuir 1997, 13 (17), 4748-4753.

111. Valente, J. S.; Hernandez-Cortez, J.; Cantu, M. S.; Ferrat, G.; López-Salinas, E., Catalysis Today 2010, 150 (3), 340-345.

112. Liang, X.; Zang, Y.; Xu, Y.; Tan, X.; Hou, W.; Wang, L.; Sun, Y., Colloids and Surfaces A: Physicochemical and Engineering Aspects 2013, 433, 122-131.

113. Das, N.; Konar, J.; Mohanta, M.; Srivastava, S., Journal of colloid and interface science 2004, 270 (1), 1-8.

114. Romeo, E.; Royo, C.; Monzón, A.; Trujillano, R.; Labajos, F.; Rives, V., Studies in Surface Science and Catalysis 2000, 130, 2099-2104.

115. Rives, V.; del Arco, M.; Martín, C., Journal of Controlled Release 2013, 169 (1), 28-39.

116. Braterman, P. S.; Xu, Z. P.; Yarberry, F., Handbook of layered materials 2004, 373-474.

117. Boclair, J. W.; Braterman, P. S., Chemistry of Materials 1999, 11 (2), 298-302.

118. Constantino, V. R.; Pinnavaia, T. J., Inorganic Chemistry 1995, 34 (4), 883-892.

119. Newman, S. P.; Jones, W., New Journal of Chemistry 1998, 22 (2), 105-115.

120. Choudary, B.; Kavita, B.; Chowdari, N. S.; Sreedhar, B.; Kantam, M. L., Catalysis letters 2002, 78 (1-4), 373-377.

121. Rives, V.; Ulibarri, M. a. A., Coordination Chemistry Reviews 1999, 181 (1), 61-120.

122. Choy, J.-H.; Kwak, S.-Y.; Park, J.-S.; Jeong, Y.-J.; Portier, J., Journal of the American Chemical Society 1999, 121 (6), 1399-1400.

123. Choy, J.-H.; Kwak, S.-Y.; Park, J.-S.; Jeong, Y.-J., Journal of Materials Chemistry 2001, 11 (6), 1671-1674.

124. Aisawa, S.; Takahashi, S.; Ogasawara, W.; Umetsu, Y.; Narita, E., Journal of Solid State Chemistry 2001, 162 (1), 52-62.

125. Miyata, S., Clays Clay Miner 1983, 31 (4), 305-311.

126. Xu, Z. P.; Niebert, M.; Porazik, K.; Walker, T. L.; Cooper, H. M.; Middelberg, A. P.; Gray, P. P.; Bartlett, P. F.; Lu, G. Q. M., Journal of Controlled Release 2008, 130 (1), 86-94.

127. Jaubertie, C.; Holgado, M.; San Roman, M.; Rives, V., Chemistry of materials 2006, 18 (13), 3114-3121.

128. Li, L.; Ma, R.; Ebina, Y.; Iyi, N.; Sasaki, T., Chemistry of materials 2005, 17 (17), 4386-4391.

129. Li, L.; Ma, R.; Iyi, N.; Ebina, Y.; Takada, K.; Sasaki, T., Chemical Communications 2006, (29), 3125-3127.

130. Shao, M.; Ning, F.; Zhao, J.; Wei, M.; Evans, D. G.; Duan, X., Journal of the American Chemical Society 2012, 134 (2), 1071-1077.

131. Vournakis, J. N.; Finkielsztein, S.; Pariser, E. R.; Helton, M., Methods and compositions for poly-β-1-4-N-acetylglucosamine drug delivery. Google Patents: 1998.

132. Choi, S. J.; Choy, J. H., Nanomedicine-Uk 2011, 6 (5), 803-814. DOI Doi 10.2217/Nnm.11.86.

133. Xu, Z. P.; Lu, G. Q., Pure Appl. Chem. 2006, 78 (9), 1771-1779.

134. Choy, J.-H.; Kwak, S.-Y.; Jeong, Y.-J.; Park, J.-S., Angewandte Chemie 2000, 39 (22), 4041-4045.

135. Kumar, G. A.; Bhat, A.; Lakshmi, A. P.; Reddy, K., Int. J. of Pharm Tech Research 2010, 2, 3658-2375.

136. Zhang, W.; Gilstrap, K.; Wu, L.; KC, R. B.; Moss, M. A.; Wang, Q.; Lu, X.; He, X., ACS nano 2010, 4 (11), 6747-6759.

137. Bokka, S. controlled release of the cytarabine and colchicine using hydrogel derived from the polymerized microemulson. university of akron, 2015.

138. Kost, J.; Lapidot, S. A.; Kumar, N.; Chaubal, M.; Domb, A.; Kumar, R.; Majeti, N., Kirk-Othmer Encyclopedia of Chemical Technology 2003.

139. Lindsay, W. L., Chemical equilibria in soils. John Wiley and Sons Ltd.: 1979.

140. Zhang, H.; Zou, K.; Guo, S.; Duan, X., Journal of Solid State Chemistry 2006, 179 (6), 1792-1801.

141. Ambrogi, V.; Fardella, G.; Grandolini, G.; Perioli, L.; Tiralti, M. C., aaps pharmscitech 2002, 3 (3), 77-82.

142. Senapati, S.; Thakur, R.; Verma, S. P.; Duggal, S.; Mishra, D. P.; Das, P.; Shripathi, T.; Kumar, M.; Rana, D.; Maiti, P., Journal of Controlled Release 2016, 224, 186-198.

143. Ambrogi, V.; Fardella, G.; Grandolini, G.; Perioli, L., International Journal of Pharmaceutics 2001, 220 (1), 23-32.

144. Li, B.; He, J.; Evans, D. G.; Duan, X., Applied clay science 2004, 27 (3), 199-207.

145. bin Hussein, M. Z.; Zainal, Z.; Yahaya, A. H.; Foo, D. W. V., Journal of Controlled Release 2002, 82 (2), 417-427.

146. Khan, A. I.; Lei, L.; Norquist, A. J.; O'Hare, D., Chemical Communications 2001, (22), 2342-2343.

147. Kim, J. Y.; Choi, S.-J.; Oh, J.-M.; Park, T.; Choy, J.-H., Journal of nanoscience and nanotechnology 2007, 7 (11), 3700-3705.

148. Pan, D.; Zhang, H.; Zhang, T.; Duan, X., Chem. Eng. Sci. 2010, 65 (12), 3762-3771.

149. Choy, J.-H.; Jung, J.-S.; Oh, J.-M.; Park, M.; Jeong, J.; Kang, Y.-K.; Han, O.-J., Biomaterials 2004, 25 (15), 3059-3064.

150. Oh, J.-M.; Park, M.; Kim, S.-T.; Jung, J.-Y.; Kang, Y.-G.; Choy, J.-H., Journal of Physics and Chemistry of Solids 2006, 67 (5), 1024-1027.

151. Choi, S.-J.; Choi, G. E.; Oh, J.-M.; Oh, Y.-J.; Park, M.-C.; Choy, J.-H., Journal of Materials Chemistry 2010, 20 (42), 9463-9469.

152. Choi, S.-J.; Oh, J.-M.; Choy, J.-H., Journal of Physics and Chemistry of Solids 2008, 69 (5), 1528-1532.

153. Rives, V.; del Arco, M.; Martín, C., Applied clay science 2014, 88, 239-269.

154. Ladewig, K.; Niebert, M.; Xu, Z. P.; Gray, P. P.; Lu, G. Q., Biomaterials 2010, 31 (7), 1821-1829.

155. Wong, Y.; Markham, K.; Xu, Z. P.; Chen, M.; Lu, G. Q. M.; Bartlett, P. F.; Cooper, H. M., Biomaterials 2010, 31 (33), 8770-8779.

156. Wong, Y.; Cooper, H. M.; Zhang, K.; Chen, M.; Bartlett, P.; Xu, Z. P., Journal of colloid and interface science 2012, 369 (1), 453-459.

157. Chen, M.; Cooper, H. M.; Zhou, J. Z.; Bartlett, P. F.; Xu, Z. P., Journal of colloid and interface science 2013, 390 (1), 275-281.

158. Li, S.; Li, J.; Wang, C. J.; Wang, Q.; Cader, M. Z.; Lu, J.; Evans, D. G.; Duan, X.; O'Hare, D., Journal of Materials Chemistry B 2013, 1 (1), 61-68.

159. Li, L.; Gu, W.; Chen, J.; Chen, W.; Xu, Z. P., Biomaterials 2014, 35 (10), 3331-3339.

160. Chen, W.; Zhang, B.; Mahony, T.; Gu, W.; Rolfe, B.; Xu, Z. P., Small 2016.

161. Yan, S.; Rolfe, B. E.; Zhang, B.; Mohammed, Y. H.; Gu, W.; Xu, Z. P., Biomaterials 2014, 35 (35), 9508-9516.

162. Williams, D. F., Biomaterials 2008, 29 (20), 2941-2953.

163. Cunha, V. R. R.; de Souza, R. B., Scientific Reports 2016, 6.

164. Choi, S.-J.; Oh, J.-M.; Choy, J.-H., Journal of Inorganic Biochemistry 2009, 103 (3), 463-471.

165. Kankala, R. K.; Kuthati, Y.; Sie, H.-W.; Shih, H.-Y.; Lue, S.-I.; Kankala, S.; Jeng, C.-C.; Deng, J.-P.; Weng, C.-F.; Liu, C.-L., Journal of colloid and interface science 2015, 458, 217-228.

166. Kwak, S. Y.; Kriven, W. M.; Wallig, M. A.; Choy, J. H., Biomaterials 2004, 25 (28), 5995-6001.

167. Monopoli, M. P.; Åberg, C.; Salvati, A.; Dawson, K. A., Nature nanotechnology 2012, 7 (12), 779-786.

168. Bartlett, D. W.; Davis, M. E., Bioconjugate chemistry 2007, 18 (2), 456-468.

169. Dobrovolskaia, M. A.; Aggarwal, P.; Hall, J. B.; McNeil, S. E., Molecular pharmaceutics 2008, 5 (4), 487-495.

170. Mahapatro, A.; Singh, D. K., Journal of nanobiotechnology 2011, 9 (1), 1.

171. Kuthati, Y.; Kankala, R. K.; Lee, C.-H., Applied Clay Science 2015, 112, 100-116.

172. Liu, Y.; Miyoshi, H.; Nakamura, M., International Journal of Cancer 2007, 120 (12), 2527-2537.

173. Liu, L.-H.; Métivier, R.; Wang, S.; Wang, H., Journal of Nanomaterials (Online) 2012, 2012 (2012).

174. Gu, Z.; Zuo, H.; Li, L.; Wu, A.; Xu, Z. P., Journal of Materials Chemistry B 2015, 3 (16), 3331-3339.

175. Li, L.; Gu, W.; Liu, J.; Yan, S.; Xu, Z. P., Nano Research 2015, 8 (2), 682-694.

176. Park, D. H.; Cho, J.; Kwon, O. J.; Yun, C. O.; Choy, J. H., Angewandte Chemie International Edition 2016, 55 (14), 4582-4586.

177. Black, W. C.; Welch, H. G., New England Journal of Medicine 1993, 328 (17), 1237-1243.

178. Sanz, J.; Fayad, Z. A., Nature 2008, 451 (7181), 953-957.

179. Gambhir, S. S., Nature Reviews Cancer 2002, 2 (9), 683-693.

180. Frangioni, J. V., Journal of clinical oncology 2008, 26 (24), 4012-4021.

181. Cherry, S. R. In Multimodality imaging: Beyond pet/ct and spect/ct, Seminars in nuclear medicine, Elsevier: 2009; pp 348-353.

182. Kuo, Y.-M.; Kuthati, Y.; Kankala, R. K.; Wei, P.-R.; Weng, C.-F.; Liu, C.-L.; Sung, P.-J.; Mou, C.-Y.; Lee, C.-H., Journal of Materials Chemistry B 2015, 3 (17), 3447-3458.

183. Wang, L.; Xing, H.; Zhang, S.; Ren, Q.; Pan, L.; Zhang, K.; Bu, W.; Zheng, X.; Zhou, L.; Peng, W., Biomaterials 2013, 34 (13), 3390-3401.

184. Gu, Z.; Shi, S.; Fliss, B. C.; Cai, W.; Xu, Z. P.

185. Shi, S.; Fliss, B.; Valdovinos, H.; Chen, F.; Nickles, R.; Cai, W., Journal of Nuclear Medicine 2015, 56 (supplement 3), 1042-1042.

186. Wong, J.; Brugger, A.; Khare, A.; Chaubal, M.; Papadopoulos, P.; Rabinow, B.; Kipp, J.; Ning, J., Advanced drug delivery reviews 2008, 60 (8), 939-954.

187. Walkey, C. D.; Chan, W. C., Chemical Society Reviews 2012, 41 (7), 2780-2799.

188. Schanen, B. C.; Karakoti, A. S.; Seal, S.; Drake III, D. R.; Warren, W. L.; Self, W. T., ACS nano 2009, 3 (9), 2523-2532.

Chapter 3

Materials and Methods

This chapter summarizes the strategies utilised in the whole PhD project, including synthetic methods for various LDH formulations, techniques for material characterizations and biological evaluations.

3.1 Materials synthesis

3.1.1 LDH synthesis
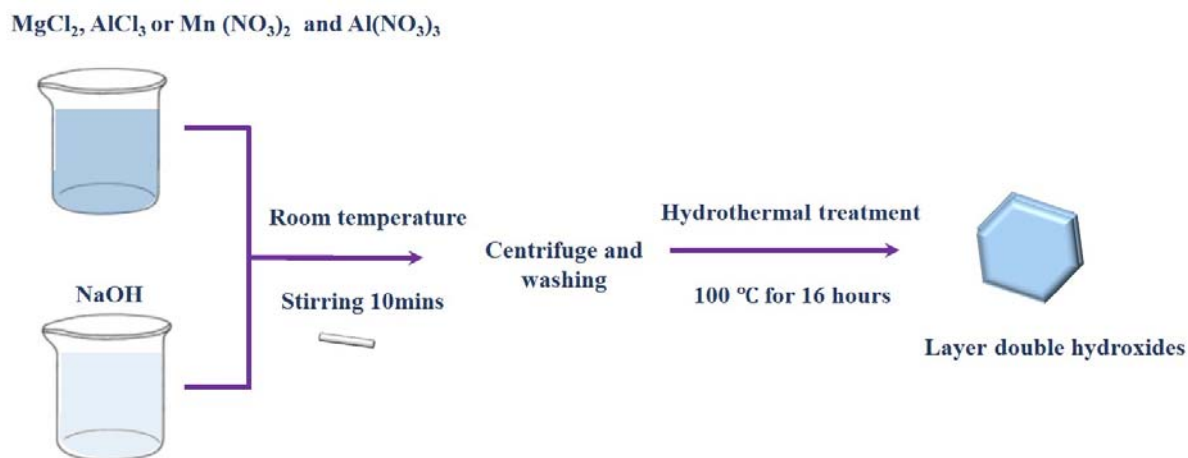
Figure 3.1 Schematic illustration of LDHs synthetic process

The co-precipitation method was used to synthesise the pristine LDHs (Mg-LDHs or Mn-LDHs). In this method, a solution containing two cations (i.e. Mg^{2+} / Mn^{2+} and Al^{3+}) was added into an alkaline solution containing desired anion for co-precipitation to occur. Vigorous stirring and bubbling with nitrogen were performed to ensure homogeneity of the reaction mixture and minimise contamination from atmospheric carbon dioxide. The resulting LDHs mixture was then washed and hydrothermally treated under 100 ℃ for 16 h to obtain

homogeneous LDH particles of good crystallinity (Figure 3.1).[1] Mn-LDHs was well dispersed with help of ultra-sonication. The aging time and temperature affected the prepared particle size.

3.1.2 Surface modification of LDH nanoparticles

Uniform and well-stabilised LDH complexes were obtained by us through adding 2 ml of 4 mg/ml LDH suspension into 2 ml of 10 mg/ml BSA solution (dissolved in deionised Milli-Q water) drop by drop under vigorously magnetic stirring for 30 mins. Furthermore, the BSA-coated LDH (BSA-LDH) nanoparticles were then crosslinked by Glutaraldehyde (GTA) solution at a BSA: GTA molar ratio of 1:135 overnight to form crosslinked BSA-LDH (BSA-LDH-GTA) (Figure 3.2). The surface modification enables LDH nanoparticle to be more colloidally stable and more easily dispersed in solution after freeze drying. The corresponding method developed by us.
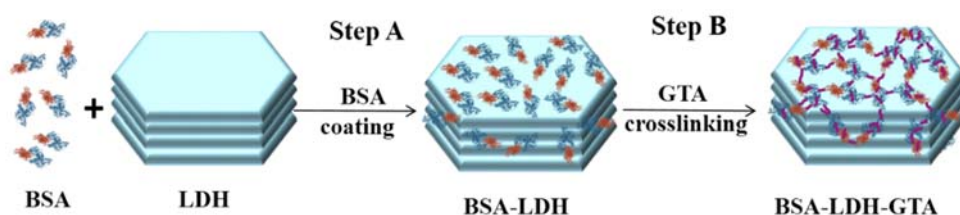
Figure 3.2 Schematic illustration of LDH nanoparticle coating with BSA coating (Step A) and subsequent GTA crosslinking (Step B).

3.1.3 Peptide or dye conjugation with BSA

We prepared peptide or dye conjugated BSA by activation of BSA with a 10-fold molar excess of sulfo-SMCC crosslinker first, producing maleimide-activated BSA. After excess non-reacted crosslinker and by-products were removed, the maleimide-activated BSA reacts with the appropriate amount of peptide or dye having sulfhydryl groups. Usually, there are several or multiple maleimide-activations per protein/antibody molecule, enabling several peptide or dye molecules to be conjugated to each BSA molecule (Figure 3.3).
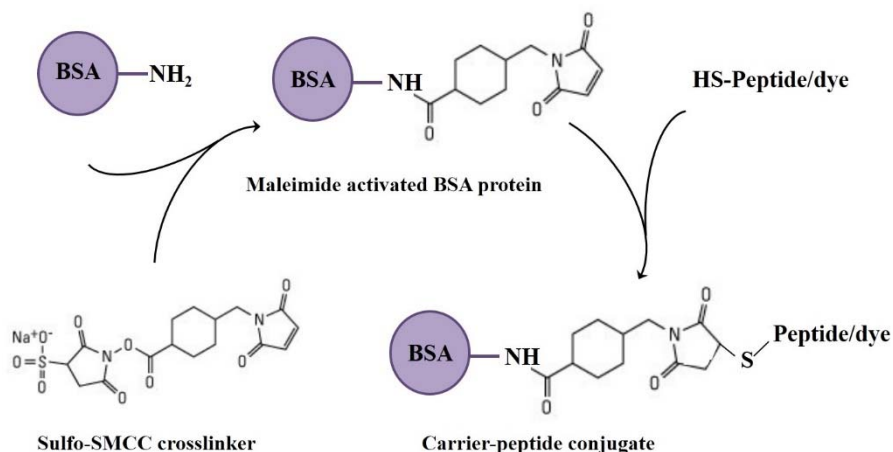
Figure 3.3 Two-step reaction scheme for conjugating peptide/dye with BSA proteins via Sulfo-SMCC.

3.1.4 Synthesis of ligand/dye modified LDHs

This was done by simply mixing the BSA and BSA-peptide conjugate (with or without BSA-dye conjugate) at a desired ratio using the similar coating and crosslinking recipe as above mentioned, as detailed in Figure 3.4. Thus, the ligand (and dye) modified LDHs were fabricated.
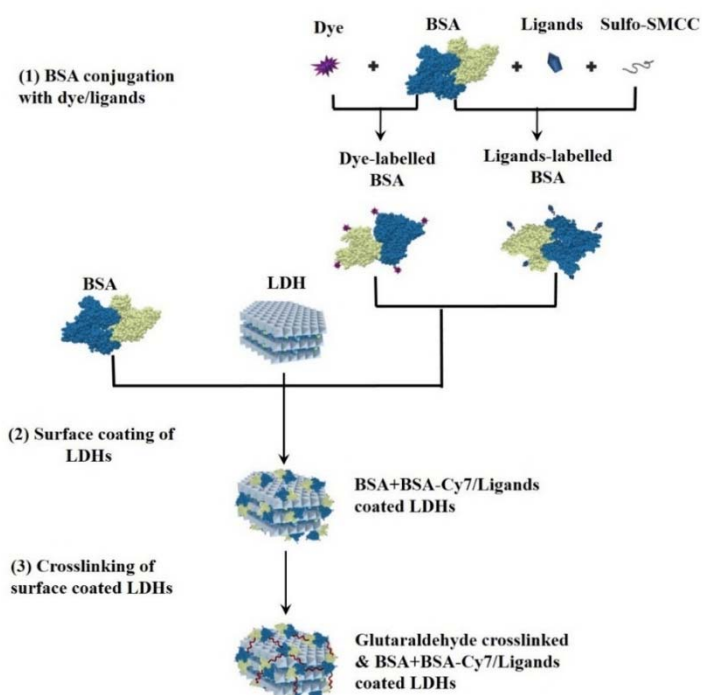
Figure 3.4 Schematic illustration of LDH surface modification with targeting ligand and/or fluorescence dye.

3.2 Characterisation

3.2.1 Powder X-ray diffraction (XRD)

XRD is a powerful analytical tool for crystalline material structure identification. The powder specimen is finely ground, homogenised and placed into a thin layer of quarz sample holder with smooth surface. The sample holder was then inserted into the X-ray beam to generate characteristic X-ray spectra. Typically, the diffraction patterns were collected on the Rigaku Miniflex X-ray Diffractometer with Co Kα source ($\lambda = 0.178897$ nm) used. The sample rotates in the X-ray beam path at an angle θ while the X-ray detector that mounted on an arm rotates at an angle of 2θ. Data were collected at scanning range from 2º to 70º and a scanning rate of 0.02º/s. In this way, all possible diffractions of the lattice should be obtained and the diffraction peaks could be converted into the d-spacings, characteristic of the mineral. The interaction of X-ray beam, diffraction angle, and the lattice spacing in the crystalline sample is demonstrated by the Bragg's Law: $\lambda = 2d \sin \theta$. The pattern of LDH materials usually show a series of strong basal reflections conventionally indexed as 003, 006, etc.[2,3]

3.2.2 MALDI-TOF mass spectra

Matrix-assisted laser desorption/ionisation (MALDI) is a commonly used technique in mass spectrometry. Biomolecules and large organic molecules such as DNA, proteins, polymers, dendrimers and other macromolecules are ionized into fragments by conventional ionization. Typical MALDI methodology contains three-step process. The samples is first mixed with a suitable matrix and applied to a metal plate. Then the ablation and desorption of sample with the matrix are triggered by a pulsed laser irradiates. Finally, the analyte materials after ionization process are accelerated into the mass spectrometer that is used to analyse. The mass spectrometer used in this study was TOF (time of flight mass spectrometer). This study took advantage of accurate molecular weight measurement to characterise various BSA and modified BSA compounds by MALDI-TOF, so that the progress of chemical reactions were monitored (Chapter 5).[4]

In this PhD studies, the spectra were recorded in a linear mode. For testing, a matrix thin layer of Sinapinic Acid saturated in EtOH was put on a ground steel target first and dried naturally. Then a sample solution (2 μl each) was premixed with an equal volume of matrix solution II (Sinapinic Acid saturated in TA30), and applied on the precoated ground steel target. Finally,

the number-average molecular weight (MW) and weight-average molecular weight (MW) were calculated from the MALDI-TOF spectra using Data Explorer software (Applied Biosystems, Framingham, MA).

3.2.3 Particle size and size distribution

Dynamic Light Scattering (DLS) was used to measure particle size. The movement of nanoparticles under Brownian motion have different speeds due to their different sizes where the scattered light from the particles was measured and converted into a size and a size distribution by the Stokes-Einstein relationship. The hydrodynamic particle diameter of LDH suspension was measured in the Nanosizer Nano ZS instrument (Malvern Instruments) at 25 °C. The LDH samples were dispersed in deionized water, PBS or cell culture medium.

3.2.4 X-ray photoelectron spectroscopy

X-ray photoelectron spectroscopy (XPS) was used to determine the amount of carbon (C), nitrogen (N), aluminium (Al), oxygen (O) and manganese (Mn) on the surface of Mn-LDHs. X-ray photoelectron spectra (XPS) were collected on a Kratos Axis ULTRA X-ray photoelectron spectrometer using a monochromatic Al KR (1486.6 eV) X-ray source and a 165 mm hemispherical electron energy analyser. Signal from adventitious carbon was used as a BE standard at 284.6 eV.[5]

3.2.5 Zeta potential analysis

Microelectrophoresis was routinely used to calculate the Zeta potential of charged nanoparticles in solution. In this technique, a cell with a pair of electrodes at each side was used to contain the particle dispersion. When an electric field is applied to nanoparticle solution, the charged nanoparticles will move to the oppositely charged electrode and their velocity is measured and expressed in unit field strength as their mobility.[6] The test was carried out by the Nanosizer Nano ZS instrument (Malvern Instruments) at 25 °C. The most known and widely used theory for calculating Zeta potential value was derived from calculation of the electrophoretic mobility using the Smoluchowski equation. The LDH samples were dispersed in deionized water, PBS or cell culture medium.

3.2.6 Scanning electron microscopy (SEM) / Energy-dispersive X-ray spectroscopy (EDS)

SEM is technique used for examining the sample's surface topography. Samples were prepared by suspending in H_2O first and then attached to the conductive carbon film and finally dried in a vacuum oven at 70 °C before observation. The prepared samples were examined on a JEOL JSM 7800 FE-SEM with a narrow beam produced by the filament under an accelerating voltage of 5-30 kV. The morphological information of the specimen was obtained by secondary electrons caused by the hits of electron beam on the surface layers of subject.

Energy-dispersive X-ray spectroscopy (EDS) is an analytical technique used for the sample elemental analysis or chemical composition characterisation. Each element has a unique atomic structure, which allows a unique set of peaks on its electromagnetic emission spectrum. Therefore, the EDS characterisation relies on the interaction of X-ray and sample. X-ray from a high-energy beam was used to stimulate the emission of X-ray from the specimen, and the change of electron state which is reflected as the X-ray energy in such a field was recorded by an energy-dispersive spectrometer. In this way, the EDS allows the elemental composition of the specimen to be measured.[7]

In this thesis, the SEM of Mn-LDHs and EDS element mapping of Mn, Al and O were conducted to investigate the morphology and distribution of manganese within the Mn-LDHs.

3.2.7 Transmission electron microscopy (TEM)

Transmission electron microscopy (TEM) images were taken using a JEOL 1010 microscope operated at 100 kV. TEM is widely used in biology to examine subcellular structure at high resolution and structure in material sciences. In this technique, a transmitted optical image is formed by electrons from a highly focused monoenergetic electron beam in vacuum that penetrate the sample. To prepare material specimen, as-prepared LDH suspension was dispersed in 75% ethanol solution via ultrasonication for 1 h and transferred to a copper grid, then the image was taken at 100 kV.

3.2.8 Fourier transform infrared (FTIR) spectroscopy

FTIR was used in this study to identify the characteristic bonds in Mn-LDHs. The Mn-LDHs powder was finely mixed with KBr powder and 32-scan infrared (IR) spectra were collected on a Nicolet 6700 FTIR (Thermo Scientific, Thermo Fisher Scientific, MA, USA) over the range 4000-400 cm^{-1} at a resolution of 4 cm^{-1}.

3.3 Biological techniques

3.3.1 Agarose gel electrophoresis

Agarose gel electrophoresis is a method used for separating a mixed population of DNAs/RNAs in a matrix of agarose. Under the electrophoresis conditions, the negatively charged DNA/RNA moves towards the positively charged anode and the speed of DNA/RNA travel through the gel is determined by their size and charge, and to lesser extent, their shape. In the nanomedicine field, migration of nucleic acids in agarose gel is retarded by the nanoparticles and the agarose gel electrophoresis technique used in this area is known as electrophoretic mobility shift assay (EMSA), which is used to separate the nanoparticle–DNA/RNA and DNA/RNA mixture. As a common affinity electrophoresis technique used to study nanoparticle–DNA/RNA interactions, this technique is widely used to determine whether the nanoparticles are capable of binding a given amount of DNA. Normally, a corresponding lane where the pure DNA/RNA fragment without nanoparticles is used as control. Under designed experimental conditions, the interaction between the DNA/RNA and nanoparticle is stabilized, the free and retarded DNA/RNA on the gel reflects the bounding ability of DNA/RNA by nanoparticles.[8]

For gel electrophoresis, the complexes were loaded into each well of 2% agarose gel and the corresponding amount of dsDNA was prepared in the absence of nanoparticles as control, which was then run in Tris-acetate-EDTA buffer at 80 V for 40 min. Genetic molecule bands were visualized using a GelDoc UV illuminator. In this thesis, gel electrophoresis analysis was performed to examine the binding ability of BSA-LDH-GTAs to genetic molecules. The association of dsDNA with BSA-LDH-GTAs was conducted by mixing dsDNA with pristine LDH, BSA-LDH, and BSA-LDH-GTA at the LDH: DNA mass ratio of 40:1 using light agitation at 37 °C overnight.

3.3.2 Flow cytometry

Flow cytometry is a common laser-based biophysical technique used for cell sorting, cell counting, biomarker detection, etc. In the nanomedince study, properties of individual particles or particles taken up by cells are able to be detected by light scattering or fluorescence emission. By suspending nanoparticles or cells in sheath fluid and passing them through an electronic detection apparatus, the fluorescence signal is generated and information about the nanoparticles or cells is provided. The scattered light collected by a lens in the forward direction

is called forward scatter channel (FSC). The FSC intensity is used to distinguish cellular debris and living cells. Side scatter (SSC) is light measured approximately at a 90° angle to the excitation line that provides information about the granularity or internal complexity. A combination of FSC and SSC can be used to differentiate different cell types in a heterogeneous sample.[9]

In this thesis, BD LSR II flow cytometer was used to measure cellular uptake of nanoparticles. For testing, Cy3 as fluorescence marker was used to label DNA and premixed with BSA-LDH-GTAs or ligand modified LDHs. Cells were seeded in multi-well plates at a certain density per well one day before the assay, followed by incubation with labelled LDH nanoaprticles for a few hours. After incubation, cells were washed 3 times with PBS and harvested by trypsination. After two more washes with PBS, the cells were re-suspended in paraformaldehyde (Merk) in PBS (PFA/PBS, 600 μl, 2 %) for FACS test. The results were analysed using FlowJo software.

3.3.3 Confocal laser scanning microscopy (CLSM)

Confocal laser scanning microscopy is an optical imaging technique used for collecting high resolution images based on selected depth (also known as optical sectioning). It enables three-dimensional reconstructions of topologically complex objects. CLSM is able to cut the specimen into single planes and image these single planes along the optical axis (Z), the slices result in a 3D data set that provides information about the spatial structure of the object.

In this thesis, a Carl Zeiss LSM 710 was used to examine cellular uptake and trafficking of LDH formulations.[10] To prepare the specimen for CLSM, cells treated with various fluorescent labelled LDH formulations were grown on the coverslips. After incubation, the liquid was removed and cells were fixed with paraformaldehyde (Merk) in PBS (PFA/PBS, 600 μl, 2 %) for 20 mins, followed with three times wash with PBS. Finally the coverslip was mounted onto glass slides by fluoroshield with DAPI (Sigma). The slides were viewed using confocal microscopy. Z-series images were taken by using optical sectioning technique to observe the location of particles.

3.3.4 MTT assay

3-[4, 5-dimethylthiazol-2-yl]-2, 5-diphenyl tetrazolium bromide (MTT) assay is a simple method applied in nanomedicine area for evaluating their toxicity via measuring the mitochondrial dehydrogenase activity in living cells. The yellow tetrazolium MTT can be cleaved by mitochondrial dehydrogenases in metabolically viable cells, and the resulting purple

MTT formazan crystals can be dissolved and quantified by spectrophotometric means. As the toxicity extent affects the cells viability and apoptosis or necrosis leads to reduction in cell viability, therefore MTT is widely employed in the cytotoxicity study.[11]

In this study, the stabilized BSA-LDH-GTAs and ligand modified LDHs toxicity to various cells were tested. Moreover, cell growth inhibition by delivering therapeutic drugs or siRNAs using LDH formulations as nanocarriers was tested in N2a and U87 cell lines. For testing, 3000-5000 cells were seeded in each well of 96-well plates one day before the test, the tested complexes were dispersed in culture medium (supplemented with 10% FBS and 1% penicillin-streptomycin) and incubated with cells for 24 to 72 hours at 37 °C. The cell viability was measured by adding MTT agent and reading the absorbance at 490 nm using a Synergy HT Microplate Reader. Results were compared to cells not exposed to corresponding nanoparticle complexes.

3.3.5 In vivo confocal neuroimaging (ICON) technique

In vivo confocal neuroimaging (ICON) technique uses the specially designed standard confocal laser scanning microscope (LSM 5 Pascal, Carl Zeiss AG, Jena, Germany) with a large probe space for positioning the animal and a long working distance objective lens. ICON is useful for repetitively visualising and analysing the passage of fluorescent carriers across the blood-retina barrier (BRB) in living animals in a real time manner, permitting to record the dynamic pattern of the fluorescent NP's BBB-passage. As the retina is ontogenetically derived from the central nervous system (CNS) and the BRB is functionally identical to that of the BBB, thus the BRB is used as a model for the BBB.[12-14]

In this study, the dynamic patterns of two-ligand modified LDH nanoparticles across the BRB in comparison with unmodified LDHs were collected by ICON.

3.3.6 Fluorescence optical imaging

Optical imaging is widely used for in vivo behaviour study of fluorescence containing system in small animal models. In the nanoparticle area, the fluorescent dyes can be physically encapsulated in nanocarrier systems or covalently conjugated with nancarriers, predicting drug release kinetics or monitoring nanoparticles biodistribution and site-specific accumulation in animal organs. To avoid the autofluorescence from natural biological tissues and obtain a high signal to noise ratio images, near-infrared (NIR) wavelengths above 700 nm where the autoflourescence emission is dramatically reduced are preferred.[15,16] A silicon semi-conductor

material called as charge coupled device (CCD) is used for detecting light in this spectral region and converting it into the electrical signal.[17]

The fluorescence optical imaging was used in this thesis for detecting the in vivo biodistribution of Cy7 labelled BSA-LDH-GTAs and comparing the brain targeting ability of ligand modified LDHs with that of unmodified LDHs.

3.3.7 Hemolysis assay

Hemolysis, also known as haemolysis, is the lysis of red blood cells and the release of their contents into surrounding fluid (e.g. blood plasma). Hemolysis may occur in vivo or in vitro (inside or outside the body). In nanomedicine area, the small size and unique physicochemical properties of nanoparticles may interact with erythrocytes, leading to potential toxicity. As hemolysis leads to symptoms such as anemia, jaundice and other pathological conditions, therefore, in vitro evaluation of biocompatibility of nanoparticles with blood samples is a necessary for early preclinical development.[18]

In this thesis, the engineered various LDH formulations were evaluated by hemolysis assay.

3.4 Summary

The LDH formulations in the whole PhD project were characterised by the techniques mentioned above, ensuring the surface modification of LDHs were successful. For the in vitro and in vivo application, i.e. the biological stability and brain penetration ability, the engineered LDHs were evaluated by a series of biological techniques interpreted in this chapter.

3.5 References

1. Xu, Z. P.; Stevenson, G.; Lu, C.-Q.; Lu, G. Q., The Journal of Physical Chemistry B 2006, 110 (34), 16923-16929.

2. Poppe, L.; Paskevich, V.; Hathaway, J.; Blackwood, D., US Geological Survey Open-File Report 2001, 1 (041), 1-88.

3. Auerbach, S. M.; Carrado, K. A.; Dutta, P. K., Handbook of layered materials. CRC Press: 2004.

4. Hortin, G. L., Clinical chemistry 2006, 52 (7), 1223-1237.

5. Kristensen, E. M.; Nederberg, F.; Rensmo, H.; Bowden, T.; Hilborn, J.; Siegbahn, H., Langmuir 2006, 22 (23), 9651-9657.

6. Kaszuba, M.; Corbett, J.; Watson, F. M.; Jones, A., Philosophical Transactions of the Royal Society of London A: Mathematical, Physical and Engineering Sciences 2010, 368 (1927), 4439-4451.

7. Goldstein, J.; Newbury, D. E.; Echlin, P.; Joy, D. C.; Romig Jr, A. D.; Lyman, C. E.; Fiori, C.; Lifshin, E., Scanning electron microscopy and X-ray microanalysis: a text for biologists, materials scientists, and geologists. Springer Science & Business Media: 2012.

8. Scott, V.; Clark, A.; Docherty, K., 1994.

9. Ornatsky, O.; Bandura, D.; Baranov, V.; Nitz, M.; Winnik, M. A.; Tanner, S., Journal of immunological methods 2010, 361 (1), 1-20.

10. Claxton, N. S.; Fellers, T. J.; Davidson, M. W., Encyclopedia of Medical Devices and Instrumentation 2006.

11. Ferrari, M.; Fornasiero, M. C.; Isetta, A. M., Journal of immunological methods 1990, 131 (2), 165-172.

12. Steuer, H.; Jaworski, A.; Stoll, D.; Schlosshauer, B., Brain research protocols 2004, 13 (1), 26-36.

13. Steuer, H.; Jaworski, A.; Elger, B.; Kaussmann, M.; Keldenich, J. r.; Schneider, H.; Stoll, D.; Schlosshauer, B., Investigative ophthalmology & visual science 2005, 46 (3), 1047-1053.

14. Voigt, N.; Henrich-Noack, P.; Kockentiedt, S.; Hintz, W.; Tomas, J.; Sabel, B. A., European Journal of Pharmaceutics and Biopharmaceutics 2014, 87 (1), 19-29.

15. Pinkerton, N. M.; Zhang, S. W.; Youngblood, R. L.; Gao, D.; Li, S.; Benson, B. R.; Anthony, J.; Stone, H. A.; Sinko, P. J.; Prud'homme, R. K., Biomacromolecules 2013, 15 (1), 252-261.

16. Frangioni, J. V., Current opinion in chemical biology 2003, 7 (5), 626-634.

17. Spibey, C. A.; Jackson, P.; Herick, K., Electrophoresis 2001, 22 (5), 829-836.

18. Dobrovolskaia, M. A.; Clogston, J. D.; Neun, B. W.; Hall, J. B.; Patri, A. K.; McNeil, S. E., Nano letters 2008, 8 (8), 2180-2187.

Chapter 4

Crosslinking to enhance colloidal stability and redispersity of layered double hydroxide nanoparticles

The present study introduces a strategy for stabilizing and redispersing layered double hydroxide (LDH) nanoparticles by crosslinking bovine serum albumin (BSA) coated onto the surface. The strategy involves optimization of the amount of the crosslinking agent glutaraldehyde (GTA) to achieve minimal aggregation and ready redispersion. LDH nanoparticles were prepared by co-precipitation and hydrothermal treatment, with subsequent bovine serum albumin (BSA) coating at the BSA/LDH mass ratio of 5:2. BSA coated onto LDH nanoparticles was crosslinked with different amounts of GTA. Aggregation studies using dilution assays, dynamic light scattering, and zeta potential analysis indicated that severe aggregation at lower LDH nanoparticle concentrations can be prevented by proper crosslinking of BSA with GTA. The GTA-crosslinked BSA-coated nanoparticles showed excellent redispersity compared to the non-crosslinked nanoparticles. In vitro cytotoxicity and cell uptake were found to be minimally affected by GTA-crosslinking. The new strategy therefore provides a much more effective method for the prevention of LDH nanoparticle aggregation and improved LDH nanoparticle redispersion for use in a wide variety of bio-applications in vitro and in vivo. **This work has been partly published in *Journal of colloid and interface science* (2015).**

4.1 Introduction

Due to their potential application in biomedical therapeutics, nanoparticles have attracted intense scientific interest. Nanoparticles normally have at least one dimension in the range of 1-100 nm, and can therefore readily enter the cell microenvironment. [1, 2] Stabilization of nanoparticles is a fundamental requirement necessary for successful use in clinical applications. Upon intravenous injection, nanoparticles often interact with biological environments that consist of biomolecules such as proteins, sugars, and electrolytes. These interactions can lead to nanoparticle aggregation and blockage of blood vessels and capillaries. Therefore, it is of particular importance that nanoparticles avoid aggregation in the in vivo situation.[3-5] The development of nanotechnology allows researchers to rationally engineer nanoparticles for targeted delivery, prolonged circulation half-life, improved therapeutic index and reduced immunogenicity.[6-8] It is therefore desirable to engineer nanoparticles with high colloidal stability in biological fluids. Additionally, maximal surface accessibility for drug/gene loading and delivery is desirable.

Previously, we reported that layered double hydroxide (LDH) can effectively deliver drug/DNA into several types of cells including fibroblasts, HEK 293, CHO cells and neurons.[9-11] LDH is a family of anionic clays, and can be found in nature and also readily synthesized in the laboratory. [12, 13] Similar to hydrotalcite, the LDH composition can be expressed as the formula $[M^{2+}_{1-x}M^{3+}_x(OH)_2]^{x+}(A^{n-})_{x/n} \cdot mH_2O$, where M^{2+} represents a divalent metal cation, M^{3+} a trivalent metal cation, and A^{n-} an anion. The typical morphology of LDH nanoparticles is a hexagonal, plate-like, stacked layer structure, with a lateral diameter tailored from 50 to 300 nm.[14] With the exchangeable property, the LDHs are able to load various negatively charged therapeutics, such as DNA and RNA, anionic drugs and peptide/proteins. Many investigations show that LDHs are a potential drug and gene delivery candidate as they have many intrinsic advantages, including good biocompatibility, low cytotoxicity, high drug loading and controllable drug release mechanism.[15-21] However, in vivo applications of these nanoparticles have been hampered by their tendency to aggregate in biological environments, resulting in inflammatory responses or death. Therefore, it is necessary to improve the stability of LDH nanoparticles for in vivo applications.

Several methods have been used to increase stability of colloidal systems, including surfactant molecule attachment on the nanoparticle surface, surface modification of functional groups and modification designed to enhance stability such as steric repulsion and electrostatic repulsion.[22]

For example, silver nanoparticles were modified with two surfactants (sodium dodecyl sulfate and polyoxyethylenesorbitane monooleate-Tween 80) to improve anti-aggregation properties.[23] PEGylation is an often used strategy to maintain colloidal stability via the steric effect. [22, 24, 25] It is well-known that charged nanomaterials adsorb strongly on oppositely charged surfaces, and they were widely used to stabilize the nanoparticles. Recently, we used BSA to coat LDH nanoparticles and found that these LDH-BSA complexes were colloidally stable in various electrolyte solutions.[26] Chemical crosslinking is one of the highly versatile methods to create a network on the nanoparticle surface by crosslinking functional groups of the surface molecules. Crosslinking with the amine-carboxylic acid, isocyanate-OH/NH$_2$ reaction and Schiff base formation, [27, 28] can prevent aggregation via steric repulsion.
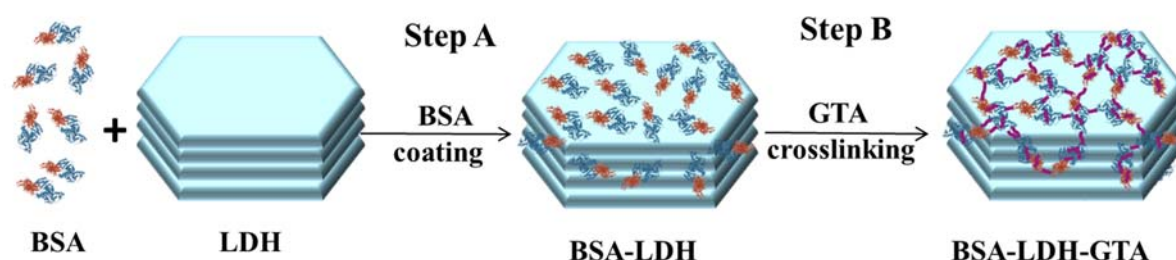
Scheme 4.1 Schematic illustration of BSA-coating onto LDH nanoparticles and subsequent GTA crosslinking.

Dynamic light scattering (DLS) is a common method to study aggregation and colloid stability of inorganic particles in the presence of oppositely charged macromolecules. For example, DLS studies pointed out that the ionic strength may induce conformational changes of the adsorbed items, therefore, the hydrodynamic thickness of the adsorbed layer on colloidal latex particles will increase. Surface charge neutralization of colloidal particles with the oppositely charged coating agents give rise to fast aggregation of the particles while the charge reversal enables stabilization of the system. It is ideal to design a well-dispersed colloidal system over a wide range of buffer conditions with ready redispersity, while simultaneously having surface accessibility for loading therapeutics. Our previous stabilization of LDH nanoparticles with BSA was achieved in specific buffer conditions (Step A in Scheme 1), but the BSA-LDH complexes became unstable at low concentrations. Moreover concentrated BSA-LDH particles are poorly redispersed in aqueous solution. Therefore, in this study, we crosslinked BSA after coating onto the LDH surface with glutaraldehyde (GTA) (Step B in Scheme 4.1) and demonstrated that this crosslinked BSA-LDH system has an enhanced colloidal stability and

excellent redispersity. The optimized crosslinking only consumed a small portion of functional groups in BSA, leaving the majority available for further surface modification. Note that the crosslinked LDHs showed cytotoxicity similar to LDH alone, indicating their good biocompatibility for biomedical applications.

4.2 Experimental section

4.2.1 Synthesis of clay nanoparticles

Materials

Complementary strands of dsDNAs were purchased from GeneWorks and annealed at 75 °C for 10 min. One strand of the duplex was covalently coupled to the cy3 fluorophore at the 5′ end before annealing. Glutaraldehyde (GTA) solution (25%) was bought from Ajax Finechem, and other chemicals and reagents from Sigma-Aldrich if not illustrated specifically. Water used in experiments was deionized Milli-Q water.

Synthesis of LDH nanoparticles

Mg2Al-Cl-LDH (pristine LDH) was prepared using a co-precipitation-hydrothermal treatment method, as reported previously.[17, 29] In brief, LDH was synthesized by mixing 40 ml NaOH solution (0.15 M) with 10 ml salt solution containing $MgCl_2$ (3.0 mmol) and $AlCl_3$ (1.0 mmol) under vigorous stirring. The resultant precipitate was washed and then hydrothermally treated at 100 ºC for 16 h, giving an LDH suspension with the mass concentration of 4.0 mg/ml.

4.2.2 BSA coating

Crosslinking of BSA coated on LDH

Two mililiters of 4 mg/ml LDH suspension was added into 2 ml of 10 mg/ml BSA solution (dissolved in deionized Milli-Q water) drop by drop under vigorously magnetic stirring for 30 min to ensure saturated adsorption. The BSA-coated LDH (BSA-LDH) nanoparticles were then added with GTA solution at a BSA: GTA molar ratio of 1:0.5, 1:15, 1:45, or 1:135, and incubated overnight to form crosslinked BSA-LDH (BSA-LDH-GTA).

Quantification of active amino groups on crosslinked BSA

GTA was applied as the crosslinking agent to react with BSA (as shown in Scheme 4.2). The determination of unreacted amino groups was performed using the reaction of TNBS (2, 4, 6-trinitrobenzene sulfonic acid) with free amino groups. As a simulation, BSA (50.0 mg) was dissolved in 10.0 ml reaction buffer (0.1 M sodium bicarbonate, pH 8.5). Aliquots of 1.0, 2.5, 5.0, 10.0, 20.0, 30.0, 60.0, 80.0 and 100.0 μl of 5% GTA solution were added gradually to 1.0 ml BSA solution and the total volume was adjusted with the reaction buffer to a total 2.0 ml. After 24 h incubation at 20 °C under constant shaking, 1.0 ml 0.01% TNBS solution was added into the reaction mixture and shaken at 500 rpm for 2 h at 40 °C. The solution was then assayed by recording the absorbance at 343 nm. The content of free amino groups on the crosslinked BSA surface was calculated in relation to BSA treated in the same manner as described above but without using GTA.
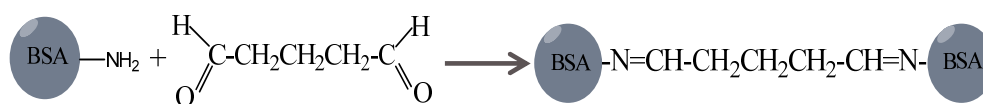
Scheme 4.2 Schematic illustration of BSA reaction with GTA

Colloidal stability test

The size and polydispersity index (Pdi) of BSA-LDH and BSA-LDH-GTA at different concentrations (diluted for 0, 10, 160, and 320 times) were measured on a Nano Zetasizer (Nano ZS, MALVERN Instruments). The same volume of PBS was then mixed with BSA-LDH or BSA-LDH-GTA under vigorous stirring for 30 min and the particle size distribution was monitored similarly. LDHs in water and in PBS were also measured for the particle size distribution on a Nano Zetasizer instrument.

Redispersion ability test

After centrifugation, BSA-LDH or BSA-LDH-GTA was collected and frozen in liquid nitrogen for 10 min, and then freeze-dried for 24 h, followed by being redispersed in water under gentle

ultrasonication. The particle size distribution of water-redispersed particles (equilibrate to the original concentration) was measured and then compared with the initial one in the suspension.

Nucleic acid association with LDH

The association of dsDNA with LDH was conducted by mixing dsDNA with pristine LDH, BSA-LDH, and BSA-LDH-GTA at the LDH: DNA mass ratio of 40:1 using light agitation at 37 °C overnight.

4.2.3 Characterisation of different LDHs

The particle size distribution and zeta potential of LDH, BSA-LDH, and BSA-LDH-GTA in aqueous solutions were measured on a Nano Zetasizer instrument. Transmission electron microscopy (TEM) images were obtained on a JEOL 1010A transmission electron microscope at an acceleration voltage of 100 kV. Powder X-ray diffraction (XRD) patterns were recorded on a Rigaku Miniflex X-ray Diffractometer using Co Kα source (λ = 0.178897 nm) at a scanning rate of 0.02º/s (2θ) from 2θ = 2º to 2θ = 80º. Fourier Transform Infrared (FTIR) spectra were recorded on a Nicolet 6700 spectrometer by accumulating 32 scans at a resolution of 4 cm^{-1} in the attenuated total reflection model.

4.2.4 In-vitro and in-vivo assays

In vitro cytotoxicity test and cellular uptake

Rat vascular smooth muscle cells (SMC) and human breast tumour cell line (MCF-7) were seeded in a 96-well or 6-well plate at a density of 4-5 × 10^4 cells/cm^2 in growth medium (Medium 199 and DMEM medium respectively, containing 10% foetal calf serum, 100 U/ml penicillin and 100 μg/ml streptomycin), and incubated at 37 °C in a humidified atmosphere with 5% CO$_2$.

Cytotoxicity of BSA-LDH-GTA was examined by the MTT (Sigma) assay. Twenty-four hours after seeding, the cells were treated with growth medium containing BSA-LDH-GTA (LDH 10, 50, 100, 200 or 500 μg/ml). The control cells were treated with growth medium only. After 24, 48 and 72 h incubation, 20 μl of 5 mg/ml MTT (3-[4, 5-dimethylthiazol-2-yl]-2, 5-diphenyl

tetrazolium bromide) solution was added, and then incubated at 37 °C for 4 h. Culture medium was then removed, and formazan crystals within cells solubilized by incubation with 0.2 ml DMSO for 10 min. Absorbance was measured at 490 nm on a SpectraMax M5 microplate reader, and cell viability calculated as (absorbance in the treatment well)/(absorbance in the control well) × 100%.

Cell uptake efficacy of BSA-LDH and BSA-LDH-GTA was determined by flow cytometry (BD LSM II). Twenty-four hours after cell seeding, the cells were treated with growth medium containing BSA-LDH-dsDNA-cy3 or BSA-LDH-dsDNA-cy3-GTA for 24 h (both contained the same amount of dsDNA-cy3). After centrifugation and washing with PBS for three times, the cells were fixed in 2% paraformaldehyde/PBS and analyzed on the flow cytometer.

In vivo fluorescence imaging

The feasibility of current surface modification for in vivo application was investigated. Cy7 labelled BSA-LDH-GTAs were prepared. Firstly, BSA was conjugated with excess amount of Cy7 through bifuncitonal Sulfo-SMCC and purified to get rid of free cy7. Then 10% BSA was substituted by BSA-Cy7 to ensure sufficient fluorescence absorbed, following the coating and crosslinking procedures described above, Cy7 labelled BSA-LDH-GTAs were obtained. The resulted nanoparticles were subjected to centrifugation and washed by milli-Q water to remove the excess BSA-Cy7. In vivo optical imaging experiments were performed on an In Vivo MS FX Pro instrument (Bruker Corporation). Cy7 images were collected with a 730 ± 20 nm excitation and 790 nm ± 20 nm emission filter set (f-stop 2.80, 4 × 4 binning, 120 mm FOV, 20 s exposure time). All images were batch exported as 16-bit TIFF images and images were processed by Image-J (National Institutes of Health) software. Fluorescence images were false coloured.

4.3 Results and Discussion

BSA-coated LDH nanoparticles and redispersity

As shown in Figure 4.1A and Figure 4.S1, after hydrothermal treatment, a monodispersed LDH nanoparticle suspension was obtained with an average hydrodynamic diameter of 105 nm and a Pdi of 0.211, in agreement with the previous report.[30] When the LDH suspension was added into electrolyte solution (e.g. PBS or culture medium), LDH nanoparticles formed aggregates

with the average particle size being in the micrometer range (>1000 nm) in PBS (not shown) and ~400 nm in culture medium (Figure 4.1A), respectively. Our previous work has successfully developed a BSA coating method to prevent aggregation of LDH nanoparticles in PBS or culture medium at BSA/LDH mass ratio of 5:2 where there were maximum 0.7 mg BSA adsorption on 1.0 mg LDH while there were 3.6 mg of free BSA in 1.0 ml aqueous suspension.[26] As shown in Figure 4.1A, the particle size distribution of BSA-LDH (5:2) in PBS or culture medium was similar to that of BSA-LDH originally suspended in water. These phenomena showed that coating LDH with BSA was able to prevent aggregation of LDH nanoparticles in electrolyte solutions. As we previously reported, the aggregation was probably due to the bridging effect of adsorbed serum from the medium or reduced electrostatic repulsion caused by adsorption of ions on the LDH surface that counteracts the intrinsic surface charge of LDHs. We believe that BSA coating probably provides a strong steric repulsion and is able to prevent LDH particle aggregation in electrolyte solutions and the culture medium.
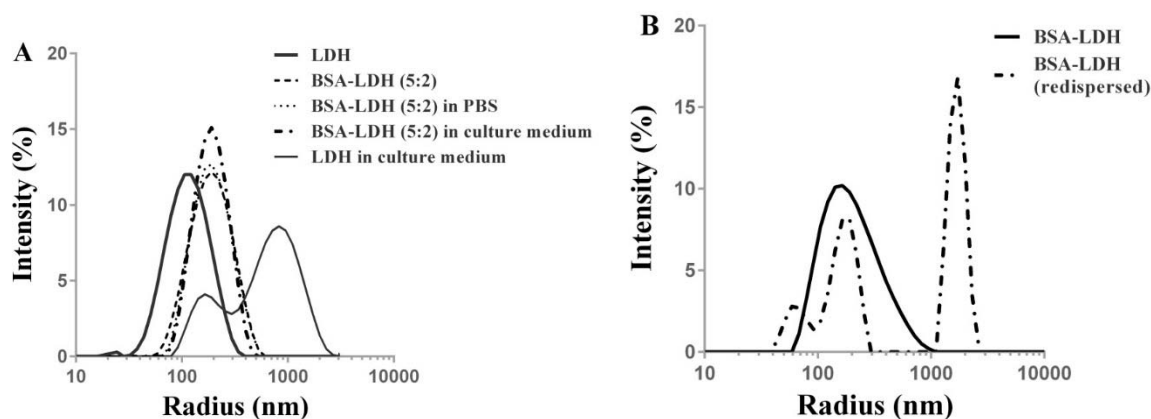
Figure 4.1 (A) Particle size distribution of LDH and BSA-LDH (5:2) in water, PBS or culture medium. Note: the size of LDH in PBS was over the measurement limit of Nanosizer and not shown here; (B) Particle size distribution of redispersed BSA-LDH after freeze-drying. Each experiment was carried out in 3 independent experiments.

Figure 4.1B shows the redispersion ability of BSA-LDH after centrifugation and freeze-drying compared with the initial BSA-LDH suspension. The data revealed that the redispersed BSA-LDH had many large aggregates with the size > 1000 nm, different from that in BSA-LDH suspension (average particle size of 171 nm). The BSA-LDH suspension contains many free BSA molecules, which are in adsorption equilibrium with the BSA adsorbed on the LDH surface, thereby maintaining colloidal stability. Freeze-drying following centrifugation

removes the free BSA from solution, preventing equilibrium being reached again during redispersion, resulting in incomplete dispersion. As freeze-drying techniques are an essential process in the manufacture pharmaceuticals, it is of great importance to enhance the redispersion ability of BSA-LDH complexes.

Colloidal stability of BSA- coated LDH nanoparticles

As shown in Figure 4.2, BSA-LDH (the BSA/LDH mass ratio = 5:2, the LDH concentration = 2000 µg/ml) had an average size of 176 nm and a Pdi of 0.229. When this BSA-LDH suspension was diluted 10 times (the LDH concentration = 200 µg/ml), the particle size distribution of BSA-LDH remained the same (the average size = 173 nm, and Pdi = 0.230). However, when the BSA-LDH suspension was continuously diluted, the particle average size increased to 298 nm (the LDH concentration = 12.5 µg/ml) and then 864 nm (the LDH concentration = 6.3 µg/ml). This aggregation can be again explained by the disturbed equilibrium between BSA adsorbed on LDH and free BSA in solution after dilution. With the addition of water, the concentration of free BSA in solution decreases and some adsorbed BSA desorbs from the surface to solution. As BSA desorption continues, LDH particles would share BSA molecules via the protein bridging effect, which leads to particle aggregation.
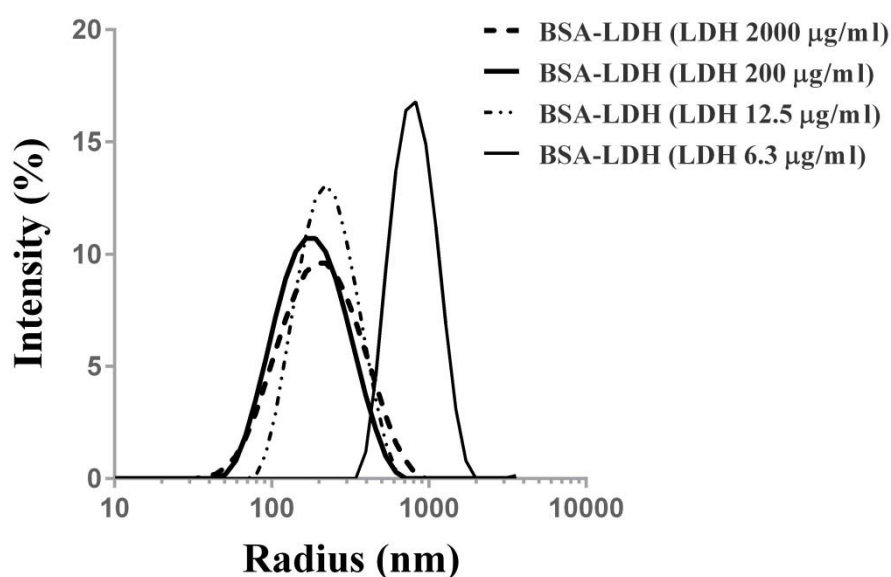
Figure 4.2 Particle size distribution of BSA-LDH (mass ratio of BSA: LDH = 5:2) at different concentrations. Each experiment was carried out in 3 independent experiments.

Enhanced colloidal stability by crosslinking BSA on the LDH surface

We next employed a crosslinking strategy to increase BSA-LDH stability and redispersity. First, the effectiveness of crosslinking BSA by using GTA was examined. The amount of unreacted amino groups deceased significantly with increasing GTA amount used (Table 4.1 and Figure 4.S2), indicating that there was a progressive degree of crosslinking.[31] After addition of 40 µl 5% GTA or more, very little change in the unreacted amino group number was observed, indicating that all available amino groups had participated in the GTA crosslinking.

Table 4.1 Free amino group in each BSA molecule after glutaraldehyde cross-linking. The number of amino groups on the crosslinked BSA was determined. GTA volumes of 1 to 100 µl for quantitative cross-linking of the 59 amino groups in the BSA molecules were employed in these tests.

5% Glutaraldehyde volume (µl)	Amino groups per BSA molecule	
	Mean	S.D.
1	37.24	1.30
2.5	34.93	0.58
5	33.04	1.42
10	18.76	0.31
20	6.09	0.57
30	2.51	0.52
40	1.77	1.29
60	1.79	0.72
80	2.01	0.53
100	1.71	1.43

To determine the optimized GTA concentration for stabilizing the BSA-LDH nanohybrids, a series of BSA: GTA molar ratios (1:0.5, 1:15, 1:45, and 1:135) were used and the obtained suspensions were subjected to dilution tests. As shown in Figure 4.3A and Table 4.S2, the average particle size of BSA-LDH-GTA was around 170 nm at the BSA/GTA ratio of 1:135 when diluted from 40 to 640 times. In all other cases (BSA: GTA molar ratio = 1:0.5, 1:15 and 1:45), the average particle size increased, indicating that some aggregation still took place even though the adsorbed BSA molecules were partly crosslinked. Therefore, the molar ratio of BSA: GTA (1:135) was applied in the following experiments.
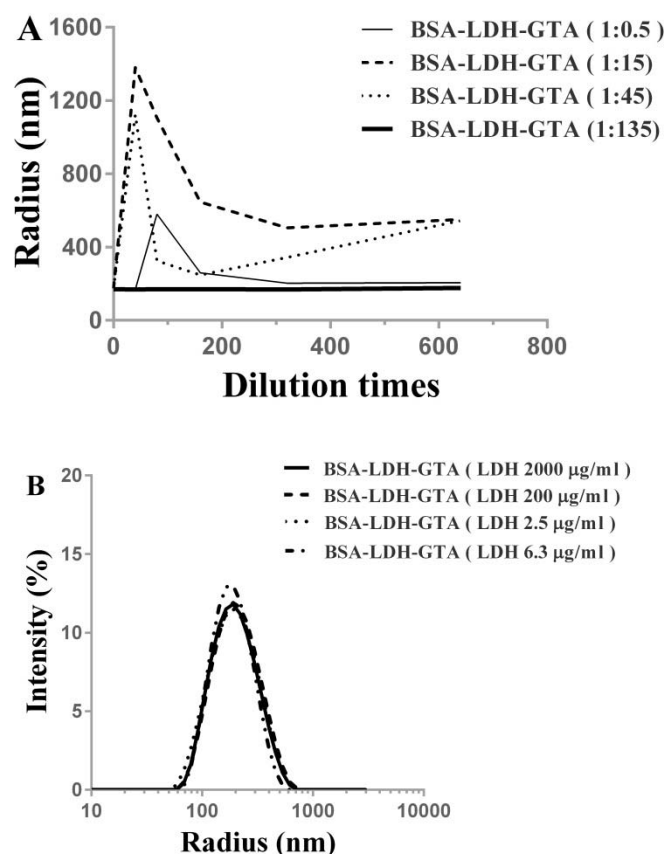
Figure 4.3 (A) The average particle size of BSA-LDH-GTA at different BSA: GTA molar ratios and dilution times; (B) The particle size distribution of BSA-LDH-GTA (the BSA: GTA molar ratio = 1:135) at different concentrations. Each experiment was carried out in 3 independent experiments.

The particle size distribution of BSA-LDH-GTA (1:135) also remained the same after 10-, 160- and 320-fold dilution (Figure 4.3B), in sharp contrast with that presented in Figure 4.2. This suggests that the crosslinking of surface adsorbed BSA by GTA can avoid/minimize the release of adsorbed BSA into solution, thus preventing LDH particles from aggregation caused by dilution. Interestingly, the BSA: GTA molar ratio of 1:135 corresponded to 5 μl 5% GTA (Table 4.1), which means that there were 33 amino groups available per BSA molecule after crosslinking. Therefore, the optimized BSA/GTA molar ratio of 1:135 ensures sufficient colloidal stability of the LDH nanoparticle system, and at the same time maintains an adequate number of free amino groups/BSA for further modification and/or loading.
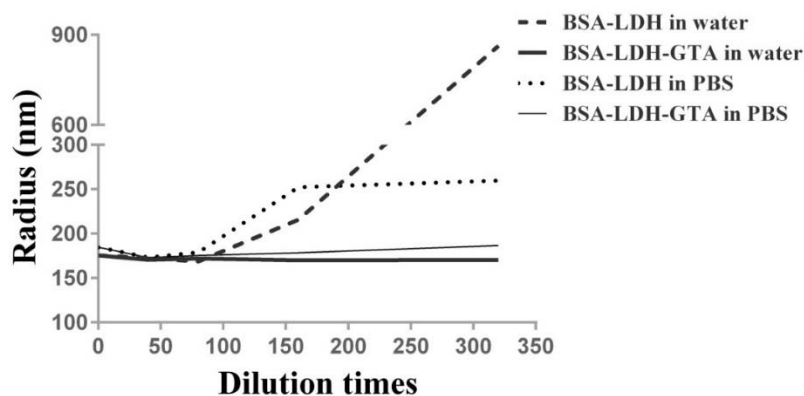
Figure 4.4 The average particle size of BSA-LDH or BSA-LDH-GTA at different LDH concentrations in water and PBS. Each experiment was carried out in 3 independent experiments.

As shown in Figure 4.4 and Table 4.S2, the average size of the initial BSA-LDH particles in water or PBS remained at about 175 nm when the suspension was diluted up to 80-fold, but increased dramatically when diluted 320-fold. In contrast, BSA-LDH-GTA nanohybrids remained the same size (around 180 nm) in both water and PBS when diluted. This stability can be attributed to the crosslinking of BSA, which immobilizes BSA onto the LDH surface and maintains the colloidal stability through steric repulsion. The comparison clearly demonstrates the enhancement of BSA-LDH colloidal stability through the crosslinking strategy.

Improved redispersity of BSA-LDH after crosslinking
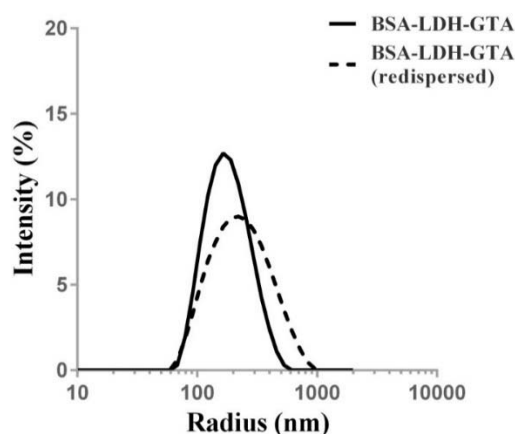
Figure 4.5 Particle size distribution of BSA-LDH-GTA and redispersed one. Each experiment was carried out in 3 independent experiments.

69

As shown in Figure 4.5 and Table 4.S1, the redispersity of freeze-dried BSA-LDH-GTA hybrids was obviously improved. After BSA-LDH-GTA hybrids were redispersed with gentle ultrasonication, the particle size distribution with an average particle size of 219 nm and a Pdi of 0.323 was very similar to that for the parent BSA-LDH-GTA hybrid. This redispersity is markedly better than that for un-crosslinked BSA-LDH (Figure 4.1B) under the same conditions. The crosslinked BSA on the LDH surface was now immobilized with a more rigid configuration, which may keep the freeze-dried particles better separated. As a result the BSA-LDH-GTA hybrids were more readily redispersed in water. This property is of importance to the pharmaceutical sector, because freeze-drying technique are essential for the storage and transport of pharmaceuticals.

Cytotoxicity of BSA-LDH-GTA

In general, the viability of cancer cell line, MCF-7, and smooth muscle cells (SMCs) after exposure to BSA-LDH-GTA (Figure 4.6A, B) gradually decreased with increasing particle size concentration and the incubation time.[29] The viability of SMCs treated with 10-100 µg/ml BSA-LDH-GTA did not change significantly after the first day of incubation, but decreased by 20 to 30% at day 2 to 3. However, a significant reduction in cell viability was observed in BSA-LDH-GTA at the concentrations of 200-500 µg/ml of BSA-LDH-GTA at day 2-3.

BSA-LDH-GTA at 10-200 µg/ml did not affect the MCF-7 cell viability significantly during the 3-day incubation period (> 80%), while 500 µg/ml significantly reduced their viability after 2 to 3 days. Compared with LDH's cytotoxicity reported previously (cell viability were over than 90% within 3 days incubation at the concentration range of 10-500 µg/ml),[32] BSA-LDH-GTA were slightly more toxic to SMCs, suggesting good biocompability. The increased cytotoxicity is possibly due to the unreacted aldehyde groups in GTA that are known to induce some toxicity.[33]

In most in vitro tests for drug and gene delivery,[30, 34, 35] the LDH concentration is normally in the range of 10-100 µg/ml. Thus this toxicity test has demonstrated that the BSA-LDH-GTA delivery platform has negligible toxicity for SMCs and the cancer cell line MCF-7 in our in vitro assay.
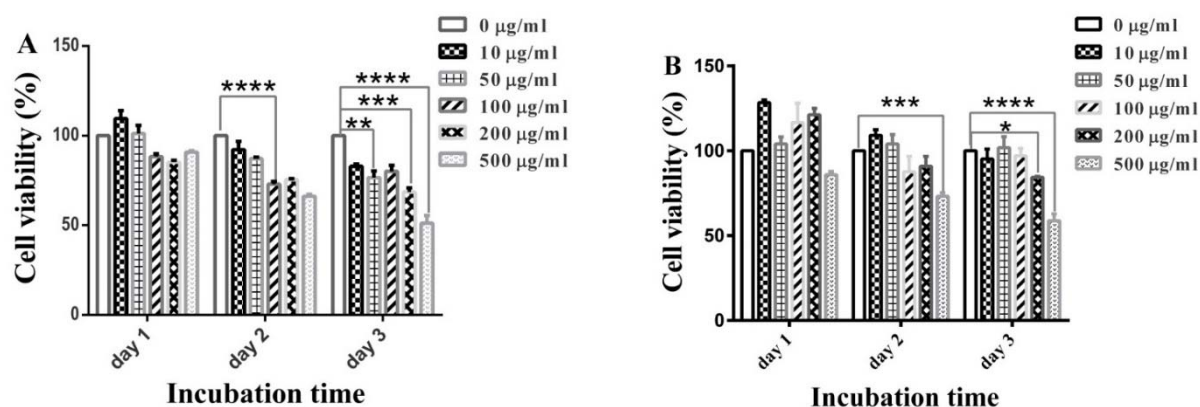
Figure 4.6 Cell viability of SMCs (A) and MCF-7 (B) after treated with BSA-LDH-GTA (BSA: GTA molar ratio = 1:135) at concentrations from 0 to 500 µg/ml. Statistics; each experiment was carried out in duplicate and 3 independent experiments were performed. The data are presented as the mean ± SEM. One-way ANOVA with Bonferroni's post-hoc test was used to assess statistical significance. * $p < 0.05$, ** $p < 0.01$, *** $p < 0.001$, **** $p < 0.0001$.

Cellular uptake
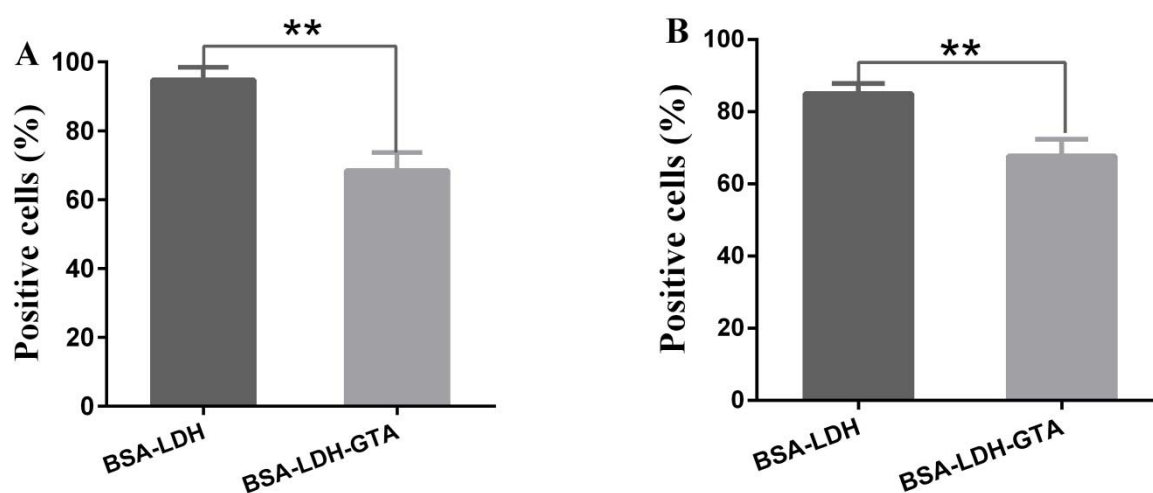
Figure 4.7 Histogram showing (A) the percentage of SMCs cells internalizing BSA-LDH or BSA-LDH-GTA and (B) the percentage of MCF-7 cells internalizing BSA-LDH or BSA-LDH-GTA monitored by flow cytometry. Statistics; each experiment was carried out in duplicate and 3 independent experiments were performed. The data are presented as the mean ± SEM. T-test was used to assess statistical significance. * $p < 0.05$, ** $p < 0.01$, *** $p < 0.001$, **** $p < 0.0001$.

According to our previous report, a five-fold excess of LDH nanoparticles is sufficient to ensure maximum association of dsDNA with LDHs.[36] The conditions required for the same amount of dsDNA intercalation were confirmed by gel electrophoresis (Figure 4.S3). Therefore, the LDH: dsDNA mass ratio of 40:1 was used to ensure BSA-LDH and BSA-LDH-GTA to contain the same amount of dsDNA.

As shown in Figure 4.7, after 24 h incubation, the percentage of SMCs internalizing fluorescent BSA-LDH-dsDNA-cy3-GTA particles was about 67%, ~30% lower than that for cells internalizing BSA-LDH-dsDNA-cy3 (96%). MCF-7 cells took up 17% less BSA-LDH-dsDNA-cy3-GTA particles (68%) than BSA-LDH-dsDNA-cy3 (85%). The results indicate that GTA crosslinking inhibits cell uptake efficiency to some degree compared to uncrosslinked nanoparticles. The possible reason is loss of functional positive amino groups on the surface of BSA-LDH nanoparticles after crosslinking. The positive charges on the particle surface increases cell surface affinity. As previously reported, increasing the amount of amine groups facilitates cellular uptake of nanoparticles for various cell lines.[37] Although BSA-LDH-GTA showed slight inhibition to cell uptake compared to BSA-LDH, the GTA crosslinking strategy provides much higher colloidal stability and much easier redispersity of LDH nanoparticles for more potential bioapplications in vivo.

In order to further confirm the stability of BSA-LDH-GTAs in in-vivo assay, intravenous injection of BSA-LDH-GTA nanoparticles into the tail vein of mice, optical imaging experiments were conducted to study the biodistribution behaviour of the nanoparticles in vivo over a long imaging times. In this study, fluorescence images of the belly and the back side of the mice were taken to display organ signals at the respective areas in the body. Figure 4.8A shows the fluorescence intensity of the optical imaging agent within the mice over a 48 h time course. Ex vivo study at 24 h and 48 h (Figure 4.8B) were used to validate the information obtained from the in vivo images. High fluorescence signal for BSA-LDH-GTA nanoparticles were observed in organs such as the liver, gut, kidney and spleen which are responsible for clearance and excretion. The distribution in the RES system other than the non-RES system was likely a direct consequence of activation of the RES clearance mechanism for the particles. Besides, the size of the current nanoparticles may also contribute to the accumulation in the liver area, as it was evidenced in many reports that the particles with around 50-200 nm tend to arrive at fenestration in the hepatic sinusoidal endothelium after intravenous injection.[38, 39]
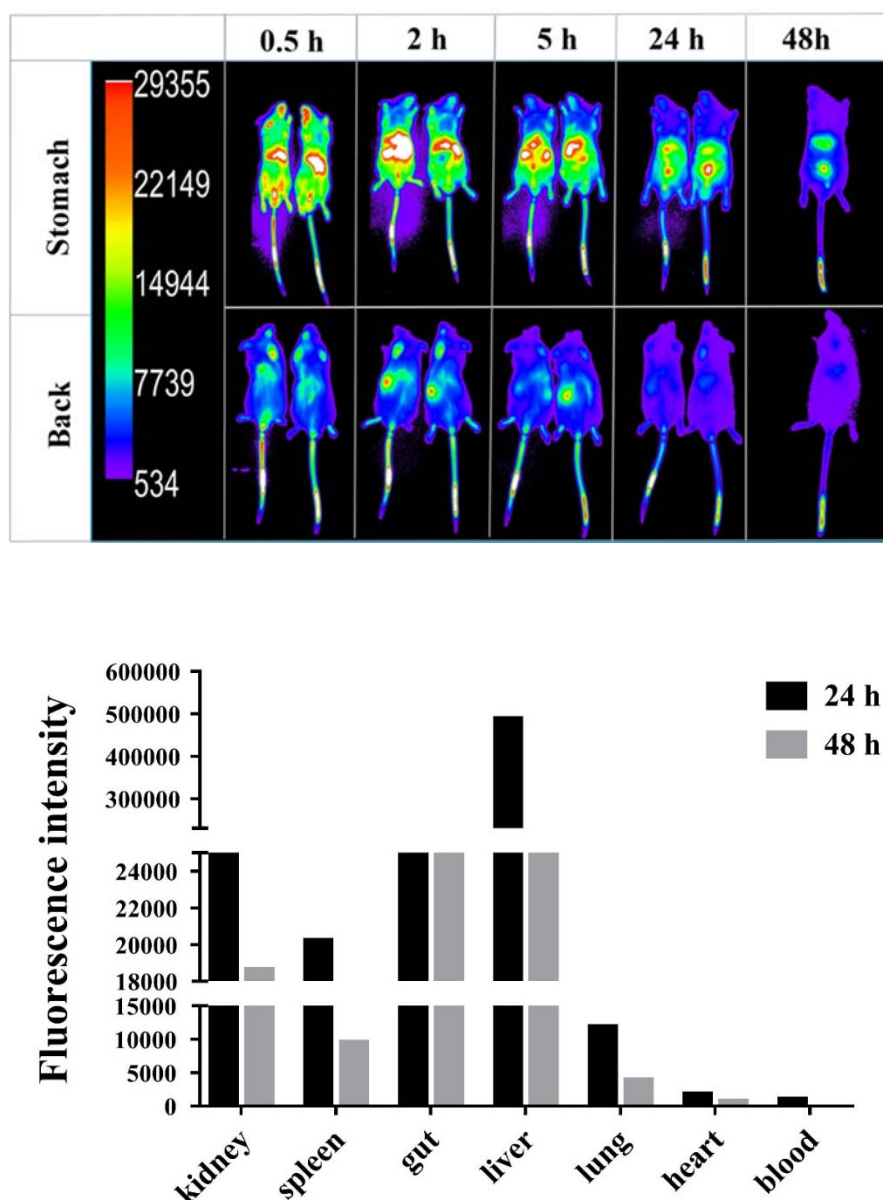
Figure 4.8 In vivo fluorescence mice image (front and back side) of BSA-LDH-GTA at 0.5, 2, 5, 24, and 48 h time courses. (II) Fluorescence intensity of organs 24hr and 48 hr post injection.

As can be observed in the Figure 4.8A, the fluorescence signal in the kidney area and bladder region can be detected following injection, implying that part of the nanoparticles experienced clearance by renal excretion. As the size of current nanoparticles have been above the renal threshold and are not able to be cleared by the kidneys, therefore, the BSA-LDH-GTAs may experience dissolution during the circulation as there was continue decrease in this signal

during 48 h. As for in vivo fluorescence imaging, the signal are always interfered by autofluorescence generated by the mice body itself, therefore, in this study a fluorophore Cy7 that can be excited in the 600–900 nm range was exploited since the biological tissues are relatively transparent in this spectral region.[40, 41] In-vivo and ex-vivo biodistribution results together indicate the feasibility of Cy7/BSA-LDH-GTAs stability for in vivo study and the clearance was through multiple pathways from the body. Thus, the current LDH engineering method with simpler conjugation process and purification procedures is flexible and adaptable for in vivo application through intravenous injection.

4.4 Conclusion

Size control of LDH nanoparticles is a challenging problem for clinical applications. This work introduced a crosslinking strategy to stabilize LDH nanoparticles based on the previous BSA coating strategy. As crosslinked BSA-coated LDH hybrids had improved colloidal stability and redispersity of freeze-dried samples. Although the cytotoxicity of BSA-LDH-GTA increased especially at the concentration of 500 μg/ml when compared to LDH cytotoxicity, the cytotoxicity of BSA-LDH-GTA at concentrations of 10-200 μg/ml had minimal effect. Importantly, our modified LDH nanoparticles can be further conjugated with functional molecules to promote target delivery to specific cells types, therefore, in the cell, drug or gene could be released from the NPs via change with electrolytes and dissolution of LDH in acid conditions and accumulated in the target cells. Overall, this new crosslinking strategy promises a more stable BSA coated LDH nanoparticles system with broad applications in vitro and in vivo. As for in vivo fluorescence imaging, the signal are always interfered by autofluorescence generated by the mice body itself, therefore, in this study a fluorophore Cy7 that can be excited in the 600–900 nm range was exploited since the biological tissues are relatively transparent in this spectral region.[40, 41] In-vivo and ex-vivo biodistribution results together indicate the feasibility of Cy7/BSA-LDH-GTA stability for in vivo study and the clearance was through multiple pathways from the body. Thus, the current LDH engineering method with simpler conjugation process and purification procedures is flexible and adaptable for in vivo application through intravenous injection.

4.5 References

1. Park, K.; Lee, S.; Kang, E.; Kim, K.; Choi, K.; Kwon, I. C., Advanced functional materials 2009, 19 (10), 1553-1566.

2. Steichen, S. D.; Caldorera-Moore, M.; Peppas, N. A., European Journal of Pharmaceutical Sciences 2013, 48 (3), 416-427.

3. I Lynch, A. S., KA Dawson Nature nanotechnology 2009 4(9), 546.

4. A. E. Nel, L. M. a., D. Velegol, T. Xia, E. M. V. Hoek,; P. Somasundaran, F. K., V. Castranova and; M. Thompson, Nat. Mater., 2009,, 8(7), , 543.

5. Vera Hirsch, a. C. K., a Marc Moniatte,d Barbara Rothen-Rutishauser,ac; Fink*ab, M. J. D. C. a. A., Nanoscale, 2013, 5, 3529–3994.

6. Zhang, L.; Gu, F.; Chan, J.; Wang, A.; Langer, R.; Farokhzad, O., Clinical Pharmacology & Therapeutics 2007, 83 (5), 761-769.

7. Acid-Paclitaxel, H.-F., a Targeting Nanoparticle, Enhances Specific Delivery of Paclitaxel to Folate Receptor-Positive Tumors Wang. Xu.

8. Davis, M. E., Nature reviews Drug discovery 2008, 7 (9), 771-782.

9. Choy, J.-H.; Kwak, S.-Y.; Jeong, Y.-J.; Park, J.-S., Angewandte Chemie 2000, 39 (22), 4041-4045.

10. Xu, Z. P.; Walker, T. L.; Liu, K.-l.; Cooper, H. M.; Lu, G. M.; Bartlett, P. F., International journal of nanomedicine 2007, 2 (2), 163.

11. Wong, Y.; Markham, K.; Xu, Z. P.; Chen, M.; Lu, G. Q. M.; Bartlett, P. F.; Cooper, H. M., Biomaterials 2010, 31 (33), 8770-8779.

12. Braterman, P. S.; Xu, Z. P.; Yarberry, F., Layered Double Hydroxides (LDHs). In Handbook of Layered Materials, Auerbach, S. M.; Carrado, K. A.; Dutta, P. K., Eds. Marcel Dekker: New York, 2004; pp 373-474.

13. Ferruccio Trifiro, A. V., Hydrotalcite-like anionic clays. In Comprehensive supramolecular chemistry Jerry L. Atwood, J. E. D. D., David D. Macnicol, Fritz Vogtle, Ed. Pergamon Press: New York, 1996; pp 251-291.

14. Xu, Z. P.; Niebert, M.; Porazik, K.; Walker, T. L.; Cooper, H. M.; Middelberg, A. P. J.; Gray, P. P.; Bartlett, P. F.; Lu, G. Q., Journal of Controlled Release 2008, 130 (1), 86-94. DOI 10.1016/j.jconrel.2008.05.021.

15. Gu, Z.; Atherton, J. J.; Xu, Z. P., Chemical Communications 2015.

16. Gu, Z.; Rolfe, B. E.; Xu, Z. P.; Campbell, J. H.; Lu, G.; Thomas, A. C., Advanced healthcare materials 2012, 1 (5), 669-673.

17. Gu, Z.; Thomas, A. C.; Xu, Z. P.; Campbell, J. H.; Lu, G. Q., Chemistry of Materials 2008, 20 (11), 3715-3722.

18. Gu, Z.; Wu, A.; Li, L.; Xu, Z. P., Pharmaceutics 2014, 6 (2), 235-248.

19. Xu, Z. P.; Zeng, Q. H.; Lu, G. Q.; Yu, A. B., Chem. Eng. Sci. 2006, 61 (3), 1027-1040.

20. Xu, Z. P.; Lu, G. Q., Pure Appl. Chem. 2006, 78 (9), 1771-1779.

21. Gu, Z.; Rolfe, B. E.; Thomas, A. C.; Campbell, J. H.; Lu, G. Q.; Xu, Z. P., Biomaterials 2011, 32 (29), 7234-7240. DOI 10.1016/j.biomaterials.2011.05.083.

22. Yu, W.; Xie, H., Journal of Nanomaterials 2012, 2012, 1.

23. Kvitek, L.; Panáček, A.; Soukupova, J.; Kolar, M.; Vecerova, R.; Prucek, R.; Holecová, M.; Zboril, R., The Journal of Physical Chemistry C 2008, 112 (15), 5825-5834.

24. Turkevich, J., Gold Bulletin 1985, 18 (4), 125-131.

25. Zhang, X.; Servos, M. R.; Liu, J., Journal of the American Chemical Society 2012, 134 (24), 9910-9913.

26. Gu, Z.; Zuo, H.; Li, L.; Wu, A.; Xu, Z. P., Journal of Materials Chemistry B 2015, 3 (16), 3331-3339.

27. Semenov, A., Macromolecules 2008, 41 (6), 2243-2249.

28. Hennink, W.; Van Nostrum, C., Advanced drug delivery reviews 2012, 64, 223-236.

29. Gu, Z.; Rolfe, B. E.; Xu, Z. P.; Thomas, A. C.; Campbell, J. H.; Lu, G. Q., Biomaterials 2010, 31 (20), 5455-5462.

30. Xu, Z. P.; Lu, G., Pure and applied chemistry 2006, 78 (9), 1771-1779.

31. Weber, C.; Coester, C.; Kreuter, J.; Langer, K., Int. J. Pharm. 2000, 194 (1), 91-102.

32. Gu, Z.; Rolfe, B. E.; Xu, Z. P.; Thomas, A. C.; Campbell, J. H.; Lu, G. Q. M., Biomaterials 2010, 31 (20), 5455-5462.

33. Lim, H.-G.; Kim, G. B.; Jeong, S.; Kim, Y. J., The Korean journal of thoracic and cardiovascular surgery 2014, 47 (4), 333.

34. Xu, Z. P.; Niebert, M.; Porazik, K.; Walker, T. L.; Cooper, H. M.; Middelberg, A. P.; Gray, P. P.; Bartlett, P. F.; Lu, G. Q. M., Journal of Controlled Release 2008, 130 (1), 86-94.

35. Wong, Y.; Cooper, H. M.; Zhang, K.; Chen, M.; Bartlett, P.; Xu, Z. P., Journal of colloid and interface science 2012, 369 (1), 453-459.

36. Ladewig, K.; Niebert, M.; Xu, Z. P.; Gray, P. P.; Lu, G. Q., Biomaterials 2010, 31 (7), 1821-1829.

37. Kettler, K.; Veltman, K.; van de Meent, D.; van Wezel, A.; Hendriks, A. J., Environmental Toxicology and Chemistry 2014, 33 (3), 481-492.

38. Li, F.-Q.; Su, H.; Wang, J.; Liu, J.-Y.; Zhu, Q.-G.; Fei, Y.-B.; Pan, Y.-H.; Hu, J.-H., International journal of pharmaceutics 2008, 349 (1), 274-282.

39. Ernsting, M. J.; Murakami, M.; Roy, A.; Li, S.-D., Journal of Controlled Release 2013, 172 (3), 782-794.

40. Lee, C. H.; Cheng, S. H.; Wang, Y. J.; Chen, Y. C.; Chen, N. T.; Souris, J.; Chen, C. T.; Mou, C. Y.; Yang, C. S.; Lo, L. W., Advanced Functional Materials 2009, 19 (2), 215-222.

41. Weissleder, R., Nature biotechnology 2001, 19 (4), 316-317.

Supplemental information

The redispersion ability and size distribution of GTA cross-linked and BSA pre-coated LDH nanoparticles were tested in order to study their potential application as drug/gene carriers. From the PCS measurements, the mean diameter of the LDH nanoparticles was around 100nm, with a monodispersed size distribution. The particle size of the nanoparticles was greatly increased when the BSA was coated. Table S1 shows that the size of the BSA-LDH nanoparticles almost has no change after cross-linked by GTA. However, the zeta potential decreased that might due to the losing of amino groups.

Table 4.S1 Particle average dimension (nm) of BSA-LDH and BSA-LDH-GTA

Sample	Size (d.nm)/Pdi	Zeta potential (mV)	redispersed
LDH	105.2/0.211	35.0	-
BSA-LDH	171.1/0.198	-22.9	>2000/1.0
BSA-LDH-GTA	174.7/0.195	-25.8	219/0.323

As shown in Figure 4.S1, after hydrothermal treatment, a nanodispersed LDH nanoparticles suspension was obtained. The nanoparticles are well-dispersed with narrowly distributed hydrodynamic diameter of 90-110 nm by PCS.

The average diameter measured by PCS is in accordance with the TEM image (90-150 nm) where the morphology of such prepared LDH nanoparticles is monodispersed and well hexagonally shaped as shown in Figure 4.2B which is consistent with previous report.[34]
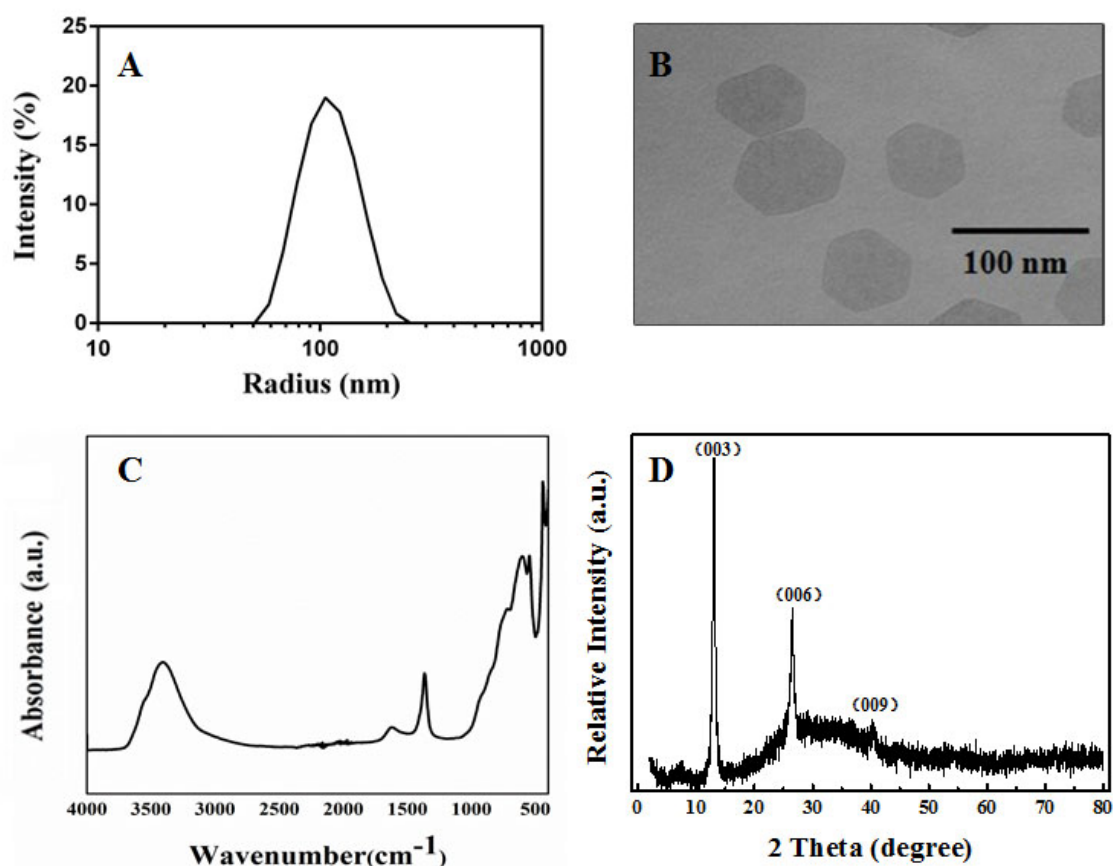
Figure 4.S1 A) Particle size distribution of LDHs; B) TEM images of LDH nanoparticles; C) FT-IR spectrum of LDH nanoparticles; D) XRD pattern of LDH nanoparticles.

LDH FTIR spectrum shows some peaks commonly appearing in MgAl-LDH spectra: (1) the intense broad band around 3400-3500 cm^{-1} associated with stretching vibration of O-H in the brucite-like layer and water molecules; (2) the sharp band at 1363 cm^{-1}; (3) the peak at 447 cm^{-1}, particularly characteristic of Mg$_2$Al-LDH materials.[17, 34]

XRD shows the pattern of the LDHs are typical of lamellar materials, characterized with basal reflections, associated harmonics at low 2θ angles and weaker nonbasal reflections at higher angles. The LDH is well-crystallized, as reflected by the sharp (003) and (006) basal reflections as well as (009) peaks.

Table 4.S2 Crosslinking effects on BSA-LDH system stability in PBS at different concentrations

Dilution times	BSA-LDH		BSA-LDH-GTA	
	In water (nm)	In PBS (nm)	In water (nm)	In PBS (nm)
0	175.5	184.7	175.5	184.7
5	172.5	173.2	170.5	172.9
160	215.8	252.3	170.1	178.4
320	863.9	259.9	170.5	186.7
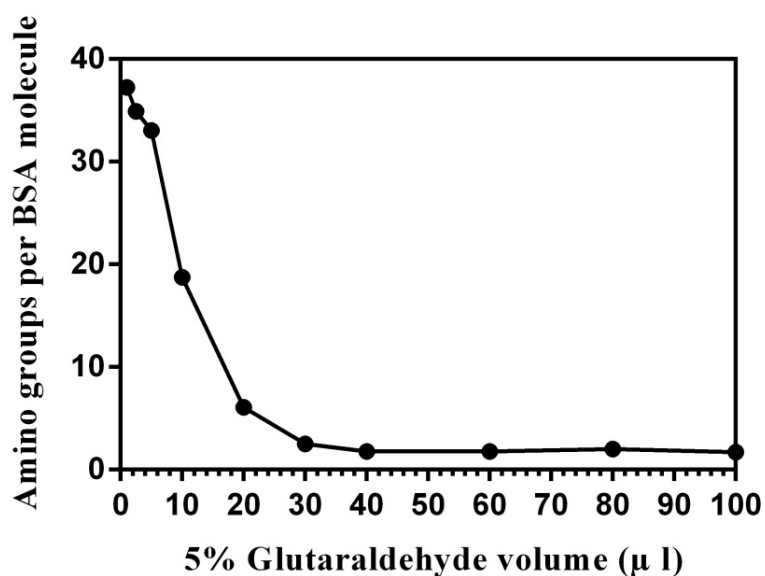
Figure 4.S2 Crosslinking of BSA with different amounts of GTA: amino group content in the solution of the BSA in correlation to the amount of GTA added. GTA volume between 1.0 and 100 μl of the theoretic amount for quantitative cross-linking of the 59 amino groups in the BSA molecule were employed.
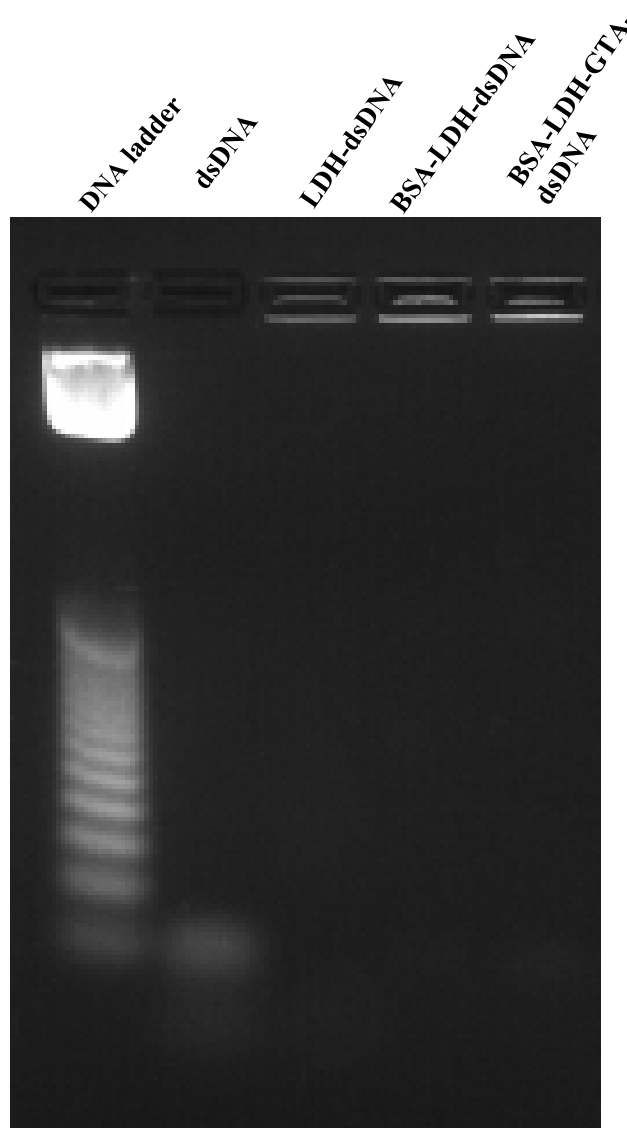
Figure 4.S3 Gel retardation assay of complexes of dsDNA with LDH, BSA-LDH, BSA-LDH-GTA at weight ratios 40:1 (LDH/dsDNA).

As shown in Figure 4.S3, the same dsDNA loading amount was achieved at a mass ratio of 40:1 (40 mg LDH: 1 mg dsDNA) when intercalation was carried out at 37 °C for overnight (Figure 4.S3). Therefore, in the following cell uptake assay, weight ratios 40:1 (LDH/dsDNA) was used to ensure BSA-LDH and BSA-LDH-GTA contain same amount of dsDNA.

Chapter 5

Surface functionalization of stabilized layered double hydroxide nanoparticles with ligands: benefit of adding targeting ligands via bovine serum albumin

In this section, non-viral layered double hydroxide nanoparticles (LDHs) were modified as a target delivery system. Two brain tumour targeting ligands, i.e. angiopep-2 (Ang2) and rabies virus glycoprotein peptide (RVG), were conjugated to the LDHs, respectively, through inter-matrix bovine serum albumin (BSA), rendering the LDHs simultaneously excellent colloidal stability and targeting capability. Two ligands were first conjugated with BSA through crosslinker sulfo-SMCC, respectively. Following our previous BSA coating and glutaraldehyde (GTA) crosslinking strategies, we successfully developed an approach to prepare colloidally-stabilised tumour-targeted LDH nanoparticles. The targeting efficacy of ligand-conjugated LDH delivery system was demonstrated in the uptake by two brain tumour cells (U87 and N2a) compared to unmodified LDHs, while the cellular uptake mechanism was similar. Importantly, ligand modified LDHs demonstrated increased anti-proliferation compared with unmodified LDHs. This new approach may contribute to rational design of targeted nanoparticles, showing great potential as a promising platform for selective and effective therapeutic treatment of neural diseases.

5.1 Introduction

Nanomaterials and colloidal drug delivery systems are believed to preferentially accumulate in the tumour area due to enhanced permeation and retention (EPR) effect.[1] To grow quickly, the tumour cells tend to stimulate blood vessel formation which is called angiogenesis. Such neovasculature with the abnormal form and architecture leads to leakage of vessels and dyfunctional lymphatic drainage, therefore, nanocarriers can extravasate into the tumour site via the defective vessels by the EPR effect.[2,3] However, the challenge is confounded by the fact that nanoparticles ubiquitously intercellular distribution within a tumour may fail the cancer treatment due to suboptimal cellular uptake efficacy.[4] Efficient and specific cell uptake is the priority for optimising treatment. Normally, cancer cells have expressed a number of receptors, which uniquely interact with specific ligands. Comparatively, decorating the nanopaticulate system with a specific targeting ligand is expected to promote the cell internalisation rate after extravasation and ultimately improve therapeutic efficacy. Moreover, active targeting greatly reduces the random distribution in the healthy tissue, thereby reducing undesired systemic side effect.[5]

Layered double hydroxides (LDHs), also known as anionic clays or hydrotalcite-like materials, are a class of two dimensional synthetic lamellar compounds that are made up of positively charged layers with an interlayer region containing charge-balanced anions and water molecules. The structure is brucite-like ($Mg(OH)_2$), where the hydroxyl anions are hexagonally closely packed with divalent magnesium cations filling all octahedral sites. Consequently, each magnesium cation is surrounded by six hydroxyl groups to form an octahedron, and octahedra share edges to form an infinite 2-D layer. The brucite layers are held together by weak hydrogen bonds and stacked on top of one another. Part of the cations can be isomorphically replaced by trivalent cations with similar size, giving positively charged sheets, which results in an LDH structure. LDHs have a general formula $[M^{2+}_{1-x} M^{3+}_x (OH)_2]^{x+} (A^{n-})_{x/n} \cdot mH_2O$, where M represents metal cations and A stands for interlayer anions. LDHs have attracted extensively clinical attention due to biocompatibility and potential therapeutic biomolecule delivery ability.[6-8] Till now, due to the colloidal instability of LDHs in the biological environment, most reports focus on in vitro cellular delivery, and ligand modification of LDHs for potential in vivo work with targeting capability has been progressed slowly.

Normally, active targeting ligands can be attached onto the nanocarriers surface through various conjugation strategies, and many researches have been devoted into this area.[9] The

traditional modification of LDH nanoparticles with targeting ligands involves serial chemical reactions either in organic solvent or electrolytic solution.[10,11] In general, for in situ surface functionalization of ligands onto nanoparticles, an excess amount of reactants are required for sufficient chemical reactions. Moreover, the ligand-modified nanoparticles fail to be precisely engineered in a meaningfully repeatable manner and easily varied from batch to batch, eventually triggering unpredictable therapeutic effect.[10,11]

In some cases, inter-matrix biomaterials were pre-conjugated with ligands and then applied to functionalize the nanoparticles with targeting ability. The pre-functionalization of biomaterials render desired nanoparticles with reduced fabrication and purification procedures, enabling narrowly variation from batch to batch.[12] Previously, we developed a strategy to improve the colloidal stability of LDHs by coating bovine serum albumin (BSA) onto LDHs surface. As-formed BSA-LDH complexes were colloidally stable in various electrolyte solutions. Further cross-linking of BSA made the complexes to be even colloidally stable and easily dispersed in electrolyte solutions after freeze-drying.[13] Based on these findings, we proposed a new strategy to conjugate angiopep-2 (Ang2) and rabies virus glycoprotein peptide (RVG) ligands to BSA and enable LDHs to target U87 glioma cells and Neuron 2a (N2a) cells, respectively in this research. It is known that Ang2 and RVG ligands can bind to low density lipoprotein (LRP) receptors and nicotinic acetylcholine receptors (nAchR) that are widely expressed in U87 and N2a cells respectively. Interestingly, the receptors for Ang2 and RVG also overexpressed in the brain endothelial cells which mainly form the blood brain barrier,[14,15] and our LDHs is expected to target these cells and help pass through blood brain barrier.

Therefore, the objectives of this research were to: (1) control-prepare BSA-coated LDH nanoparticles with Ang2/RVG ligand conjugated in a designed number; (2) ascertain that target ligands on the LDH surface enhance delivery to U87 and N2a cells; (3) investigate the effect of target ligands on the cellular uptake mechanism, and (4) confirm that target ligand enhances the cytotoxicity of drug-LDH nanoparticles. The current methods for LDHs surface modification may provide a feasible way to apply LDH nanoparticle for target in vivo delivery.

5.2 Experimental section

5.2.1 Materials

Complementary strands of dsDNAs were purchased from GeneWorks and annealed at 75°C for 10 min. One strand of the duplex was covalently coupled to the Cy3 fluorophore at the 5′end before annealing. Glutaraldehyde (GTA) solution (25%) was bought from Ajax Finechem, and sulfo-SMCC (sulfosuccinimidyl 4-[N-maleimidomethyl] cyclohexane-1-carboxylate) and other chemicals were from Sigma-Aldrich if not illustrated specifically. Water used in experiments was deionized Milli-Q water. Angiopep-2 (Ang2: TFFYGGSRGKRNNFKTEEYC) and Rabies virus glycoprotein (RVG: YTIWMPENPRPGTPCDIFTNSRGKRASNGC) peptide were purchased from Biomatik. Sulfo-SMCC (MW =436 Da) was obtained from Sigma-Aldrich. Amicon ultra-0.5 centrifugal filter units were purchased from Millipore Company. All the other solvents were of analytical or chromatographic grade.

5.2.2 Synthesis of peptide-modified LDH delivery system

Synthesis of LDH nanoparticles and LDH-5-FU

Mg_2Al-Cl-LDH (pristine LDH) was prepared using a co-precipitation-hydrothermal treatment method, as reported previously.[16-18] In brief, LDH was synthesised by mixing 40 ml NaOH solution (0.15 M) with 10 ml salt solution containing $MgCl_2$ (3.0 mmol) and $AlCl_3$ (1.0 mmol) under vigorous stirring. The resultant precipitate was washed and then hydrothermally treated at 100 ºC for 16 h, giving an LDH suspension with the mass concentration of 4.0 mg/ml. The 5-FU/Mg_2Al-LDH hybrid (5-FU/LDH) was synthesised via ion exchange, prior to hydrothermal treatment. In this process, the resultant precipitate was collected and resuspended in 40 mL of the basic solution containing 0.3 mmol of 5-FU (neutralized with dilute NaOH solution, with pH 8–9) under stirring for 1 h. After washing two times, the suspension was transferred to an autoclave (stainless steel with a teflon lining) and incubated at 100°C for 16 hours. After hydrothermal treatment, a transparent, homogeneous 5-FU/LDH suspension was obtained.[19,20] The loading amount of 5-FU drug was determined using UV-Vis at 265 nm.

BSA activation and conjugation with peptides

10 mg/ml BSA solution in conjugation buffer (phosphate-buffered saline:100 mM sodium phosphate, 150 mM sodium chloride, 3 mM EDTA, pH 7.2) was Size/Pdi and added to a solution containing 10-fold molar excess of sulfo-SMCC crosslinker over the amount of BSA

protein to activate sufficient maleimide groups and conjugate sulfhydryl-containing Ang2/RVG peptides with BSA. The reaction of the maleimide groups and the thiol groups proceeded rapidly and selectively under mild coupling conditions (pH 6.5-7.5) to yield a stable, covalently linked 10 mg/ml of Ang2/RVG-SMCC-BSA conjugate. The resulting complex was purified by Millipore ultrafiltration tube with a molecular weight cutoff (MWCO) of 30 KD to get rid of the free excess peptide and salts.

Characterisation of ligand number

Matrix Assisted Laser Desorption Ionization—Time of Flight (MALDI-TOF) and Ellman's reagent 5, 5'-dithio-bis-(2-nitrobenzoic acid), also known as DTNB, were used for quantitating the molecular weight or free sulfhydryl groups in solutions before and after BSA activation and peptide conjugation. MALDI-TOF mass spectra were obtained using a Bruker Autoflex III Smartbeam TOF/TOF 200. All spectra were recorded in linear mode. For testing, a matrix thin layer on a ground steel target using matrix solution I (Sinapinic Acid saturated in EtOH) was prepared. Equal volumes (2 μl each) of sample solution and matrix solution II (Sinapinic Acid saturated in TA30) was pre-mixed and 0.5 μl of this mixture was applied on top of the matrix thin layer prepared. The number-average molecular weight (MW) and weight-average molecular weight (MW) were calculated from the MALDI-TOF spectra using Data Explorer software (Applied Biosystems, Framingham, MA). The number of thiol groups before and after BSA conjugation with peptides was calculated by the changes of the DTNB concentration. DTNB reacts with free thiol groups to yield a mixed disulfide and 2-nitro-5-thiobenzoic acid (TNB), where the TNB has a high molar extinction coefficient at 412 nm. During the test, 125 ul tested sample was mixed with 50 μl of Ellman's reagent solution and 2.625 ml of reaction buffer (0.1M sodium phosphate, pH 8.0, containing 1mM EDTA) and left to react for 15 mins at room temperature. As a blank, 125 μl of reaction buffer was added instead of the tested sample. The absorbance at 412 nm was then measured.

Preparation of NPs and Ang2/RVG-NPs with or without 5-FU

Two millilitres of 4 mg/ml LDH or LDH-5-FU suspension was added into 2 ml 10 mg/ml of BSA (or BSA mixed with BSA-Ang2/RVG at a mass ratio of 19:1) stock solution drop by drop with vigorously magnetic stirring for 30 mins to ensure saturated adsorption. Then the adsorbed BSA was crosslinked by glutaraldehyde overnight as previous reported.[13,21] The resulted Ang2/RVG-modified and unmodified nanoparticles were named as Ang2/RVG-NPs (5-

FU/Ang2-NPs or 5-FU/RVG-NPs) and NPs (5-FU/NPs), respectively. Nanoparticles were subjected to centrifugation and washed by milli-Q water to remove the excess BSA-SMCC-Ang2/RVG before conducting cellular uptake.

Preparation of NPs and Ang2/RVG-NPs loaded with dsDNA-Cy3

Loading dsDNA-Cy3 onto NPs and Ang2/RVG-NPs was similar to the preparation of LDH/dsDNA as reported previously.[6,22] Briefly, dsDNA-Cy3 loaded nanoparticles were prepared by adding dsDNA-Cy3 to the Ang2/RVG-NPs and NPs at an LDH/dsDNA mass ratio of 40:1. The obtained dsDNA-Cy3 loaded NPs and Ang2/RVG-NPs were then cross-linked by glutaraldyhyde overnight as previously interpreted.[13] The acquired nanoparticles were subjected to centrifugation and washed by Milli-Q water to remove the excess BSA-SMCC-Ang2/RVG before conducting cellular uptake test.

Characterisation of physicochemical properties

The hydrodynamic size and the surface charge (zeta potential) of LDH NPs, Ang2-NPs and RVG-NPs were characterised with a Nano Zetasizer instrument utilizing dynamic light scattering (DLS).

5.2.3 In-vitro assays

Cell line

The U87 cell line was obtained from the QIMR Berghofer medical research institute. U87 cells were cultured in RPMI medium, supplemented with 10% FBS, 100 U/ml penicillin and 100 μg/ml streptomycin. The Neura 2a (N2a) cells were obtained from the Queensland brain institute and cultured in DMEM medium, supplemented with 10% FBS, 100 U/ml penicillin and 100 μg/ml streptomycin. All cells were cultured in incubators maintained at 37 °C with 5% CO_2 under fully humidified conditions. All cell experiments were performed in the logarithmic phase of growth.

Cellular uptake assay

U87 and N2a cells were seeded at a density of 1×10^5 cells/well in 12-well plates (Corning Coaster) and incubated for 24 h. Then U87 and N2a cells were incubated with dsDNA-Cy3 labelled Ang2/RVG-NPs and NPs at the dsDNA-Cy3 concentration range of 20-120 μM for 2

h at 37 °C. Cells without any treatment were used as control. Time dependent cellular uptake was also tested by incubating cells for 0.5, 1 and 2 h at the concentration of 60 μM and 120 μM of dsDNA-Cy3, respectively. After treatment, the culture medium was removed and the cells were washed three times with ice-cold PBS (pH 7.4) and harvested. The cellular uptake was measured by flow cytometry analysis using FL-2 log filter for collection of fluorescence intensity. Each experiment was carried out in duplicate and 3 independent experiments were performed.

Cellular uptake mechanism of Ang2/RVG-NPs

U87 and N2a cells were seeded at a density of 1×10^5 cells/well in 12-well plates (Corning Coaster) and incubated for 24 h. After checking the confluency and morphology, chlorpromazine hydrochloride (CPZ, 10 μg/mL), sucrose (0.45 M), nystatin (25 μg/mL), Ang2/RVG (200 μg/mL) were added into each well and incubated for 20 mins. Then the culture medium was withdrawn from the well, and dsDNA-Cy3 labelled Ang2/RVG-NPs along with different compounds in the medium (the concentration of each compound was equal to that described above) were added. After 120 mins incubation, the medium was discarded and the cells were washed three times with ice-cold PBS. The cellular uptake was measured by flow cytometry analysis using FL-2 log filter for collection of fluorescence intensity. Each experiment was carried out in duplicate and 3 independent experiments were performed.

Intracellular tracking of NPs and Ang2/RVG-NPs

U87 cells and N2a cells were seeded on coverslips that were placed in 6-well plates. After 24 h, cells were incubated with dsDNA-Cy3-labeled Ang2/RVG-NPs or NPs for 4 h at 37 °C. Cells were washed twice with PBS buffer, fixed and moved to the glass slides containing DAPI mounting medium. After nucleus staining, the confocal images were taken on Zeiss LSM 710 confocal microscope equipped with an inverted microscope. For U87 and N2a cells, z stacks of typically 0.3 μm, 30-40 slices were imaged, each slice being the average of four laser scans. Microscopes Axio Imager Azure was also used to take images.

In vitro cytotoxicity and anti-proliferative activity against U87 and N2a cells

U87 and N2a cells were seeded in a 96-well at a density of 3000 cells/well in growth medium (RPMI and DMEM medium respectively, containing 10% foetal calf serum, 100 U/ml penicillin and 100 μg/ml streptomycin), and incubated at 37 °C in a humidified atmosphere with 5% CO_2. Cytotoxicity was examined by the MTT (Sigma) assay. Twenty-four hours after

seeding, the cells were treated with growth medium containing NPs, Ang2-NPs or RVG-NPs (LDH 10, 50, 100, 200 or 500 µg/ml). Growth medium was used as control. For anti-proliferative activity test, U87 and N2a cells were seeded in 96-well plates at a density of 3000 cells/well and cultured at 37℃ for 24 h. Then cells were incubated with 5-FU/NPs and 5-FU/Ang2-NPs or 5-FU/RVG-NPs at the 5-FU concentration of 0-20 µg/ml for 72 h, and the culture medium was used as control. At the end of incubation, 20 µl of 5 mg/ml MTT solution was added into each well. After incubation of 4 h in darkness, MTT solution was removed, and 200 µl DMSO added in each well to dissolve MTT formazan crystal. Absorbance was measured at 490 nm on a SpectraMax M5 microplate reader, and cell viability was calculated as (absorbance in the treatment well)/(absorbance in the control well) × 100%. Concentrations of 5-FU showing 50% reduction in cell viability (i.e. IC50) were calculated. Each experiment was carried out in duplicate and 3 independent experiments were performed.

5.2.4 Hemolysis assay

Fresh ethylenediamine tetraacetic acid (EDTA)-stabilised blood samples were collected from C57BL/6 male mice in the AIBN animal facility, University of Queensland Biological Resources. Whole blood was diluted in PBS (1 ml blood in 10 ml PBS), and the packed red blood cells (RBCs) were isolated via centrifugation at 1600 rpm for 5 mins, and further washed for more than five times with sterile isotonic PBS (until no red color could be seen in supernatant). Then, 200 µL of packed RBCs were diluted into 4 mL of PBS. The diluted RBCs suspension (0.2 mL) was then mixed with BSA-LDHs, NPs, Ang2-NPs or RVG-NPs PBS solution (0.8 mL) at various concentrations. PBS and water (0.8 mL) were used instead of LDH nanoparticles solution as negative and positive control, respectively. The mixture was gently shaken and incubated at room temperature for 2 h, followed by centrifugation at 1600 rpm for 5 min. The supernatant absorbance at 541 nm (Abs) was measured by a multifunctional microplate reader (infinite M200, Tecan). The percentage of RBCs hemolysis was calculated using the following formula:

$$Hemolysis\ Percentage = \frac{(Abs_{sample} - Abs_{negative\ control})}{(Abs_{positive\ control} - Abs_{negative\ control})} \times 100\ \%$$

Statistics

The data are presented as the mean ± SD. One-way or two-way ANOVA with Bonferroni's post-hoc test was used to assess statistical significance. $*p < 0.05$, $**p < 0.01$, $***p < 0.001$, $****p < 0.0001$.

5.3 Results and Discussion

Preparation and characterisation of ligand modified LDH nanoparticles

As shown in Figure 5.1, the first reaction step in our strategy was to conjugate a heterobifunctional crosslinker sulfo-SMCC to activate BSA where the amine groups of BSA reacted with N-hydroxysuccinimide (NHS) ester to form amide bonds. In the second step, the thiol groups of peptides reacted with reactive maleimide groups in activated BSA. Therefore, the peptides were conjugated with BSA (BSA-Ang2 or BSA-RVG).[23, 24]
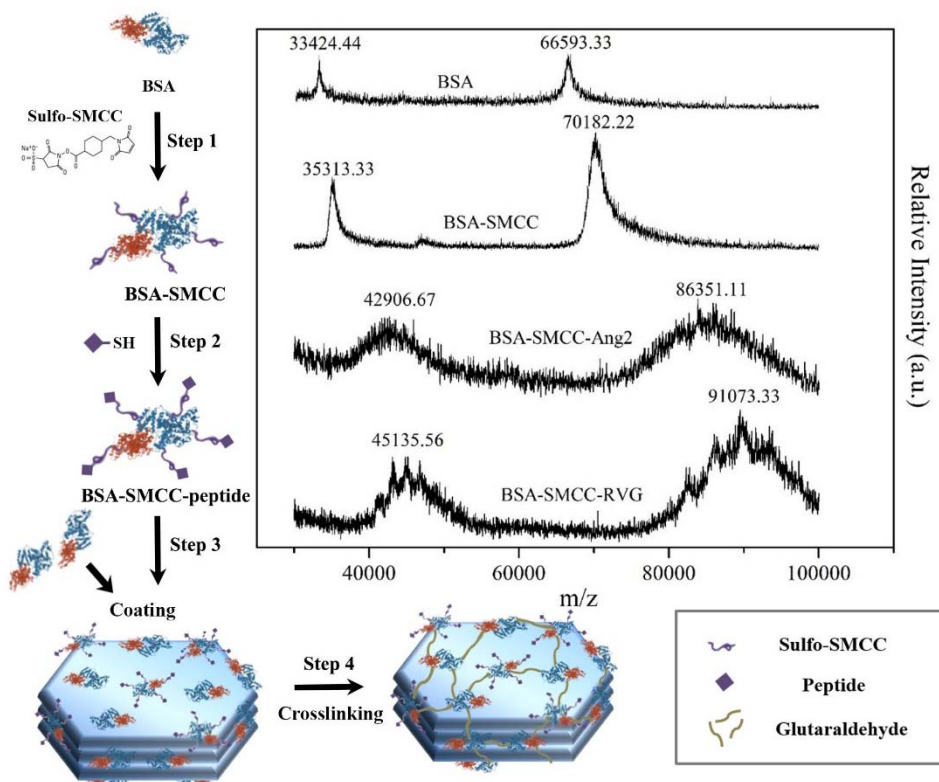
Figure 5.1 The strategy of constructing peptide-conjugated nanoparticles and MALDI-TOF detection of BSA molecular weight after activation and peptide conjugation

Table 5.1 MALDI-TOF detection of BSA molecular weight after activation and peptide conjugation

	MW	Sulfo-SMCC* number	Peptide* number
BSA	66593	-	-
BSA-SMCC	70182	8.2	-
BSA-SMCC-Ang2	86351	8.2	6.7
BSA-SMCC-RVG	91073	8.2	6.2

* Sulfo-SMCC MW: 436; Ang2 MW: 2404.66 RVG 29 MW: 3369.82

Maldi-tof is a very powerful analytical technique for the analysis of biomolecules (such as DNA, proteins, peptides and sugars) and large organic molecules (such as polymers, dendrimers and other macromolecules),[25-27] by providing accurate molecular weight.[28] As shown in Figure 5.1 and listed in Table 5.1, the original BSA had a molecular weight of 66593 D, similar to the reported for BSA.[29] After activation by the linker sulfo-SMCC, the synthesised complex BSA-SMCC had a molecular weight of 70182 D, which means that approximately 8.2 sulfo-SMCC were conjugated to each BSA. The yielding peptide-conjugated BSA (BSA-Ang2 or BSA-RVG) had a molecular weight of 86351 D and 91073 D, respectively, which indicate that there were around 6.7 Ang2 and 6.2 RVG peptides conjugated to each BSA. Moreover, the Ellman's method was also used to identify that the peptide ligand was successfully conjugated with activated BSA.[30] As shown in Table 5.S1, the absorbance value at 412 nm tested by Ellman's method decreased after reaction, which means that the sulfydryl-groups containing peptide was used to react with maleimide groups in the activated BSA. This adjuvant method also indicated that the peptides have conjugated with BSA successfully.

Following our previous experience, the mixture of BSA-Ang2/RVG and BSA was prepared at a molar ratio of 19:1 (BSA: BSA-Ang2/RVG=19:1) and then coated onto the surface of LDHs through electrostatic interaction and subsequently crosslinked by GTA (Figure 5.1, step 3 and 4) to obtain stabilised and ligand modified LDH-BSA complexes, [13,21,31,32] In such a way, Ang2

or RVG peptides were conjugated to LDH nano-carrier surface via BSA (Ang2-NPs and RVG-NPs), respectively for brain cell targeting delivery.

Table 5.2 Size distribution and zeta potential of the conjugates (mean ± SD, n = 3).

	Z-Average (d.nm)/PDI	Zeta Potential (mV)
LDH	103.3/0.179	30.5
BSA-LDH	170.5/0.198	-22.9
BSA-LDH-GTA (NPs)	170.4/0.197	-25.5
BSA-LDH-Ang2-GTA (Ang2-NPs)	169.9/0.201	-18.4
BSA-LDH-RVG-GTA (RVG-NPs)	170.3/0.185	-16.0
5-FU/LDH	90.8/0.185	28.9

5-FU (wt%): the loading capacity of 5-FU/LDH hybrids determined via UV-vis at 265 nm was 14.59% .

Table 5.2 shows the size and surface charge of LDH nano-carriers. The particle size before and after BSA coating increased from original 100 nm to around 170 nm while the zeta potential decreased from 30.5 mV to approximately -23 mV, which is in consistence with previous study.[13,21] After GTA crosslinking, the size was kept the same while the zeta potential slightly reduced due to the reaction of amino groups for crosslinking. Clearly, the particle size distribution was all moderately narrow in three cases, with the polydispersity index (PDI) close to 0.20. Attaching Ang2 or RVG peptides to the LDH nano-carriers did not significantly affect the size and the size distribution. Meanwhile, the zeta potential slightly changed from -22.9 mV to -18.4 mV (Ang2 peptides) and -16.0 mV (RVG peptides) after peptides conjugation, because the side chains of both peptides carry 2 net positive charges (2 negative charges and 4 positive charges). Altogether, these evidences suggest that Ang2 or RVG peptides are conjugated.[33] Such active targeting nanoparticles may accumulate more readily in tumour

tissue and facilitate targeted cell uptake due to the enhanced permeability and retention effect. [34,35]

Compared with LDHs, the average size of 5-FU incorporated LDHs (5-FU/LDH) was decreased to 90.8 nm (Table 5.2), which can be attributed to the inhibition of incorporation anionic organic drug 5-FU to the hydroxide layer lateral growth, as previously interpreted. [36] The similarity in zeta potential suggests that 5-FU loading was conducted through ion exchange, [37] with the loading of around 0.60 mg/ml (5-FU) in 4.0 mg/ml (LDH) suspension.

Here we developed a new and facile method to synthesise colloidally stabilised targeting LDH system by pre-conjugating Ang2 or RVG with BSA, followed by coating and crosslinking. The pre-conjugation of BSA with desired ligands has successfully offered a simplified and amenable procedure with narrowly variation and avoided the complicated post-particle modification on LDHs. The conventional modification includes serial chemical reactions in organic solvent for targeting ligand conjugation, which leads to concerns of increased toxicity and colloidal stability for biological application. [10,11] Moreover, the variation of surface property would be accompanied with a serious of downstream chain reactions, consequently compromising other properties such as antibiofouling property, stability and drug release. [38] Here, the colloidal stability of LDH nanoparticles in electrolytes buffer is always the first concern. Previous studies have evidenced that the LDH nanoparticles immediately form aggregation once exposure into the electrolytes buffer (physiological environment). [17] The aggregation has been well prohibited by coating BSA onto the LDH surface. [21] In this study, a further conjugation of the other modalities such as specific targeting ligands with BSA does not only keep the colloidal stability, but also makes the LDHs as a targeting delivery nanoplatform. [13,21,10]

Improved uptake of Ang2/RVG-NPs by U87 and N2a cells

Cy3-labeled nanoparticles were used to quantifying concentration- and time- dependent cellular uptake kinetics, the results of which are shown by flow cytometry. In this study, two receptor-mediated transport promoting ligands (Ang2 and RVG) were exploited for the modification of LDH NPs and target to U87 and N2a cells, respectively. As shown in Figure 5.2A and 5.2B, Ang2-NPs increased the U87 cell uptake efficiency compared to ligand-unmodified NPs. In particular, the U87 cell uptake efficiency was significantly higher at the dsDNA-Cy3 concentration of 40 and 60 μM with the incubation time of 2 h. Similarly, the N2a

cellular uptake of Cy3-labeled RVG-NPs also demonstrated a time- and concentration-dependent mode (Figure 5.2C and 5.2D). After 2 h incubation, cellular uptake of Cy3-labeled RVG-NPs was significantly higher than Cy3-labeled NPs at the dsDNA-cy3 concentration of 60 and 120 μM, increasing by 41% and 36%, respectively. To further confirm whether the specific uptake was induced by ligand-receptor mediated endocytosis other than the change of surface properties, we particularly incubated N2a cells with Ang2-LDHs and U87 cells with RVG-LDHs (they were non-target cells), respectively. Figure S5.2 shows that there was no specific enhancement induced by the exchange targeting, as N2a and U87 do not have the receptors for Ang2 and RVG, respectively. These results were in agreement with reports that target ligands (Ang2 and RVG) facilitated nanoparticles uptake by the target cells other than non-target cells.[39]
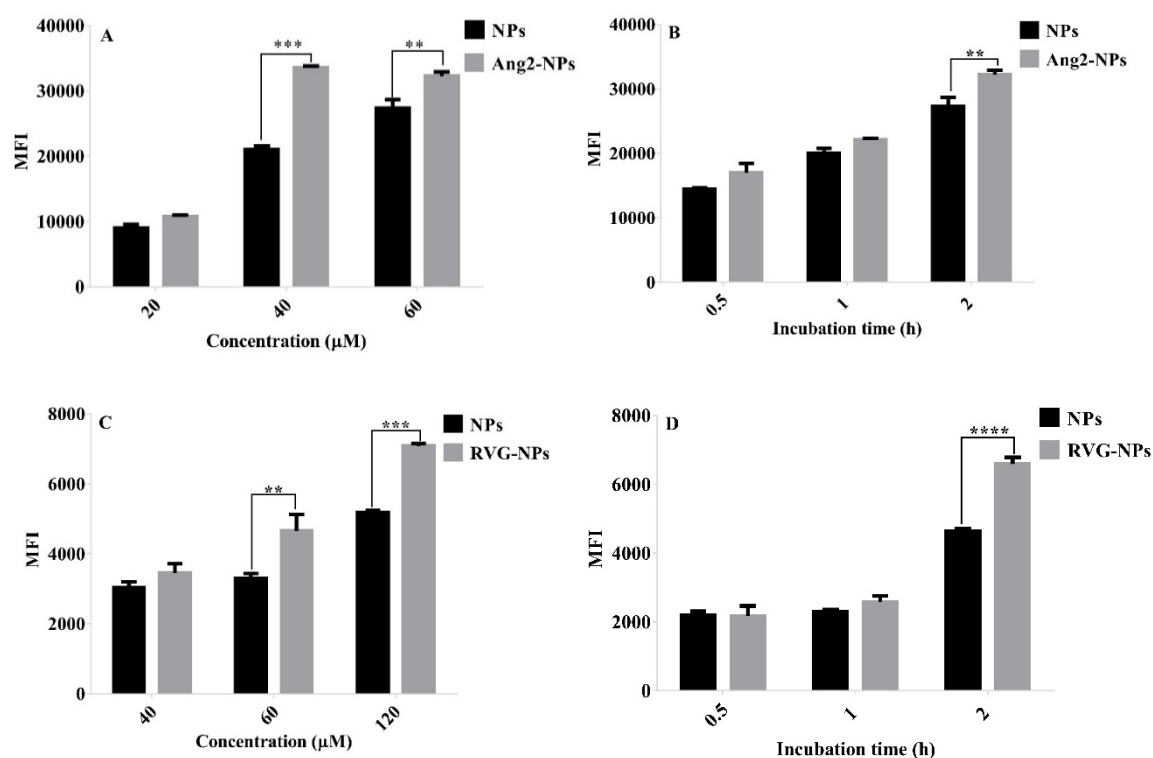

Figure 5.2 Cellular uptake of Ang2/RVG-NPs/NPs. (A) and (C) Cellular uptake of Ang2-NPs/NPs by U87 cells and RVG-NPs/NPs by N2a cells at the dsDNA-Cy3 concentration range of 20-120 μM for 2 h. (B) and (D) Cellular uptake of Ang2-NPs/NPs (60 μM dsDNA-Cy3) by U87 cells and RVG-NPs/NPs (120 μM dsDNA-Cy3) by N2a cells for different periods of incubation times.

Active targeting mediated by affinity ligands provides an alternative delivery for cancer treatment. Nanoparticles functionalised with targeting ligands preferentially increase the drug delivery to the target cells expressing cognate counterparts.[40] In a similar study about Ang2-conjugated poly(ethylene glycol)-co-poly(e-caprolactone) nanoparticles (Ang2-PEG-PCLs) drug delivery system for U87 cells, the cellular uptake of 500 mg/ml rhodamine isothiocyanate (RBITC)-labelled Ang2-PEG-PCLs exhibited a time-dependent mode and significantly higher than RBITC-labelled PEG-PCLs when the incubation time ranging from 30 to 120 mins.[41] As proposed, surface modification with Ang2 or RVG endows LDH NPs with enhanced cellular uptake efficiency, in good agreement with previous studies. Such uptake profile may provide view for optimizing the therapeutic intervention.[15, 42, 43]

Intracellular localisation of NPs and Ang2/RVG-NPs and uptake mechanism

The intracellular localisation of Cy3-labelled Ang2/RVG-NPs and NPs in U87 and N2a cells was evaluated by confocal microscopy (Figure 5.3A and 5.3B) and fluorescence microscope (Figure S5.3A-S5.3B). Both confocal images and fluorescence images show that U87/N2a cells treated with Cy3-labelled Ang2/RVG-NPs exhibited higher fluorescent intensity in comparison with Cy3-labeled NPs. Particularly, the intracellular location examination by confocal ortho-images of z-stacks illustrates that the nanoparticles were mainly present in cytoplasm. The images indicate that Ang2/RVG peptide modified LDHs could facilitate the internalisation process, leading to enhanced nanoparticles accumulation throughout the cytoplasm of U87 and N2a cells, while the localisation seems to be very similar in both cases for target and non-target LDH nanoparticles, which is in consistence with our previous report.[44]
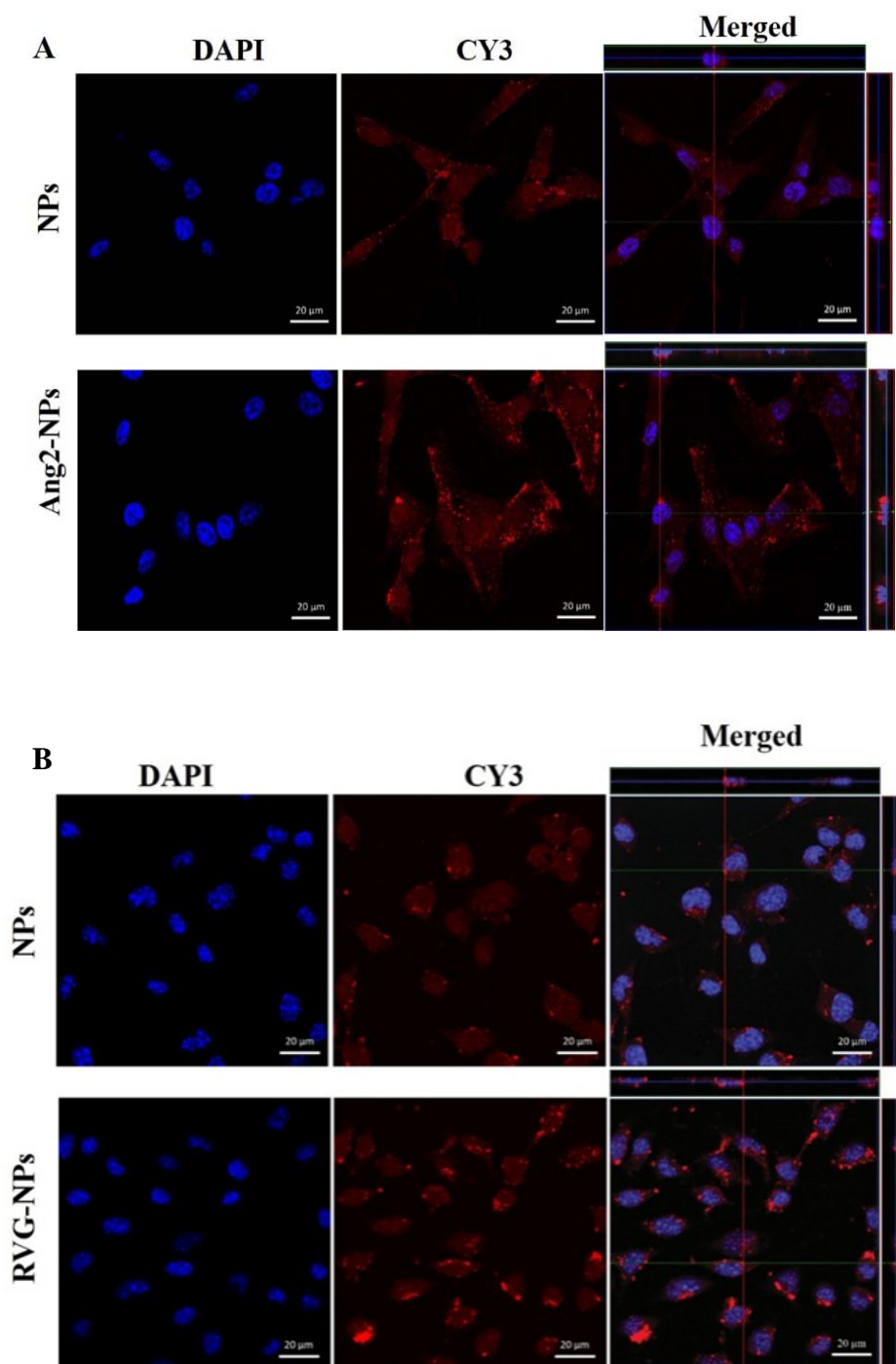
Figure 5.3 Intracellular localisation of Ang2-NPs/NPs incubated with U87 cells for 4 h (A) and RVG-NPs/NPs incubated with N2a cells for 4 h (B). The nuclei were stained with DAPI. The centre merged confocal ortho-images of z-stacks were X-Y view, the images above and right were X-Z and Y-Z views (cross section at the red and green line).
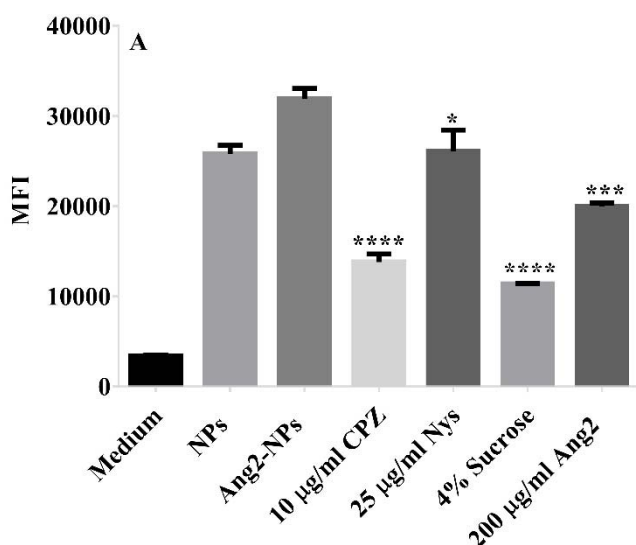
Figure 5.4 Cellular uptake of NPs and Ang2/RVG-NPs by U87 cells (A) and N2a cells (B) in presence of specific inhibitors. Cells were pretreated with various inhibitors for 20 mins, followed by treating with Ang2/RVG-NPs for 2 h.

In order to elucidate the internalisation mechanism of Ang2/RVG-NPs, the effects of endocytosis inhibitors on cellular uptake kinetics were evaluated quantitatively. Inhibitors for clathrin-mediated (CPZ and surcose) or caveolin-mediated (NYS) endocytosis were selected. As shown in Figure 5.4A, both CPZ and sucrose were found to inhibit the U87 cellular uptake of Ang2 -NPs, decreasing by 63% and 37.6%, respectively. Incubation of U87 cells with nystatin also significantly reduced the cellular uptake of Ang2-NPs. These results suggest that clathrin-mediated endocytosis and caveolae-mediated endocytosis are the main contributor to internalisation of Ang2-NPs by U87 cells.

Similarly, Figure 5.4B shows that incubation of N2a cells with CPZ and sucrose effectively reduced the cellular uptake of RVG-NPs to 50.8% and 83.2%, respectively, indicating the involvement of clathrin-mediated endocytosis in the cellular uptake of RVG-NPs. However, nystatin was not found to significantly affect the cellular uptake of RVG-NPs by N2a cells. Thus, clathrin-mediated endocytosis may contribute to major internalization of RVG-NPs by N2a cells.